Master's Dissertation in Mechanical Engineering on:

Biodegradable cog threads: design, characterization and application

Catarina Filomena da Silva Baptista Soares

Supervisor at FEUP: Prof. Rita Rynkevic
Co-Supervisor at FEUP: Prof. Marco Parente

Mestrado Integrado em Engenharia Mecânica

October 7, 2021

"It always seems impossible until it's done."

Nelson Mandela

This page was intentionally left blank.

Resumo

Nesta dissertação, o objetivo foi analisar a aplicabilidade dos *cogged threads* comerciais de policaprolactona e poliadioxanona, atualmento utilizados em cirurgia plástica para *lifting* facial, na reparção do prolapso em orgãos pélvicos; bem como o desenvolvimento e análise de suturas semelhantes através de *meltelectrowriting* e corte convencional.

Começou-se, então, pela análise das suturas comercializadas com auxílio de Microanálise por Raios X e Análise de Padrões de Difracção de Eletrões Retrodifundidos, e de testes de tração uniaxiais.

Através das dimensões retiradas das imagens da Microanálise por Raios X e Análise de Padrões de Difracção de Eletrões Retrodifundidos, realizaram-se diversos códigos de impressão (código G) para criar filamentos de policaprolactona com geometrias semelhantes às observadas. Devido a incompatibilidade das dimensões dos pormenores das suturas e das limitações da impressora de *meltelectrowriting*, apesar das várias tentativas de imprimir suturas com geometrias e dimensões mais simples, não foi possível obter resultados satisfatórios.

Assim sendo, imprimiram-se filamentos lineares através de um *nozzle* de $600\mu m$ com diferentes parâmetros de impressão (temperatura de extrusão, velocidade da mesa coletora, tensão aplicada, quantidade de material extrudido), tendo sido a temperatura mínima de extrusão obtida de 165^oC e o diâmetro máximo atingido $650\mu m$. Além disso, através de observação das suturas e da realização de testes de tração uniaxiais, considerou-se que $6.25kV$ seria, das tensões testadas, a que produzia filamentos com melhores propriedades mecânicas e 170^oC a temperatura ideal tanto a nível de propriedades mecânicas como de degradação térmica do material.

Após a impressão dos filamentos tentaram-se realizar cortes para criar a geometria dentada que se pretendia desenvolver. Assim sendo, criou-se um protótipo de máquina de corte com duas possíveis inclinações de corte (130^o e 150^o). Os filamentos foram cortados e posteriormente testados através de testes uniaxiais de tração. Observou-se que os cortes realizados foram inconstantes e que não conseguiam cumprir a função para o quais foram criados.

Não tendo obtido os resultados pretendidos com os filamentos impressos e cortados, realizaram-se testes adicionais apenas às suturas de policaprolactona comercializadas. Testou-se, então, a capacidade das suturas se fixarem ao tecido quando as mesmas estão a ser puxadas numa direção, e testou-se ainda o efeito fortalecedor que a introdução das suturas em tecidos vaginais de suína pode fornecer.

This page was intentionally left blank.

Abstract

The objective of this thesis was to analyse the application of commercial polycaprolactone cogged threads used for face lifting, in pelvic organ prolapse repair, as well as develop and study new polycaprolactone threads produced by melt electrowriting and conventional cutting.

The research starts by analysing the polycaprolactone and polydioxanone commercialized threads with the help of Scanning Electron Microscope examination and uniaxial tensile testing. It was attempted to generate G Codes, to print sutures with identical geometries to commercial ones, using the dimensions obtained from the pictures acquired from Scanning Electron Microscope exam analysis. Due to the small dimensions of the barbs and the movement limitations of the machine used, it was not possible to obtain sutures with acceptable geometries.

As a result, linear filaments with various printing parameters were produced in order to determine which parameters generated filaments with the best properties. The largest filament diameter achievable with a $600\mu m$ nozzle was $650\mu m$, while the lowest extrusion temperature possible was 165^oC. Through uniaxial tensile testing, it was determined that $6.25kV$ would be the most appropriate of the two voltages utilized, and that the optimal temperature used would be 170^oC, not only because of the tests but also due to the thermal deterioration of the polycaprolactone. There were no meaningful findings gotten about the speed of the collecting plate.

To manufacture the barbs, a cutting device prototype with two potential cutting inclinations was built. The cut filaments were evaluated using uniaxial tensile testing, and the cuts were found to be inconsistent and did fulfil the desired function.

Having failed to obtain the desired results with the cuts, additional tests were carried out only on the commercial polycaprolactone cogged threads. The ability of these sutures to hold up within the sow's vaginal tissue and the strengthening effect when the threads meet within the tissue were evaluated, and the results seemed promising.

This page was intentionally left blank.

Agradecimentos

Em primeiro lugar, gostaria de agradecer à minha orientadora, Professora Rita Rynkevic, pelo seu cuidado, boa disposição e disponibilidade durante todos estes meses. Ao co-orientador, professor Marco Parente, gostaria de agradecer a ajuda proprocionada na reta final da realização desta dissertação.

Gostaria de agradecer o financiamento do Ministério da Ciência, Tecnologia e Ensino Superior, FCT, Portugal e do Programa Operacional Competitividade e Internacionalização - POCI o projeto SPINMESH - Melt electrospinning of polymeric bioabsorbable meshes for pelvic organ prolapse repair - POCI-01-0145-FEDER-029232. Gostaria ainda de agradecer ao Professor António A Fernandes, coordenador do projecto *SPINMESH* por ter possibilitado a minha integração neste projeto.

Não poderia deixar de agradecer a todos os colegas que me receberam da melhor forma no Laboratório de Desenvolvimento de Produto e Serviços e, em especial, à Ana Pais, por toda a ajuda fornecida nos últimos meses de realização da minha dissertação. E gostaria ainda de agradecer ao Professor Jorge Lino e à Dona Emília Soares permitido a utilização do microscópio óptico do laboratório de materiais.

Aos meus amigos da faculdade, um obrigada especial por me terem acompanhado ao longo desta "caminhada" tanto nos momentos bons como nos menos bons. Obrigada ainda pela partilha de conhecimentos e experiências, e por toda a paciência. Foram, sem margem de dúvida, das melhores coisas que a FEUP me deu.

Aos meus amigos em geral, um obrigado por me ajudarem a manter a minha saúde mental e me ajudarem a ter uma melhor visão do mundo.

Em último lugar, mas não menos importante, queria agradecer à minha família por me aturarem mesmo nos momentos em que eu não me aturo a mim própria. Por fim, um obrigado especial não pode faltar aos meus pais pelo o amor incondicional que toda a vida me fizeram sentir.

This page was intentionally left blank.

Contents

Notation

Abbreviations

ABS	Acrylonitrile butadiene styrene
AM	Additive manufacturing
BB	Ball burst
FDA	United States Food and Drug Administration
FDM	Fused deposition modelling
HME	Hot-melt extrusion
MES	Melt electrospinning
MEW	Melt electrowriting
MFI	Melt flow index
PCL	Polycaprolactone
PDO	Polydioxanone
PLA	Polylactic acid
POP	Pelvic organ prolapse
PP	Polypropylene
SEM	Scanning Electron Microscope
SES	Solution electrospinning
SUI	Stress urinary incontinence
TT	Uniaxial tensile test

This page was intentionally left blank.

List of Figures

This page was intentionally left blank.

List of Tables

This page was intentionally left blank.

Chapter 1

Introduction

1.1 Framework and motivation

Pelvic Organ Prolapse (POP) is a pelvic floor disfunction that affects millions of women worldwide [1]. Although not all women have symptoms, many have seen their quality of life change negatively due to POP symptoms. The main purpose of POP treatments is to restore life quality; therefore, a variety of non-surgical and surgical options are used to prevent and treat POP [2].

The surgical treatment of POP has grown significantly over the past decades. Currently, there is no clear evidence of which of the available techniques assures the best results, since surgical treatment with mesh may offer a long-lasting repair of the prolapse than suture-based surgeries, but they can cause several graft related complications [3].

To reduce graft-related problems, new implant production techniques have been studied. Injection molding, 3D printing, hot-melt extrusion (HME) and electrospinning are some of the processes most recently used to manufacture medical devices like vaginal meshes [4].

Currently, surgeons seem to rely in prosthetic techniques to treat gynecological disfunctions. Considering the advantages of using cogged threads over standard sutures in wound closure, and face lifting surgeons may also rely on this technique to, in the future, treat POP [5].

Conventional cutting and injection modeling are the two main methods used to create the barb suture's. Since, for medicine particular field, fused deposition modeling has been combined with electrospinning to mimic extracellular matrices, the motivation of this thesis is to find a way to reduce graft related complications through the development of biodegradable cogged sutures using recent printing technologies [6].

1.2 Objectives

The long-term goal of this thesis is to find a more cost-efficient and less invasive treatment with reduced graft related complications than the existing ones for POP. Since the meshes, despite their post-operative problems, are having satisfactory results in the treatment of prolapse symptoms, it was considered that a good solution would be to develop meshes with melt electrowriting (MEW), which allows the production of microfiber of biomaterials that can also be combined with other biologic agents. Furthermore, since the use of cogged threads is a less invasive process used in plastic surgery, it was considered that the combination of these two methods could be a good solution for POP treatment in the future, since it also simplifies the adaptation of the mesh to the patient by the introduction of more or fewer threads.

Therefore, this thesis tried to take a step in the development of this hypothetical new treatment. The main objective was to create cogged threads through MEW with better properties than the ones commercialized. Thus, throughout the development of this thesis, other objectives were defined and presented to try to accomplish the main objective.

The first was to test the commercialized cogged threads and analyse the results obtained for later comparison with other threads. In addition, it was also intended to understand if the introduction of these threads in pelvic tissue would have any benefit.

The second was to understand the ability to manufacture cogged threads through MEW and, if possible, also try different geometries and printing parameters to compare and see the best-suited option. It was also planned to compare the properties of these threads with those already existing in the plastic surgery market.

1.3 Outline

In this Section, the contents of the remaining Chapters of this document are summarised.

Chapter 2 - In this chapter, relevant concepts were presented to serve as a basis to the study conducted throughout the thesis. Moreover, previous works done towards achieving pelvic organ prolapse treatment and melt electrowriting developments are also mentioned.

Chapter 3 - In this chapter, an important practical part of this thesis is presented. It shows the visual characterization of commercial cog threads and the design and production of novel cog threads through melt electrowriting and conventional cut. In addition, to compare the utility of commercial cog threads and the novel ones, some tests will be carried out to simulate some of the conditions found in women's pelvic floor. The production process of new prototype devices needed to manufacture the sutures and to perform the tests aforementioned are described in this chapter.

Chapter 4 - This chapter describes the preparations for all of the tests done (uniaxial tensile test, pulling test and ball burst test) as well as the data collected, along with brief comments on them.

Chapter 2

Studies review & state of the art

In this chapter, relevant concepts will be presented to serve as a basis to the study conducted throughout the thesis. Moreover, previous works done towards achieving pelvic organ prolapse treatment and melt electrowriting developments will be presented.

2.1 Female pelvic cavity

The pelvic cavity is a complex group of bones, connective tissues and muscles in males and females. However, there are several differences between women's and men's pelvic anatomy [7, 8]. Further analysis of the female pelvic floor anatomy and function will be done in this report.

2.1.1 Anatomy and function

The pelvic cavity is divided into anterior and posterior compartments, separated by the vaginal walls attached to the pelvic sidewalls. The anterior compartment contains the bladder and urethra (figure 2.1, and only the anterior vaginal wall is flexible. The other components (pubic bones and pelvic sidewalls) are inflexible and establish the anterior and lateral boundaries. In contrast, in the posterior compartment, from which the rectum and anus are part, the only inflexible element is the sacrum. Consequently, the other components (*levator ani* muscles, *perineal* body and posterior vaginal wall) are flexible [9].

The *puborectalis*, *pubovisceral* and *iliococcygeus* muscles are comprised in the deep layer of the pelvic floor. The *puborectalis* muscle is foremost responsible for preventing of feces leakage due to its ability to maintain the anorectal angle. Moreover, the *pubovisceral* muscles and the *iliococcygeus* muscle are also named *levator ani* muscles. These muscles hold the vagina and the pelvic cavity closed and resist the forces applied due to the abdominal and pelvic organs placed above and the abdominal and the atmospheric pressure [7, 9].

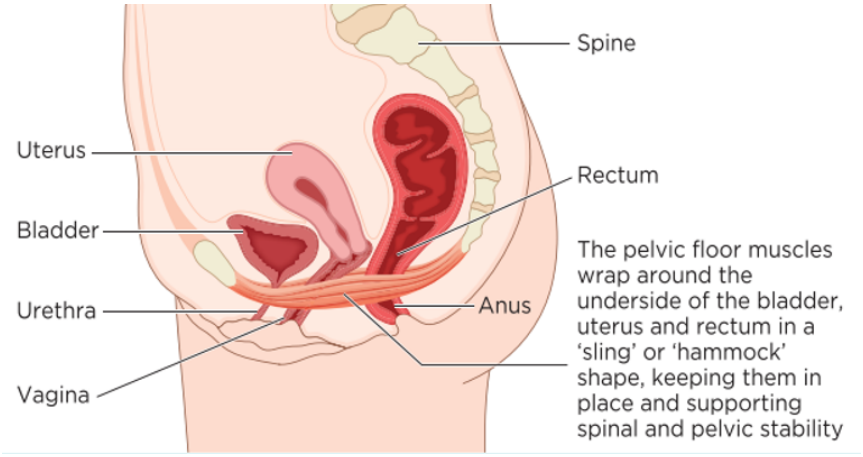

Figure 2.1 Side view of general anatomy of female pelvic floor [7].

On the other hand, the *bulbocavernosus* muscles along with the sphincter muscles form the superficial layer, in which the muscles' primary function is "to support and anchor the deep muscles to the pelvic girdle" [7]. Additionally, the urethral and anal sphincters are responsible for the external opening of the bladder and the rectum, respectively.

Another interesting pelvic components are the connective tissues. These elements connect the vagina and the uterus to the pelvic walls and are divided into three levels. In level I, mesenteric structures suspend the upper third of the vagina and the cervix to the pelvic walls. In level II, the middle third of the vagina is attached laterally to *fascial* structures. Finally, in level III the distal third of the vagina is fused with the surrounding structures [9].

To sum up, the complex mechanical function of the female pelvic floor is to support the female pelvic organs and the unborn child and to control the opening of the bladder and rectum (continence) without interfering with micturition, defecation, sexual functions and parturition [7, 8]. It is possible to see that each of the components above has a different function; understanding its role is fundamental to prevent and treat pelvic floor dysfunctions [7].

2.1.2 Pelvic floor dysfunctions

Various factors, usually related to muscle and connective tissue disorders, lead to pelvic floor weakness and dysfunction. Female pelvic floor dysfunction is the term applied to a variety of conditions that include urinary incontinence, anal incontinence, POP, sensory and emptying abnormalities of the lower urinary tract, defecatory dysfunction, sexual dysfunction and several chronic pain syndromes are most of the female pelvic dysfunctions [7, 9, 10]. The focus in this research is POP and its treatment solutions.

2.2 Pelvic organ prolapse (POP)

POP is a pelvic floor dysfunction with minor significant morbidity (except in its most severe forms), and it primarily influences women's quality of life. It affects millions of women worldwide and occurs when pelvic floor tissues and muscles that hold the organs become weakened or stretched. These may cause the failure of the connective tissues and the pelvic organs can bulge into the vaginal wall [2, 11].

2.2.1 Epidemiology

Although POP can occur in women of all ages, the prevalence of organ prolapse increases with age until a peak that some researchers believed to be around 60 to 69 or 70 to 79 years old women [12, 13, 14].

Demographic changes have significant implications for the future of women‘s health services. In Portugal, the number of citizens aged >65 years is expected to increased from 2.2 to 3 millions from 2018 to 2080 [15]. Therefore, the number of hospital admission due to POP is also expected to increase. This progression of POP cases is also mentioned in studies conducted in the Netherlands and the USA population [16]. Thus, several researchers believe that the number of women suffering from POP can increase more than 40% by 2050 [13, 17]. These studies took into account the future projections of Luber *et al.* (2001) and J. M. Wu *et al.* (2009) to conclude that during the next few decades the number of elderly women will increase substantially.

This growth in cases of prolapse has an economic impact on both the individual and the health care system, since the most effective treatments, although not totally effective, are quite expensive. In 1997 the direct cost of POP surgeries in the USA was around 1012 million dollars. In some European countries, such as Germany, France and England, the surgery costs were, respectively, around 144 million euros, 83 million euros and 81 million euros [18, 19]. Therefore, it is crucial to understand this condition better and find a more effective treatment, to reduce the social and economic burden on society.

2.2.2 Symptoms and risk factors

Despite 41% to 50% of women have some degree of POP; however, only around 3% to 6% of women report symptoms. Although not all women present symptoms, the ones who have, saw their quality of life changed negatively due to those symptoms [2, 13, 20].

Patients often describe prolapse as heaviness, and the most common symptoms are a bulge of tissue or organs that protrudes to or past the vaginal opening, pelvic discomfort or pain, urinary incontinence and sexual difficulties [2, 7, 20].

Although the “risk factors for severe POP may differ from those for mild prolapse”, aging and pregnancy are the most commonly accepted risk factors for both degrees of prolapse. Several researchers claim that around 50% of women above 50 years old with at least one vaginal childbirth have some type of prolapse [2, 11]. According to recent

research, following vaginal birth, 21% to 36% of the damage caused in the *levator ani* muscles persist. Nevertheless, prolapse can have multiple causes, from which the most reported are the number of vaginal deliveries, the weight of vaginally delivered infants, diabetes, menopause, chronic cough, constipation, previous vaginal surgeries and heavy lifting [1, 11, 13, 21].

Even though there is some knowledge about the influence of the previous factors, other factors that more recently started to be considered as components of risk, such as genetics and ethnicity. Although clinicians have a greater interest in amenable risk factors, it is interesting to understand that Jelovsej *et al.* (2007) confirmed that a higher risk of prolapse was seen in women with a history of prolapse in close relatives. A few researchers believe in the effect of race on POP, reporting different levels of risk to different ethnicities and types of prolapse [1, 22].

2.2.3 POP types

As already mentioned, POP occurs when pelvic floor tissues and muscles that hold the organs are weakened or over stretched. Depending on the organ that prolapses, the condition may have another designation. *Cystocele* is the name given when the bladder prolapses (figure 2.2), *procidentia* or *uterocele* is for when it is the uterus (figure 2.3), *rectocele* for the case of the rectum (figure 2.4), apical prolapse to the top of the vagina, and even *enterocele* when referring to intestinal prolapse. "The reported incidence for *cystocele* is around 9 per 100 women-years, 6 per 100 women-years for *rectocele* and 1.5 per 100 women-years for uterine prolapse" [23]. However, it is essential to understand that occasionally more than one organ aforementioned can prolapse simultaneously and that sometimes the prolapsed organs can pass through the vaginal opening [12, 20].

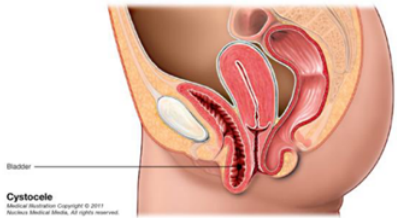

Figure 2.2 Lateral cut-away view of female pelvis with *cystocele* [20].

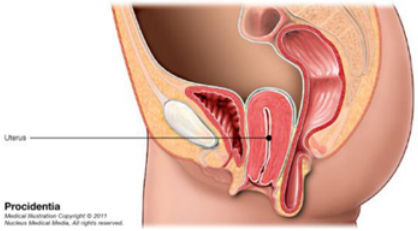

Figure 2.3 Lateral cut-away view of female pelvis with *uterocele* [20].

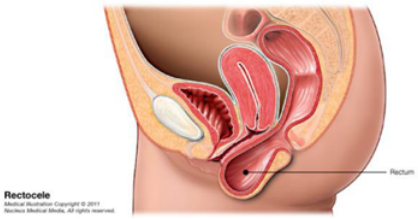

Figure 2.4 Lateral cut-away view of female pelvis with *rectocele* [20].

It is possible to establish a relationship between the prolapse type and some of the risk factors in certain cases. Hendrix *et al.*. (2002) reported the influence of four ethnicities (Hispanic, African American, Asian and Caucasian) on the probability of developing different types of prolapse. It was observed, that Hispanic women had the highest risk for *uterocele* and an increased risk for *cystocele*, Asian women had the highest risk for *cystocele* and *rectocele* and African Americans had a lower risk of all types of prolapsed evaluated in the report [22]. These results are compatible with the ones given by Yates (2019) who stated that "Hispanic and Caucasian women are at greater risk of pelvic floor weakness and dysfunction" [7]. Moreover, *cystocele* and *rectocele* can be influenced by waist circumference, increasing parity and constipation, while uterine prolapse is strongly associated with parity [22].

2.2.4 Diagnostics

POP is a dynamical disfunction, since the symptoms and examination findings vary day to day and depend on the level of activity and dilatation of the bladder and rectum. Therefore, a pelvic examination should fully describe the location and extent of prolapse and at the same time examine other dysfunctions that may be related to this disorder [13]. Usually, pelvic organ diagnostic is performed by external visual examinations followed by internal examination when indicated and necessary.

Nurses can do the external examinations to check for red, excoriated skin; infections, infestations, piercings; skin tags; abnormal lumps; fecal and/or urinary leakage; POP; signs of *atrophic vaginitis* and/or *lichen sclerosis*; alterations to the genital area that may indicate female genital mutilation (FGM) [24].

The internal examinations should only be done by a specialized professional in pelvic floor assessment and if there is any sign of infection, infestation, or a foreign body; fragile tissues, soreness, pelvic pain, tension in the pelvic floor area; history of sexual abuse; or menstruation, the internal examination should be postponed. Internal examinations make it possible to check for pelvic floor muscle strength and nerve damage [24].

2.3 POP treatment

The main purpose of POP treatments is to restore organ function and improve women's quality of life; therefore, a variety of non-surgical and surgical options are used to prevent and treat POP. Although these treatments are usually effective, they may not be completely effective in solving some symptoms including pelvic pain or pressure. Nowadays, the treatment options consist of conservative management, vaginal pessaries and surgery, with or without mesh [2, 20, 25].

2.3.1 Conservative management

The most important goal of conservative management is to reduce prolapse progression. Pelvic floor muscle training exercises and pessaries are the two conservative methods used to treat POP [13].

2.3.1.1 Pelvic floor muscle training exercises (*Kegel*)

It has been showed that pelvic floor muscle training exercises (*Kegel*) can reduce some symptoms of mild prolapse but do not treat POP. These exercises consist of frequent contraction and relaxation of the *levator ani* muscles to improve pelvic function and strengthen the pelvic floor [13].

To improve function, *Kegel* exercises should be performed to maximum strength and in different positions, and the muscle overload should be progressively adapted. Several indications may help patients to perform these exercises correctly; therefore, women should search for professional help [24].

Rehabilitation exercises are more commonly used in symptomatic women; however, some believe this conservative method can help women with a POP predisposition [24].

2.3.1.2 Pessary devices

A pessary is intensely used to manage POP since it is "an inexpensive, simple, low risk and effective treatment" [26]. This method relies on removable silicone devices (pessaries) inserted into the vagina to restore pelvic anatomy [2, 13].

This method can be used in all stages of prolapse and its main objective is to prevent progression and postpone future surgeries. Although the pessary use is limited in patients with dementia, pelvic pain and difficulty adhering to instructions, more than 85% of the patients who desire to use pessary are successfully fit with one, due to the variety of shapes and sizes available.

As already mentioned, the pessary is a very used treatment; however, as all the treatments, it has its complications: irritation, ulceration, pain, bleeding, urinary retention, defecatory dysfunction, urethral mucosal prolapse and erosion [13, 26].

2.3.2 Surgical treatment

The surgical treatment of POP has grown significantly over the past decades. There is no clear evidence of which of the available techniques assures the best results; therefore, a wide variety of techniques (hysterectomy, *fascial* defect repair, reinforcement with different meshes) and approaches (vaginal, abdominal, laparoscopic) are presently used. The currently available techniques can be divided into reconstructive surgery, with or without mesh, and obliterative surgeries. To decide the nature of the surgery, the patient's goals and expectations (body image, future sexual function, vagina intercourse) must be considered; however, the longevity and durability of POP surgery are also essential variables to be taken into account [12, 16, 27].

At the present time, mesh surgical methods are not used in several countries since the non-mesh ones have shown to be as effective without increasing the risk of subsequent surgeries in response to difficulties concerning the mesh. Nevertheless, surgical treatment with mesh may offer a long-lasting repair of the prolapse than suture-based surgeries [2, 20, 25].

Although several techniques have been developed since 1500 BC (the first evidence of an attempt to treat prolapse), ideal surgical treatment is yet to be found [3]. The main goal of vaginal prolapse surgery is to provide mechanical support; hence research for innovative materials and techniques is fundamental.

2.4 Implants

Mesh implants started to be used to reduce the risk of relapse. Several reports consider that the risk of reoperation because of POP is between 30 and 50%; however, recent studies found that this percentage is much lower (around 10%). It could be explained by the improvement of the new approaches and also by the number of conditions addressed in the older studies, since both urinary incontinence and POP were addressed [5].

Currently, mesh implants are mainly used due to the belief that their use in vagina surgeries can improve both objective and subjective cures. The implemented implants should restore normal anatomy and function to the vagina and the surrounding pelvic organs and have more extended longevity than *autologous* tissue. Therefore, similar biomechanical properties as the tissues nearest their application site are one of the key factors of implant success [5, 8, 28].

Surgical mesh is a screen-like material intended to be implanted to provide additional support to the weakened or damaged soft tissues or bones. Surgical meshes were initially used for hernia repair and abdominal repair of POP. Lately, gynecologists began to use this method to treat transvaginal POP and stress urinary incontinence (SUI) [20, 25, 29]. This market kept growing with the development of surgical mesh kits that included new insertion tools, tissue fixation anchors, surgical techniques and materials until the safety

of mesh procedures for transvaginal POP and SUI treatment became the subject of several court actions against manufactures internationally [20, 30].

This report will slightly address the POP implants' evolution to better understand the current use of the available materials and techniques.

2.4.1 History of implants

As already states, the first evidence of an attempt to treat prolapse was registered around 1500 BC. However, only after a few millennials (1521), the first surgical procedure for prolapse was performed by Berengario da Carpi. Although the first procedures were quite inchoates, they represent the first step of the consequent evolution. Surgical procedures evolved during the next several centuries, and due to disappointing outcomes of patient´s native tissues, surgeons started to experiment with a variety of natural and synthetic grafts to improve surgery's efficiency [3, 16].

According to traceable information, the first mesh repair of *cystocele* was performed in 1955 and used a tantalum mesh. Over the years, new materials suitable to be used in humans were found, and in the 1970s, the first use of *xenogenous* collagen mesh in urogynecology was described [3]. At the beginning of the 1990s, gynecological surgeons began using nonabsorbable synthetic meshes because of the success of these meshes in abdominal hernia and SUI treatments. At the end of the 1990s, polyglycolic acid or polyglactin-10, two fully absorbable mesh materials, were the most frequently used. However, probably due to unsatisfactory long-term results, they stopped to be used [3].

In 1996 US Food and Drug Administration (FDA) gave clearance to use synthetic meshes for urinary incontinence treatment and polypropylene (PP) mesh showed great results when used for *cystocele* treatment. Four years later *xenogenous* tissues ("originating outside of the organism, or from a foreign substance that has been introduced into the organism") [31] were used in *cystocele* surgeries. Although some reports state that porcine collagen implants successfully reduced the prolapse recurrence rate, other researchers claim that similar recurrence rates are found in conventional repair [3, 5].

Despite all the research and discoveries done since 1955, an ideal mesh material has yet to be found. Although surgeons are currently relying upon prosthetic materials for POP treatment, the search for a more effective solution is ongoing [5].

Considering the new knowledge and strategies studied in tissue engineering[1] and the use of robot-assisted technology in surgeries, the future of prolapse treatment seems promising [3, 5, 16].

[1]Tissue engineering is the process of creating functional materials for implantation into a live host by growing new tissues from cells and collagen scaffolds. Tissue engineering is heavily reliant on a thorough understanding of the mechanical and material characteristics of the original tissue that has to be replaced or augmented [8]. The biomechanical similarity between native tissue and the implant must be maximized to create functional site-appropriate tissue.

2.4.2 Implant types and materials

Due to the implant's material nature, implants can be classified as biologic grafts or synthetic meshes. As a result of the similarities between biologic grafts and native tissue, biologic implants are more likely to undergo tissue remodelling and, thus, less likely to cause erosion [5]. Biologic implants are divided in:

- *Autografts*: Grafts taken from the patient. They cause a minimal foreign body reaction, integrate well into native tissue and can theoretically be used in a contaminated area. Surgical morbidity associated with tissue harvesting, and the unpredictability of the repair's longevity, and the uneven quantity and consistency of the specimen restrict their use. *Fascia lata* and *rectus fascia* are the most widely used *autografts*.

- *Allografts*: Mostly processed from the cadaveric fascia of human donors. *Allografts* reduce the morbidity associated with *autologous* fascia harvest, but not the unpredictability of the resorption and integration process. Despite the meticulous preparation, there are still concerns about the potential danger of viral particles and infection, especially prion transmission. As compared to *autografts* and synthetic meshes, *allograft's* efficiency is consistently inferior.

- *Xenografts*: A cellular collagen-based scaffolds extracted from non-human (porcine, most used, and bovine) species raised for that purpose. Their theoretical risk of infection and incompatibility with some religious and cultural beliefs are some of the obstacles in applying these grafts [5, 32].

Biologic grafts can be expensive, scarce and come with the risk of perioperative morbidity or potential infectious disease transmission. As a result synthetic meshes are the most common choice [5].

Synthetic grafts are usually characterized by four distinct characteristics: their absorbability, pore size, weave and weight.

1. Absorbability

    - Non-absorbable prosthetic material, such as PP or polyester, remains in the body indefinitely and is considered a permanent implant. These materials induce undesired connective tissue reactions; however, there is permanent reinforcement in strength to the urogynaecological repair due to the implant and the scar formation.
    - Absorbable mesh polymers, for example, polyglycolic acid and polycaprolactone (PCL), degrade and lose strength over time. These materials cause a prolonged foreign body reaction and stimulate the activity of fibroblasts. Their goal is to provide additional strength while a new tissue develops; however they do not provide a long-term repair strength [5, 20, 25, 29].

2. Pore size: The most important mesh feature that influences cellular infiltration, risk of infection and mesh density and flexibility (smaller pore size increases flexural rigidity).

    - Microporous ($< 10\mu m$): This type of material increases the risk of infection because of the impossibility of large immune cells to access the interstices to phagocyte bacteria.
    - Macroporous ($> 75\mu m$): At $75\mu m$ the risk of infection decreases and the collagen infiltration is maximized because of this pore size, the entry of fibroblasts, macrophages, blood vessels and collagen fibres is viable.
    - Submicronic ($< 1\mu m$): It is rarely and only used in gynecological surgeries associated with other meshes for adhesion prevention [5].

3. Weave: Synthetic meshes can also be divided into mono or multifilament. In multifilament implants, the interstices between the threads are much smaller than the pores ($< 10\mu m$). These interstices increase the risk of infection, since they allow bacteria to enter and replicate, but stop the penetration of host immune cells. Moreover, as the interstices increase the contact surface with the host when compared to monofilament implants, multifilament implants elicited a shorter-lasting acute inflammatory response that progressed into a more pronounced chronic inflammatory response [5, 32].

4. Weight: Lightweight materials are more elastic and may be less susceptible to infection and subsequent erosion. It is possible to find light-weight, mid-weight and heavy-weight materials.

The absence of infectious disease transmission from donor to host and the easy accessibility are the two main advantages of synthetic materials; however, the main drawbacks are the infectious and erosive complications. From all the possible meshes aforementioned, lightweight microporous and monofilament meshes are considered the best choice for pelvic floor reconstructive surgery [5].

In reconstructive surgery, the aim of using grafts is to strengthen the existing tissue. Consequently, the ideal mesh should be biologically compatible, sterile, affordable, non-carcinogenic, resistant to infection, non-allergenic, non-inflammatory and must provide both anatomic and functional results. Nevertheless, a perfect material is yet to be found. Although PP meshes are widely used, they seem to cause severe body reactions that can affect the healing process. Therefore, partially absorbable meshes have been used to lower the erosion rate and improve the success of pelvic surgeries [3, 5, 33].

2.4.3 Graft related complications

Understanding the principal risks and their causes while using transvaginal surgical meshes in prolapse treatment may help the development of a less invasive, more lasting, and less problematic method.

Although there are several risks while using surgical meshes, the two main ones occur when the surgical mesh devices break down or wear away. This happens when the mesh part becomes exposed or protrude the vagina (vaginal mesh erosion) or when the mesh erodes into pelvic organs such as the urethra, bladder and rectum (erosion of the mesh into pelvic organs). It is important to understand that vaginal mesh erosions are widespread while using non-absorbable synthetic surgical meshes, for example, meshes made of PP or polyester [11].

The physical and structural characteristics of the prosthesis determine the histology response to reconstructive material utilized in surgery. The host reaction is divided into many stages: Incorporation (host cells infiltrate the reconstructive material, enabling for neovascularization and collagen deposition), encapsulation (collagen and connective tissue deposit at the periphery of the material), mixed response (integration takes place at the graft pores and the leftover material is encapsulated) and resorption (material is replaced by host neo-connective tissue) [5].

The main complications associated with surgical mesh devices for POP are:

-Vaginal mesh erosion Non-absorbable synthetic surgical mesh can break down or wear away over time. Part of the mesh may become exposed or protrude through the vagina.

-Vaginal mesh contraction Shortening or tightening of the mesh over time can cause vaginal shortening, tightening or pain.

-Dyspareunia Pain during sexual intercourse.

-Erosion of mesh into other organs The mesh may erode into the other pelvic organs.

-Urinary problems.

-Infections.

-Bleading.

Other, less frequent, problems are recurrent prolapse, neuro-muscular and emotional problems and vaginal scarring. Surgery may be needed to correct some of these complications, and, even after removing the mesh, some problems may persist [20, 25, 33]. Due to the long list of complications, FDA has forbidden the use of transvaginal meshes [2].

2.5 Social and economic impact

As already mentioned, our society is aging, and consequently, the number of POP surgeries is increasing as the years' pass. Moreover, several women require reoperation due to graft-related complications, unsatisfactory results, along other reasons. Studies were done in three different countries, USA, UK and Denmark, have shown that the risk of reoperation is respectively in each country, 25%, 10.8% and 11.5% the last two within 11 years after the initial procedure [12, 34, 35]. Some authors believe that surgical procedures are improving since more recent studies showed a significantly lower reoperation rate, around 13%, than the older ones. Around 30% of women undergoing POP surgery needed reoperation. However, the risk of reoperation after the first procedure on younger women (18 to 49 years), 26.9%, is much higher than in older women (50 to +90 years), 10.1%. In addition, although the risk of having more than one reoperation is low, there are patients (around 0.05% of women that underwent the first procedure) that need a third reoperation procedure, and all these operations have an economic impact [12, 33, 34].

Understanding the economic impact of all these factors together is extremely important. Some authors believe that in 30 years, "with the increasing number of aging women, the cost of prolapse surgeries is expected to grow at twice the rate of population growth", because the risk of undergoing prolapse surgery increases each year [36].

The cost-effectiveness of transvaginal mesh procedures has yet to be proved. Therefore there is the need to develop and study new strategies to produce cost-effective solutions to treat POP [37].

2.6 Novel implant production technologies

To reduce graft-related problems, new implant production techniques have been studied. Injection molding, 3D printing, HME and electrospinning are some of the processes most recently used to make medical devices such as vaginal meshes. When selecting a manufacturing method, several aspects must be evaluated, including cost, efficiency and changes in the properties of the produced devices.

Injection molding, during which the molten material is injected into a mold and allowed to solidify, may be used to create implantable devices from thermoplastic polymers (figure 2.8). This process is extremely consistent, and reliable for high volume production and its ability to scale production in mass is its main benefit. However, injection molding is extremely difficult, sometimes even impossible, to create complex objects and to modify the final product in a minute. Moreover, the up-front costs of this technology (design, testing and equipment) are very high [4].

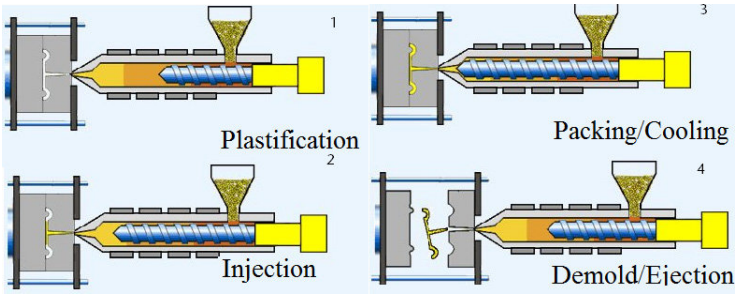

Figure 2.5 Injection molding process [38].

3D printing is based on the principle of layering material to create a tangible three-dimensional item, has shown to be a reliable method to prototype and develop novel mesh implants, including surgical urogynecological meshes, hernia meshes and breast implants. This method allows mesh representation before its final release, reducing the time and cost associated with product development and allowing the CAD file alteration whenever a modification is needed. From 3D printing types shown in figure 2.6, fused deposition modelling (FDM) is the most frequently used. It is low cost, simple, and versatile. However, due to some difficulties, it is hard to scale up 3D printing technologies production for industrial manufacturing. FDM, on the other hand, can be used to manufacture patient-matched urogynecological surgical meshes. Advances must be made towards finding solutions to the actual limitations imposed on the use of biomaterials in 3D printing technologies for the fabrication of tissue and organ constructs [4, 23].

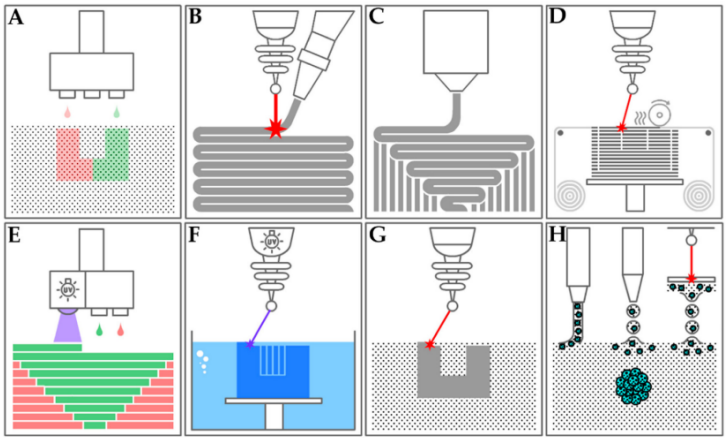

Figure 2.6 Types of 3D printing technologies. (A) Binder jetting; (B) Directed energy deposition; (C) Material extrusion; (D) Sheet lamination; (E) Material jetting; (F) Vat polymerisation; (G) Powder bed fusion; (H) Extrusion based bioprinting [39].

HME is a well-known method rapidly being employed in pharmaceutical and biological applications. HME is a continuous process that uses heat and pressure to soften a material and force it through an aperture to produce a product with a consistent shape and density (figure 2.7). The capacity to enhance the solubility of weakly water-soluble compounds and the capacity to design controlled, prolonged, sustained, and targeted drug delivery

systems are only a few of the benefits of this technology. One possible disadvantage of this technology is that it is incompatible with thermolabile polymers or medicines. Nevertheless, HME has already been combined with FDM to manufacture implants, catheters and surgical meshes [4].

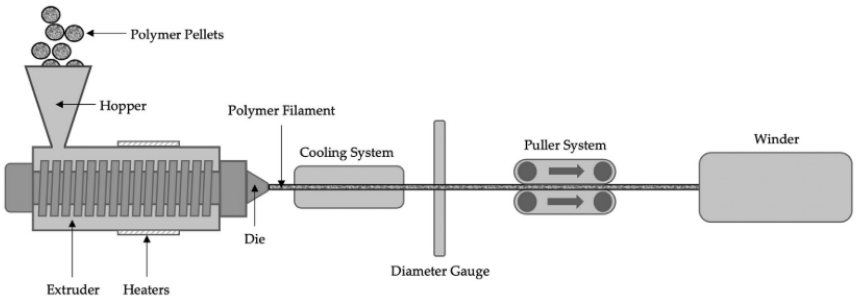

Figure 2.7 Schematic diagram of a typical HME system [4].

Finally, electrospinning is a simple and effective technique for manufacturing nanofibers using an electric field. The fibres produced by this technology have characteristics (high surface to volume ratio and very high and tunable porosity) needed in biomedical applications. Organic solvents are often used in electrospun nanofibers, and this might be a severe concern for biomedical applications like surgical meshes, as these solvents might constitute a health risk to consumers. Therefore, to manufacture surgical meshes, it is better to use melt electrospinning (MES). This technology uses molten polymers instead of polymeric solutions. Electrospinning's adaptability allows implants to be designed to replicate the biomechanical characteristics of natural tissue. Textile meshes can induce tissue regeneration by their three-dimensional structure and bioactivation instead of being only a passive support. As a result, electrospinning polymeric biomaterials have emerged as a possible strategy for overcoming some of the issues with commercially available transvaginal meshes [4, 40].

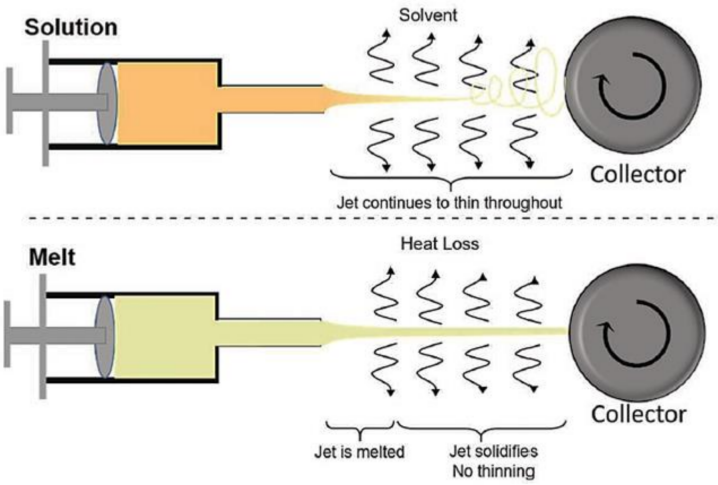

Figure 2.8 Electrospining vs melt electrospining [41].

2.7 Novel POP correction techniques and cogged threads

Since, at this time surgeons are relying on prosthetic materials for the treatment of POP, in this report, the use of technologies currently applied in thread lifting may be a solution to treat POP.

A telltale feature of aging is people's faces. As years pass by, some face-shaping supports are lost, "especially around the cheeks, the eye area, the jowls and the neck" [42]. This happens due to progressive soft-tissue laxity and facial fat loss [43, 44].

There are various invasive and non-invasive surgical facial rejuvenation techniques, but they require sedation or general anaesthesia and long-lasting recovery. Consequently, less invasive treatments were proposed to reduce the procedure and recovery time. Therefore, less invasive procedures, like thread lifting and high-intensity focused ultrasound lifting, have become popular, despite their less effective lifting result [42, 43].

Thread lifting is a semi-invasive procedure that only uses surgical suture threads to restore sagging facial skin [43, 45]. This method has several advantages, such as:

- can be performed under local anaesthesia;
- has shorter operative time;
- has a shorter recovery;
- has lower complication risk;
- usually does not present visible scars;
- is cheaper than conventional procedures [42, 43].

However, it is important to understand that "thread lifting is less effective and has a shorter maintenance period" [42]. The only mechanical anchoring of the thread is the surface cogs on the thread, so it is challenging to obtain a long-term effect. Depending on the material and geometry of the threads used, the effect can prevail for a longer or a shorter time [42, 44]. Also, this procedure is not appropriate for people with severe facial aging because they will show unsatisfactory results [42, 45].

Ideal candidates are usually between 30 to 49 years old with mild to moderate degree of sagging skin and soft tissue. As expected, this procedure shows better results in healthier patients (without skin allergic reactions, immunologic diseases, diabetes, among other problems) [42, 45].

There are different ways to perform a thread lifting procedure, but these have to guarantee that the threads are inserted deeply enough in the skin to prevent skin rippling [42]. Nowadays, one of the three major types of threads used in thread lifting is cogged thread. These threads are mono threads with tiny barbs strategically placed and designed according to the desired final effect, being their main advantage in providing a non-slip

attribute when the threads are correctly placed under the skin the "barbs along with the thread act as cogs to grasp, lift and suspend a relaxed facial area", not requiring additional knots [45].

2.7.1 History

Although, to most surgeons, knots are fundamental to the use of sutures, aside from their anchoring purpose, surgical knots provide little to no benefit and present several adverse characteristics. By weakening and stretching the material, surgical knots lower the tensile strength of all sutures. Therefore, several studies reported a reduction in tensile strength on the knot and on its adjacent parts by 35 to 95%, depending on the suture material used. Moreover, tight knots lead to a lower strength of the healed wound; however, knot slippage can occur if the knot is not tight enough. Therefore, knot tying is sometimes difficult, time-consuming and ineffective [46].

Several surgeons tried to find new solutions to improve wound closure results. The first patent in this direction was registered in 1958 by Nathaniel A. Matlin about a method for manufacturing wool-like artificial fibres with a wavy surface [47, 48, 49].

John H. Alcamo, a general surgeon and inventor, can be considered the author of modern cog threads since he filed the first patent of surgical cog threads. Alcamo submitted his idea, "An elongate cord of a diameter and tensile strength adapted for sewing and holding human flesh, and comprising a body portion and sharp-edged, resilient barbs projecting therefrom, at acute angles relative to, and directed toward, the trailing portions of the body, and adapted to yield toward the body when pulled through the flesh and of a size adequate to penetrate the flesh when the cord is pulled against the barbs.", to the US Patent office in 1956 but only in 1964 the US Patent number 3,123,077 was issued. Alcamo patented several different designs, but as it is possible to see in figure 2.9, his sutures were all barbed and unidirectional [50, 51, 52, 53].

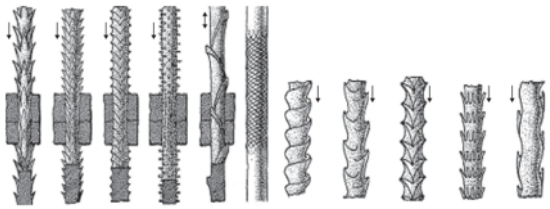

Figure 2.9 Alcamo's cog thread designs [47].

Between 1967 and 1999, several inventors presented distinct designs and techniques for knotless suture development. In 1971 Lemole patented suture design involving a notched suture and a latched collar and in 1978 Akiyama patented a surgical suture with spherical projections on the surface [47].

Nevertheless, in 1999, the so-called father of modern microsurgery, Harry J. Buncke, filed a patent in which he describes various designs of unidirectional and bidirectional

sutures, their methods of deployment and even some manufacturing techniques. According to him, these sutures may have an advantage in general wound closure, tendon repair and other internal tissue repairs, such as facelifts ("where the sutures would provide lines of tissue support beneath the skin") [51, 52]. Buncke presented bi-directional sutures with one needle at each end of the monofilament suture and unidirectional sutures only with one (see figure 2.10). Moreover, while with unidirectional sutures he proposes the use of two sutures used in opposite directions, with bidirectional, the use of two sutures is no longer needed [47, 51].

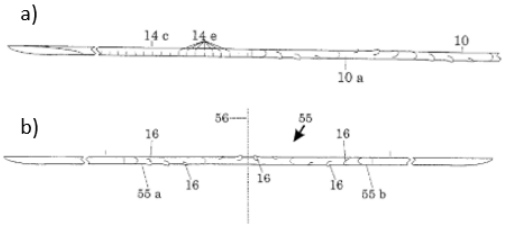

Figure 2.10 Example of Buncke's sutures: a)unidirectional; b)bidirectional [51].

Like Harry J. Buncke, Gregory Ruff started to investigate the possibility of cutting barbs in sutures to lift tissues, in order to prevent the necrosis that inevitably occurs with knotted loops and tensioned sutures. This would disperse the suture's holding force along its whole length, preventing node necrosis. Also, in addition to developing cog threads, he developed a thin brass tube to insert these sutures, and in June 2001, he received the first of many patents describing cog threads, an insertion device and a variety of design variations. After his first design, made of polydioxanone (PDO), several revisions and modifications were made, and in 2005 the initial design of Contour Threads™, showed in figure 2.11, received FDA clearance for midface suspension [52, 54].

Figure 2.11 First FDA-approve Contour suture. 25cm 2-0 polypropylene with barbs cut in middle 10cm [52].

Contour Threads™ complications can include nerve injury, breakage or migration of the suture, infection, bruising, or surface irregularities such as dimpling or grooving. These complications can be mainly due to the use of a nonabsorbable material and the device's position. Ruff believes a realistic goal for barbed sutures would be a consistent two-year period of benefit, ideally with an absorbable suture material [52, 54].

Around the same time that Gregory Ruff was developing and patenting his new designs and techniques of barbed sutures in the US, in Europe, Marlen A. Sulamanidze began to test barbed suture designs and to publish articles about thread lifts. He designed several sutures from which he was not very proud until he started to produce APTOS, a short bidirectional suture made of nonabsorbable polymer (PP) and that was designed to be used in freely mobile tissue. In these sutures, the barbs were cut at an angle in the suture and organized facing toward the midline in a bidirectional fashion. The devices developed by Marlen A. Sulamanidze were widely used and copied around the world; however, as reports of complications and relapses began to appear, threads and needle design and their placement method suffer several changes over time.

As years passed by, some scientists tried to improve the already patented sutures. One of these scientists was the plastic surgeon Nicanor Isse who believed that he could enhance suture designs by extending the sutures and employing unidirectional barbs. Looking at the technologies already developed, he had four significant concerns [52]:

- PP, one of the least reactive suture materials, does not cause a significant inflammatory response. Without this response, the production of new collagen around a PP suture is negligible, so the durability is brief.

- Both at the anchoring knot in the fascia and the contact of the barbs with the fatty tissues, there is still the possibility of "cheese-wiring."

- The used materials can be problematic considering the influence of the time and stress of facial animation, which predisposes the material to the linear shredding of the suture in the cleavage plane where the barbs are cut in the suture.

- "The amount of relaxation of the threads for reduction of lift effect is surprisingly very small" [52].

Considering the concerns mentioned above, Isse redesigned a suture called Silhouette Suture® that, instead of having barbs it has $10mm$ spaced knots and small unidirectional absorbable floating cones (trumpets) along the distal $10cm$ of the suture (Figure 2.12).

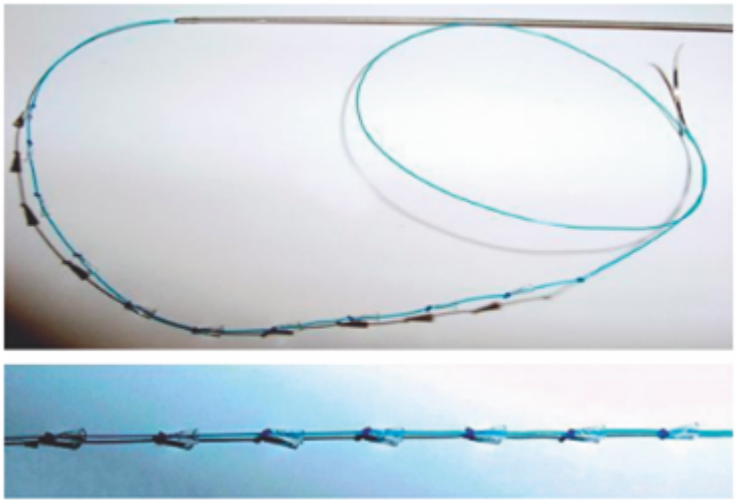

Figure 2.12 Silhouette Suture by Isse showing knots and "trumpets" [54].

The trumpets provide a significant increase in the suture's holding power at the time of deployment. Furthermore, since the trumpets are made of an absorbable material, their absorption will result in an intensified inflammatory response, an increase in new collagen surrounding the knots and threads and greater thread effects durability. It is essential to understand that silhouette suture is not used for wound closure. It is only used for lifting and relocating soft tissues [52, 54].

More suture designs were patented worldwide, some unidirectional other bidirectional, some with linear barbs and others with conical ones. Woffles T. L. Wu was another surgeon that developed practical investigation and created another type of suture, called Woffles (figure 2.13), from which he improved and developed different versions [52].

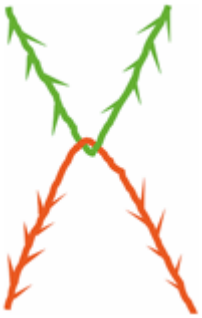

Figure 2.13 Version 3 Woffles X-lift [52].

V-loc and Quill sutures in 2013 were the two FDA-approved barbed devices for wound closure and were considered by some specialists to be a safe and effective option for plastic surgeries. V-loc was introduced in the market by Covidien, and Quill Medical produced Quill sutures. The most significant difference between these two types of sutures is the barb geometry. As a result of these disparities, the failure modes are different. As shown

in figure 2.14, the V-loc suture design is characterized by a dual-angle cut, which enables to generate barbs with high anchoring force due to its lower-angle cut while maintaining the integrity of the strand's strength. Quill suture. On the other hand, a Quill suture is a single-angle cut suture with a more significant cut angle that is more absorbable by the body [55, 56, 57].

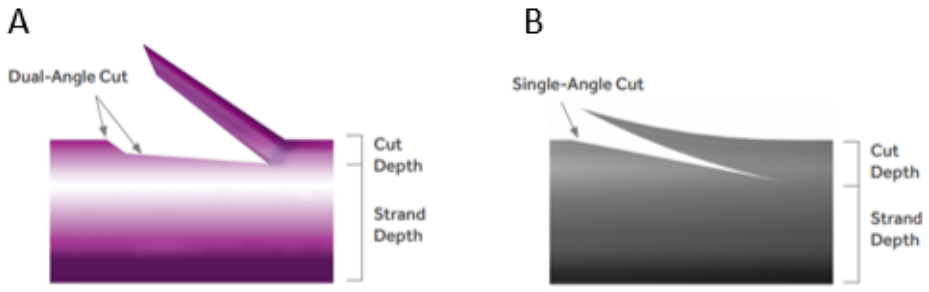

Figure 2.14 Design representation of V-loc (A) and Quill (B) sutures [57].

2.7.2 Materials and types

To find the right thread for the right patient, it is important to consider several factors, such as barb length, thread density, angles and barbs' direction, which may significantly influence the final results [44].

The threads' length should not be long enough to "become too flexible and incapable of lifting the facial tissue" [44] but should be long enough to provide some support to the facial tissue [44]. Another important factor is the density of barbs along a thread. A thread must have barb-free areas to avoid skin wrinkling and provide adequate anchoring; however, a good density of barbs is also needed to lift the tissues. To decide the density of barbs on a thread, the volume and weight of the tissues to be lifted must be considered [44].

Considering the barbs, at least two important aspects must be carefully chosen: their angle and thickness, spatial distribution and their direction. The angles of the barbs influence how much hold is achieved; in other words, more extensive angles mean stronger lifts. Nevertheless, it is necessary to ensure that barbs do not dig into the thread because this can make the threads thinner or break them. "Ideally, the length of the base of the barb should be equal to the thickness of the thread" [44]. Finally, focusing on the spatial distribution of the barbs along the thread and their direction it is also possible to provide better results. While increasing the contact between the barbs and the facial tissue, the efficiency of the lift may as well increase. Also, as bi-directional threads inhibit movements in either way, these are considered more efficient than uni-directional threads [44].

Regarding the thread's effect in the thread lifting procedure, the mechanical effect was the only effect analysed; however, it is essential to explore the biological effect of the threads [58].

Although, thread-lifts were performed with permanent sutures a few years ago, nowadays, they are performed with absorbable materials that disappear after a few months [43]. In this research, three of the materials currently used in thread lifting, PDO, polylactic acid (PLA), and PCL, will be analysed.

In this study field, PDO threads are the most used due to the results obtained over the years that have been used. They are colourless and made of a synthetic biodegradable polymer that is used in surgeries for many years. They stimulate the production of type 1 collagen in the lifted area [42, 44]. According to some studies, PDO seems to induce less pain in the patients "because it is hydrolysed and released into the urine after 6 months" [42].

PLA threads started to be used after the PDO ones and seem to provide more extended type 1 collagen regeneration, maybe because they remain in the tissues for about twice the time that PDO threads remain. PLA threads are made from a biocompatible polymer derived from lactic acid already used in several medical fields [44].

PCL threads are bio-absorbable, monofilament suspension threads of synthetic origin that regenerate type 1 and type 3 collagen. PCL stays in the tissue for around 12 to 15 months and, even after being absorbed by the body, it seems to preserve the lifting effect [44].

Collagen is one of the most abundant proteins produced in humans and can be categorized into different types that exhibit distribution, structural and functional differences. Type 1 and type 3 collagen are the most common in human skin. As already seen before, long-lasting threads stimulate more collagen. Nevertheless, the amount of collagen does also depend upon the thread surface area. As the collagen production in the targeted area helps restore volume and improves the skin texture, the choice of the material and the geometry of the threads appear to have a significant role in the biological effect of the threads [43, 44].

The mechanical effect is responsible for the immediate lifting outcome; the threads' barbs will practice their sustaining action on the tissues once positioned in the subcutaneous tissue. On the other hand, the biological reaction fortifies and extends the lifting effect even when all threads are absorbed [58].

2.7.3 Applications for POP correction

Considering the advantages of using cogged threads over standard sutures in wound closure and face lifting, it may be possible to apply this technique in different medical fields in which the standard sutures succeed in lifting or reallocating intern organs. In obstetric and gynaecologic practices, this type of thread was firstly used for tissue reapproximating in a laparoscopic myomectomy in 2008 and has been used since then in myomectomies

and some hysterectomies. Therefore, with some effort and investigation, it seems possible to start using this technique in POP treatment [46].

2.7.4 Evolution of cogged thread manufacture process

The methods used to create the several, above mentioned, patterns on the suture's body are cutting and injection molding. The oldest technique is cutting the barbs onto the filament body. Initially, this process was done by hand, but quickly new machines started to appear [53].

The production of barbs by cutting into the surface of conventional sutures is a reliable and precise mechanical technique to generate cog threads. A standard cutting machine for producing cog threads has a cutting bed, where the filament is placed, a Vise which holds the filament, one or more blade assemblies in order to cut a plurality of axially spaced barbs disposed on the exterior of a suture filament and, sometimes, a template or guide for the blades [48, 53]. Although there are several manufacturing benefits while using this method, there are also quite a few drawbacks. The most significant clinical disadvantage is that cutting barbs into suture weakens the suture's core and narrows its useful diameter, reducing its tensile strength. Nevertheless, the barb openness and engagement with surrounding tissues are also obstacles since there is no effective way to open the barbs especially while using flexible materials [46, 48].

Due to some of the issues mentioned above, other manufacturing processes were developed. Korean manufacturers started using molding technology to produce cogged threads. They initially started with creating threads with bumps, but not long after, using a mold pressing process, they could transform those bumps into barbs (Figure 2.15). This mold pressing manufacturing technique conserves the integrity of the thread [59].

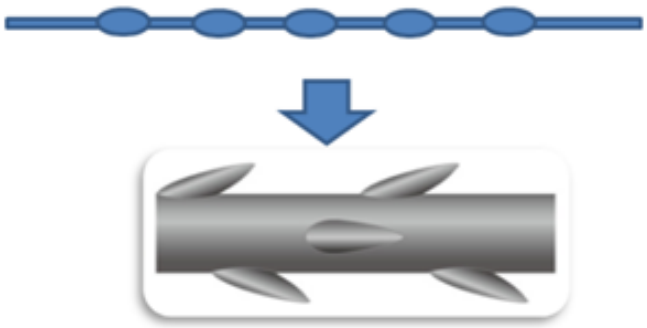

Figure 2.15 Mold pressing manufacture process [59].

Different molding manufactured threads are being used and tested. The most recent in the market is Mold Cutting Thread, which offers much more benefits in terms of strength, duration, tissue trauma and cost price [59].

2.8 3D printing/ Additive manufacturing

Three-dimensional (3D) printing, also known as additive manufacturing (AM), is a revolutionary manufacturing technique that enables the direct fabrication of an object layer by layer, *via* digital information from a computer-aided design file, without any part-specific tool (figure 2.16) [60, 61].

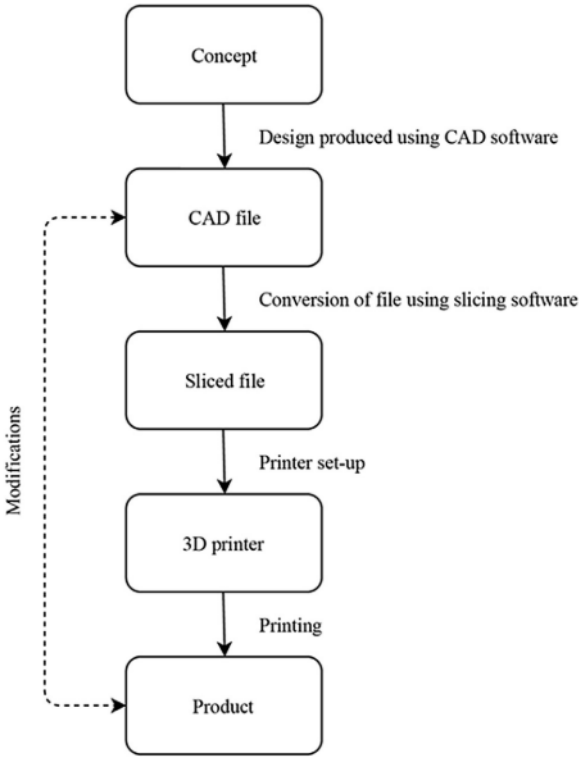

Figure 2.16 Outline of the steps generally performed during the 3D printing process [4].

In 3D printing, the first step is to create the 3D CAD (Computer-Aided Design) model of the object and convert it to any standard STL (Standard Tessellation Language) format. Through slicing software, the designed model is divided into several layers. Different printing parameters must be defined to create the final object. Thus, it is expected that a 3D printer allows the construction of an object by stacking 2D slice information [60, 61].

The first industries that employed 3D printing technology were the automobile and aeronautical. Over the past few decades, 3D printing processes have been implemented in numerous industries, "such as research, automotive, aerospace, healthcare, and medical, architecture and construction, fashion industries, and food industries" [61]. Nowadays, AM has revolutionized the healthcare system due to its ability to create small and personalized components. Accordingly, 3D printing has been widely used to produce implants, prostheses, biomedical models, surgical aids, tissues and living scaffolds (figure 2.17) [60, 62].

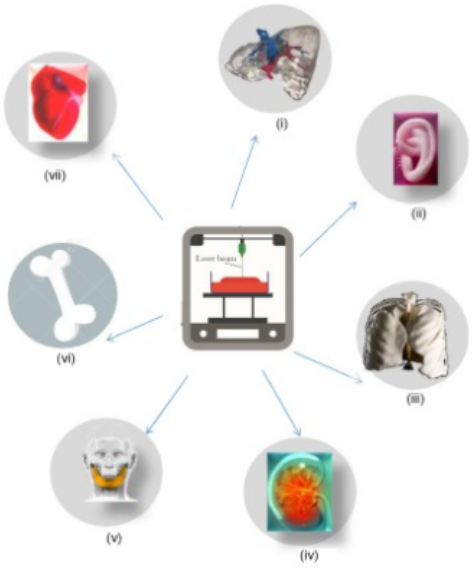

Figure 2.17 Development of various human organs: (i) liver, (ii) ear, (iii) lungs, (iv) kidney, (v) skull and jaw bones, (vi) limb bones, and (vii) heart [63].

One of the reasons why 3D printing has developed so much in the past few decades is its unique list of advantages. Some people say that AM offers "complexity for free" as it allows the manufacture of complex products with minimal time, material and money waste compared to subtractive and traditional techniques [60, 61]. Nevertheless, parts made through 3D printing exhibit an anisotropic nature and tend to have worse mechanical properties, probably due to material limitations or defects between adjacent layers [60, 61].

Various materials are used in 3D printing; currently, metals, polymers, concrete, and ceramics are generally used. It is important to know that material selection depends mainly on the future application of the achieved parts. Focusing the attention more on the medical field, it is necessary to select biomaterials with specific requirements [61, 64].

Biomaterials are biological or synthetic substances that can help repair or replace any part of the body for some time. Biomaterials are being deeply studied to replace petroleum-based polymers due to their abundant and sustainable sources and versatile properties. Some of the most desirable attributes in an ideal biomaterial for optimal 3D printing are biocompatibility, morphological mimicking capability and adjustable degradation printing capability [61, 62].

As the final application of the printed element is one of the main factors on which the choice of material depends, stiff materials, such as metals, ceramics, hard polymers and composites, are commonly chosen for orthodontic and orthopedic applications due to their mechanical stiffness and slower degradation rates. On the other hand, soft polymers are usually elected for visceral organ applications as a result of their flexibility and their faster degradation rates [62].

Although these materials may seem the perfect solution for several challenges in the medical field, there are a few concerns about their application in real life. Beyond the

aforementioned 3D printing challenges (difficulty to achieve mechanical properties, durability and others), the application of bioprinting leads to more specific challenges, namely regulatory issues and difficulty to manufacture in a sterile environment [60].

Although the 3D printing technologies have remarkably evolved in the past few decades, this research will be focused on FDM, one of the several existing 3D printing technologies [60].

2.8.1 Fused Deposition Modelling

FDM is a simple, expedite, versatile and low-cost AM technique. Scott and Lisa Crump developed this technique a few years after the emergence of stereolithography (SLA) technology and it is usually used due to its ability to quickly create a complex object [6, 60, 61, 62].

In this 3D printing procedure, a heated thermoplastic filament passes through the extrusion nozzles and it is deposited layer-by-layer onto the build platform according to the information in the CAD file (figure 2.18). When a new layer is deposited it fuses with the previous ones and solidifies. This process continues until the final product is obtained [60, 61, 62, 65]. Due to the necessity to reach high temperatures to melt the materials, usually, FDM printers suffer from thermal degradation and can also show unsatisfactory spatial resolution [65, 66]. FDM technique is extensively studied in the medical field because it enables the fabrication of ultrafine polymer fibers in the absence of solvents. Although FDM is widely used for prototyping in the industry due to its dimensional accuracy, high porosity and excellent mechanical properties, its use in medicine is limited since the industrial materials used lack biocompatibility. At this point, there is a lack of biocompatible thermoplastic materials with great thermal and rheological properties [61, 62, 65].

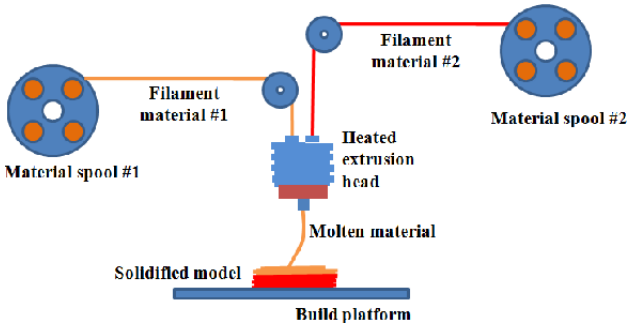

Figure 2.18 Mechanism of fused deposition modeling [67].

The materials used in this process must have a low melting temperature and a high enough viscosity to build but low enough to extrude through a thin head. Therefore, thermoplastics, such as polyvinyl chloride (PVC), nylon, acrylonitrile butadiene styrene (ABS) are usually used. For bio-applications, PCL and PLA are commonly used despite being petroleum-based materials [61, 65]. Ideal material for FDM application must "have a

processing temperature higher than the transition temperature and lower than the degradation temperature" [61]. Besides, sometimes for medicine applications, the thermoplastic polymers are doped with bioactive agents and biocompatible rheological modifiers. Although it is possible to dope thermoplastics with bioactive agents, it is often unwise to do so since the filaments reach excessively high temperatures (110 to 140^oC) [62, 65].

Printing parameters can have a big influence on the final properties of the printed part. Parameters as "layer thickness, build direction, raster angle, raster with, infill density, extrusion temperature and bed temperature" influence the final porosity and mechanical properties [61].

To overcome some of the aforementioned challenges, depending on the application field and the desired properties of the manufactured part, this technique has been combined with some conventional techniques. For medicine particular field, FDM has been combined with electrospinning (ES) to mimic ECM matrices[2] [6].

2.9 Electrospinning

Electrospinning can be described as a fusion of electrospray and spinning techniques. This process is based on the belief that the surface tension forces can be overcome by stronger mutual electrical repulsive forces in a charged liquid polymer. Therefore, it uses an electrical field to shape fibres from a melt polymer or a polymeric solution and allows the fabrication of 1D, 2D, and 3D nonwoven structures [23, 69, 70]. Consequently, this technique is a simple, efficient and user-friendly approach to produce continuous nano to micro-scale polymer fibres that can also be named nanofibers [71, 72, 73].

Some centuries ago (around 1890), electrostatic forces started to be used to deform liquid materials. The electrospinning technique, which is an extension of electrohydrodynamic atomization applied to higher viscosity fluids, was first observed in 1897 by Rayleigh; a few years later, it was studied in detail by Zeleny (1914) and then patented by Formals (1934). Although only in the 90s the term electrospinning was created, the first description of an electrospinning experimental setup can be found in the Formals' patents from 1934 to 1944 [72, 69].

In the past few decades, as nanotechnology and nanoscience fields have been growing, consequently electrospinning became the focus of further investigations due to its ability to produce ultrafine fibers and structures that can be used in the aforementioned fields [74, 69].

2.9.1 Procedure

Electrospinning begins by inducing a large electric potential in a polymer solution or melt, depending on the desired procedure. A static electric field is created separating, by a

[2] An extracellular matrix is a three-dimensional non-cellular network present in all tissues that provide structural and biochemical support to surrounding cells [68].

defined distance, the initially charged polymer reservoir and the final target with an opposite charge. This electrostatic field promotes the formation of Taylor's cone. As the field strength grows, the electric field reaches a critical value and a thin jet is ejected from the tip of Taylor's cone. This jet accelerates toward the target as a function of charge repulsion between and within the jet. As the jet begins solidification, by solvent evaporation or temperature decrease, the fibre is formed and small perturbations in the jet such as Rayleigh, axisymmetric, and bending instabilities are exaggerated by the electrostatic repulsion of like charges. As a result, these instabilities expose the jet to a whipping phenomenon that elongates and reduces the diameter of the fibre but leads to an unpredictable deposition of the polymer [23, 69, 75, 76].

2.9.1.1 Taylor's cone

Taylor was the first person to analytically describe the shape of the liquid cone as the result of a "force balance of surface tension, gravity, viscosity, electric polarization stress, and electrostatic forces" [77], as it can be seen Figure 2.19.

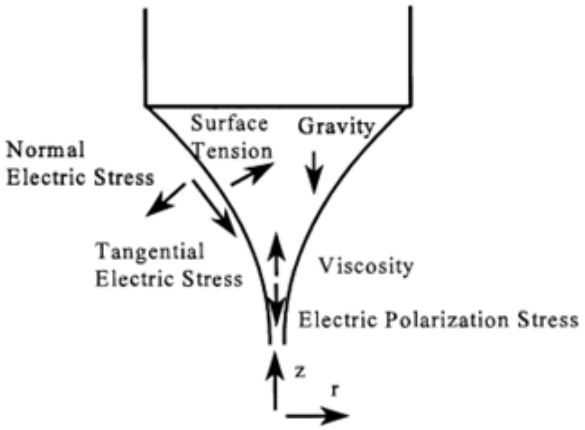

Figure 2.19 Forces in the liquid cone [78].

The Taylor's cone describes the shape of the liquid or polymer at the spinneret when the electrostatic pressure, p_e, overcomes the capillary pressure, p_c. Therefore, the condition for the formation of the Taylor cone can be written as $p_e \geq p_c$. The electrostatic pressure on the liquid surface, p_e, can be analytically described as

$$p_e = \frac{1}{2} \cdot \epsilon \cdot E^2 \tag{2.1}$$

where ϵ is the relative permittivity of the surrounding gas and E symbolizes the intensity of the electric field. The capillary pressure, p_c, derivates from the *Laplace Young* equation and is defined as

$$p_c = \frac{2 \cdot \gamma}{r} \tag{2.2}$$

where γ is the surface tension and r is the mean curvature of the surface [23, 79].

2.9.2 Set up and equipment

Nowadays, due to the popularity of electrospinning, several sophisticated systems have been studied and fabricated; however, the vertical and horizontal setups schematically represented in Figure 2.20 are two standard electrospinning systems [69]. Although the horizontal configuration is the most used because it eases the length control and its benefits to electrospinning systems that use heavy devices, the vertical configuration is also used, especially for applications that cannot use the horizontal one due to the configuration limitations [80].

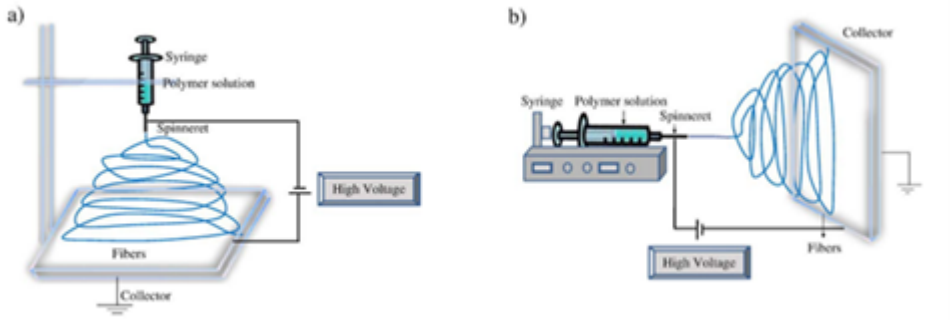

Figure 2.20 Schematic diagram of standard electrospinning setup (a) vertical setup (b) horizontal setup [69].

To build an electrospinning system, the three fundamental components are a high voltage power supply, a spinneret, and a grounded collecting plate. Since in solution electrospinning (SES) some polymers may emit toxic smells, this system should be built in a chamber with a ventilation system. However, as MES must be performed in a vacuum condition, it is necessary to provide this condition, and there is also the need for a heater to melt the filament [69].

2.9.3 Parameters that influences fibres' morphology and diameter

Electrospinning is ruled by several parameters that can significantly impact the fiber's final morphology and diameter when correctly manipulated. The impact of these parameters can be explained by the influence that the forces applied to the electrospinning jet have on the fibre's morphology. In addition, the parameters can be divided into solution parameters (concentration, molecular weight, viscosity, conductivity, surface tension), process parameters (applied voltage, flow rate, tip to collector distance), or ambient parameters (temperature, humidity), taking into account their nature [23, 69].

2.9.4 Solution electrospinning (SES)

The SES technique was more studied in the past than MES. Several researchers utilized polymeric solutions to produced fibres that exhibit millimetric and nanometric diameters.

This procedure relies on solvent evaporation from the polymer solution before it reaches the collector due to the potential difference applied [23, 66, 72].

2.9.5 Melt electrospinning (MES)

Although MES has not been as investigated as SES, since it generates fibres with larger diameters, this technique allows the production of sub-micron fibres avoiding technical issues, such as solvent retention and toxicity, increasing the fields of applications of electrospun fibres. MES must be performed in a vacuum condition, and, as the name says, instead of polymeric solutions a molten polymer is used [23, 69, 80].

The flow rate, temperature, voltage, spinneret-collector distance, and collecting speed all have a role in the MES product's result. Several analyses of the influence of these parameters on fibre outcome and the creation of numerical models to quantify the result have been published in the literature. The viscosity of the polymer melt increases the uniformity of the fibre diameter and the technique's natural biocompatibility makes MES suitable for industrialization, particularly in the tissue engineering area [23, 69, 81].

2.9.6 Solution electrospinning vs melt electrospinning

MES and SES differ not only in terms of the nature of the polymer state but also in terms of process control, with the first allowing for more predictable fibre deposition because it is based on AM techniques that allow the production of highly ordered and customized structures [77]. The MES method allows for the collection of 100% of the polymer, whereas the solution variation only allows for collecting of 2 to 10% of the produced volume of material [82].

Regarding the stability of the polymer jet path, lowering the viscosity of the solution polymer to the point where it can no longer inhibit repulsive *coulombic* charge interactions causes bending and randomization during fiber deposition. In contrast, the viscosity of the polymer melt provides for a more stable deposition of the fibers in MES [23, 82].

2.9.7 Advantages and disadvantages

Electrospinning offers versatility and flexibility that no other standard mechanical fiber-spinning process was able to match. This process allows the reliable production of nanofibers with a high surface area to volume ratio and good malleability. Due to the fiber's malleability and process flexibility, this technique can adapt the fiber to a wide variety of sizes and shapes and achieve the desired mechanical properties by controlling the nanofiber composition. Nevertheless, a usual problem associated with electrospinning is the accumulation of charge on the deposited fibres (after deposition, the solidified threads retain part of the charge produced by the electric field and form a dielectric that interacts with freshly formed fibres, producing repulsion and uneven deposition). Overall, electrospinning is

a very attractive technique for several applications due to the possibility of large-scale production, the simplicity of the process, and the final fiber properties [71, 69, 73, 74].

As mentioned before, one of the drawbacks of SES is random fiber deposition due to the whipping effect caused by the polymeric solution's incapacity to suppress repulsive *Coulombic* charge interactions. Moreover, the use of solvents may not be compatible with some industries, where nanofibers are widely used, because of environmental, health, and productive limitations [23, 72, 75].

In MES, the viscosity and conductivity of the polymers restrict the influence of instabilities. However, while stability is desired for better control, it is also disadvantageous since it does not drive thinning as SES does, allowing for a more predictable but coarser structure. The use of additives to improve electrical conductivity increases the diameter reduction in MES [81, 82].

2.10 Melt electrowriting (MEW)

The ability to generate consistent fibers with smaller diameters, using electrospinning techniques, provided the basis for expanding this approach to more complex structures with unique properties. As indicated in the preceding part, the growth of scientific researches about electrospinning was matched by the continued development of AM systems, resulting in the merging of both predictable and practical domains. This combination enables the production of structures with well-defined dimensions, form, and volume, which would otherwise be difficult to achieve using SES [82, 83].

The effect of high voltage is a significant difference between electrospinning and electrowriting: in electrospinning, the electrical potential induces extra extensional tension, which accelerates the material and forces whipping effects, whereas in MEW, the high voltage electrical field allows a continuous fibre to be electrospun. Intermittent fibre electrospinning is caused by low flow rates [83].

MEW is the outcome of the confluence of AM, often known as 3D printing, and electrospinning of polymer melts. As stated in a preceding section, AM processes are characterized as layer-by-layer manufacturing methods based on CAD models, and the nature of the polymer used makes the employment of FDM technologies more suited for the intended application. The combination of two processes - extrusion AM and MES - yields a precise technique with excellent dimension control and subsequent collection of thin fibres to produce extremely porous structures [81, 82, 84].

The translation of the collector plate in respect to the spinneret allows for movement in MEW (figure 2.21). There are examples of designs with fixed and moveable spinnerets in the literature. In a similar fashion to 3D printing, the patterns created by the movement are the result of instructions transmitted from a computer. Overlapping is permitted, allowing for the fabrication of thicker components. The method's flexibility extends to the

collector since a spinning mandrel may be used in place of the flat collector plate to create tubular structures [81, 82, 85].

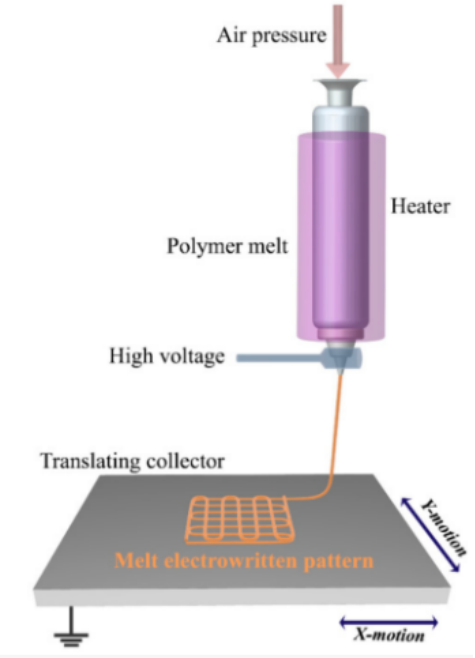

Figure 2.21 Schematic representation of melt electrowriting [86].

2.10.1 Parameters that influence fibers' morphology and diameter

MEW, like MES and SES, is governed by solution parameters (molecular weight, viscosity, conductivity), process parameters (applied voltage, flow rate, tip to collector distance, collection speed, spinneret temperature), and ambient parameters (temperature, humidity). When correctly manipulated they can have a huge impact on the fiber's final morphology and diameter [23, 69].

2.10.1.1 Solution parameters

Molecular weight/viscosity

Viscosity has a considerable impact on fibre drawing, and in MEW, where there is no solvent, the polymer viscosity is the sole viscous characteristic to concern. Studies state a need to find an optimal viscosity for electrowriting because it must be high enough to obtain a continuous fiber but low enough to allow an easy ejection of the solution and the production of Taylor's cone. Also, although very high viscosity polymer solutions could prevent the fracturing of the ejected jets during electrospinning and allow uniformization of the fiber due to their longer stress relaxation times, the higher the viscosity the larger the fiber diameter. Therefore, researchers related that maximum spinning viscosities between 0.1 to 21.5 ($Pa{\cdot}s$). Furthermore, researchers also believe that 0.1 to 2 ($Pa{\cdot}s$) is the viscosity range in which is possible to produce uniform nanofibers by electrospinning [69, 82].

Heating is the most often used method for reducing viscosity in melts; nevertheless, this method has limitations owing to thermal deterioration. Another successful technique is using low molecular weight polymers with low viscosity [82].

In addition, molecular weight has some influence on a variety of rheological and electrical properties, such as viscosity, surface tension, conductivity, and dielectric strength [69]. Reducing the molecular weight leads to lower viscosity and, as a result, higher melt flow index (MFI).

Many MES and MEW solutions use heating in the melt reservoir before going through the spinneret, with this step remaining at high temperatures for extended periods, allowing for a decrease in molecular weight. The polymer's storage conditions must be examined since moisture exposure might change the raw material's molecular characteristics [82].

Conductivity

Electrical conductivity is a critical characteristic in an electrohydrodynamic process since the entire process is jeopardized without creating an electric current between the electrodes. Because the polymer melt is dielectric most of the time, this parameter has a significant impact on the process outcome [82]. As in the aforementioned parameters, it is necessary to find an adequate range of conductivity where it is possible to produce a continuous fibre with the desired diameter and morphology. A low conductive solution produces beads and uniform fibres due to the insufficient elongation of a jet. On the other hand, researchers believe "that the jet radius varied inversely with the cube root of the electrical conductivity of the solution" [69].

The generation and mobility of charge carriers or ions govern the mechanism of electrical conductivity in polymeric materials. In contrast, insulating materials have charge transport due to convection throughout the jet, and the externally applied electric field is unaffected by diminishing surface charges [82].

2.10.1.2 Process Parameters

Applied Voltage

As should be expected, the applied voltage to the solution is a crucial parameter to define the success of the electrowriting process. However, as already mentioned, the applied voltage effect is different from electrospinning and electrowriting. While in MES and SES the applied voltage accelerates the material and forces whipping effects, in MEW the high voltage electrical field allows a continuous fibre to be electrospun [83].

Flow rate

The flow rate is considered by several studies the most significant parameter on the fibre diameter since it impacts the jet velocity and the material transfer rate. While keeping all other parameters constant, raising the flow rate should result in thicker fibres since more material is pulled from the nozzle under the same circumstances. At the same time, it is critical to remember that a minimal amount of material must be fed so that Taylor's cone is formed [69].

Tip to collector distance

As the spinneret and collecting platform constitute the electrodes in MEW devices, their distance significantly influences the electrical field force. The distance between the spinneret and the collector interferes with the electrical field strength and restricts the height of the jet [87].

To maximize the thinning effects, an intermediate value of the distance from the tip to the collector is the optimum approach since, due to the balance of forces that primarily oppose surface tension and electrical force, the fibres tend to shrink their section along with the jet. However, the electrical force in the field and the impact of high voltage diminish as the distance between electrodes increases, which reduces the effect of tensile forces [87].

When working in MEW, the dimensional precision and integrity of the final part are crucial. As the distance between the jet and the fiber increases, the amount of heat transmitted from the jet increases, and the fibers are more eager to solidify before deposition, affecting fiber adhesion while constructing 3D structures. Simultaneously, the jet's placement precision is compromised because instabilities might arise from either charge interference or other electrical interferences [88].

The typical inter-electrode spacing ranges from $1cm$ to $8cm$; however, distances of less than $1mm$ are conceivable [89].

Collector

The deposited fibres on MEW provide a tiny amount of residual charge and cause insulation of the melt from the collector, preventing the jet path from following its usual course since it is rejected from the places where fibres have previously been deposited. When constructing 3D structures with fibres placed on top of each other, this impact becomes more pronounced. The more conductive substrates lead to a reduced influence of these *coloumbic* repulsive charges, especially if the collector is grounded since it assures a larger discharge area. On the other hand, an insulating collector will accelerate the build-up [89, 90].

Because the size of the fibres is small in MEW, placement precision is critical, and the result precision is reliant on the moving portion [89].

Collection speed

Controlling the pattern of fibre deposition in MES is accomplished by moving either the collector or the printing head. With the head fixed, the movement will be regarded at the collector, which is one of the foundations for a successful output in electrowriting. The collector speed has a significant impact on MEW deposition accuracy because the rapid moving jet reaches the collector and, if the movement speed of the collector is not quick enough to match the vertical speed of the jet, fibre buckling occurs. . The reference value is critical translation speed to achieve straight fibers, and processing should be performed at speed greater than the reference [84].

When building patterned structures, placement precision must be considered, and lag arises when the pace is too fast.

Spinneret Temperature

To properly melt electrospun the polymers, the materials must be at a high temperature, above the T_m, to be drawn successfully. The high viscosity of the polymer, and the long relaxation time, limit the rate of jet thinning, so as Tm grows, the viscosity decreases, which is beneficial to the thinning impact of electric field forces.

If the processing conditions were isothermal, the target temperature of the fibres would be the lowest feasible temperature below thermal deterioration. However, most configurations are non-isothermal, and to maintain a thinning-compatible temperature away from the spinneret, the temperature must be raised higher. Higher temperatures can cause a decrease in viscosity with smaller diameters on the generated fibres. However, this rise is restricted by the continuity of the jet, which can be compromised at high temperatures due to a decrease in elongational viscosity limiting a continuous jet [82].

It is crucial to note that when the temperature rises, viscosity decreases, favouring thinning; nevertheless, flow is facilitated, and a higher flow rate may ensue.

2.10.1.3 Ambient parameters

Temperature

The rise in temperature in the surrounding environment reduces heat transfer at the jet, causing cooling of the fibre to slow and additional thinning to be feasible, enabling quenching to be postponed. There are solutions used to heat the surrounding atmosphere using heated gas flow or by regulating the operating temperature to maximize fibre thinning [89].

Humidity

When it comes to humidity, two types of polymers behave differently depending on the quantity of moisture in the air: hydrophilic and hydrophobic polymers. Because surface tension is lowered in the presence of water, the former may achieve smaller diameters in humid conditions, whereas the latter has the reverse effect [91].

The presence of water in the environment induces hydrolysis at the ester linkages of certain polyesters, resulting in the dissociation of the chain into oligomers of lactide acid and, eventually, alcohol and acid monomers [89, 91].

2.10.2 Materials

2.10.2.1 Polypropylene

Due to the lack of a suitable solvent for SES, PP has been employed in MES. Several studies with high molecular weight PP have been done; however, because this parameter significantly impacts the fibre diameter result, it is usually coupled with additives that increase the fibre section reduction [92].

Because of its long-term stability and superior mechanical performance over other biocompatible polymers, PP is widely used in medical equipment. The use of PP in medical devices dates back more than 50 years, with the introduction of PP sutures and, more recently, PP meshes to treat abdominal wall herniation. Even when using pure PP, fibres with a wide variety of sizes can be obtained following electrospinning. As previously indicated, MFI has a major influence on the outcome of MEW and MES, and pure PP can be found with MFI values ranging from 160 to $2000g/10min$ [89, 92].

2.10.2.2 Polylactic acid

PLA is a polyester produced from maize and sugar beets that may be made *via* condensation of lactic acid or ring-opening polymerization of cyclic lactide. It is a biocompatible and biodegradable polymer that has undergone extensive research in recent years, allowing it to be commercially accessible with various characteristics, most notably a high molecular weight and low MFI. PLA is thus an eco-friendly nontoxic polymer with features that alow its use in the human body. PLA is one of the most well-known materials in the AM industry since it is the most often used polymer in FDM machines as filament. Despite all the information that rigorous study, inspired by the industrialization of 3d printers, has delivered, it is a material that is not widely used in MEW. The feeding system is one of the most challenging aspects of using PLA in MES equipment, with the filament feeding version previously being overlooked since it needed mechanical strength in the rods that were not possible to achieve with many other materials, limiting the process' versatility [61, 89, 93].

In MES, as well as in other electrospinning processes, material properties are determinants for the outcome. PLA is highly susceptible to thermal deterioration, and it is hard to store due to its propensity to absorb water and hydrolyse. Mixing these factors, much work has gone into combining PLA with other polymers to make it acceptable for MEW, such as combining Polyethylene glycol (PEG) and PLA in blends. By regulating the surrounding environment of the jet, several tests were done utilizing inert gases to decrease PLA's oxidation problems as well as hydrolysis [61, 89].

PLA's primary benefits are its high strength and stiffness, which are balanced by its high brittleness and low viscosity, and its heat tolerance and solvent resistance. These characteristics of the pure polymer allow it to mix with other polymers such as rubbers, polybutylene succinate (PBS), PP, polystyrene (PS), and ABS. The glass transition temperature is around 55^oC to 65^oC, with a fusion temperature of 170^oC to 180^oC. PLA has a very low MFI, ranging between 4 and $8g/10min$[89, 94].

2.10.2.3 Polycaprolactone

PCL is a biodegradable aliphatic synthetic polyester made *via* ring-opening polymerization of caprolactone with the aid of a catalyst. Because of their biocompatibility and

biodegradability, aliphatic polyesters are becoming increasingly important in biomedical applications. PCL's characteristics are highly unique, making it ideal for biological applications such as tissue engineering and drug delivery. One of PCL's strategic benefits is that it has been approved for medical usage by the FDA. Additionally, PCL has been explored in composite bioink structures because of its known long-term degradation, and it is also a material with high mix compatibility, allowing it to be used with a variety of different polymers [95, 96, 97].

Among other rheological properties, PCL has a low melting point of about 60^oC, a negative glass transition temperature of -55^oC, and a variable molecular weight. MFI's most common values result from its molecular weight and vary from 10 to $30g/10min$. PCL is used in most PCL studies because of its low melting point and large molecular weight making it an excellent basis for blending with other polymers [89, 95, 96].

Chapter 3

Materials and Methods

In this chapter, an important practical part of this thesis is presented. It shows the visual characterization of commercial cog threads and the design and production of novel cog threads through melt electrowriting and conventional cut. In addition, to compare the utility of commercial cog threads and the novel ones, some tests will be carried out to simulate some of the conditions found in women's pelvic floor. The production process of new prototype devices needed to manufacture the sutures and to perform the tests aforementioned are described in this chapter.

3.1 Commercial cog thread characterization

Before developing sutures through MEW, commercialized sutures were characterized to obtain important information regarding their design and properties. Therefore, $100mm$ sutures of two different materials, namely Polycaprolactone (PCL) and Polydioxanone (PDO), were ordered. The cost of each suture ordered was approximately 22 euros, and the sutures' properties provided by the manufacturer, *Yastrid*, are presented in table 3.1:

Table 3.1 Commercial cog thread - manufacture information.

	Yastrid PDO cog thread	**Yastrid PCL cog thread**
Thread's material	Absorbable Polydioxanone	Absorbable Polycrapolactone
Needle's material	Stainless Steel (Japan imported)	Stainless Steel (Japan imported)
Cannula's Type	R/W/Bullet Cannula	R Blunt Cannula
Thread size	UPS 2/0	USP 2
Shelf life	2 Years	2 Years
Duration	180-240 days	180-240 days
Certification	CE & ISO13485	CE & ISO13485

The first analysis of commercial cog threads was carried out with the assistance of the

SEM exam. This exam was performed using a High resolution (*Schottky*) Environmental Scanning Electron Microscope with X-Ray Microanalysis and Electron Backscattered Diffraction analysis: **FEI Quanta 400 FEG ESEM / EDAX Genesis X4M**. The samples were coated with a Au/Pd thin film by sputtering, using the SPI Module Sputter Coater equipment, and the images obtained are shown in figure 3.1 and figure 3.2.

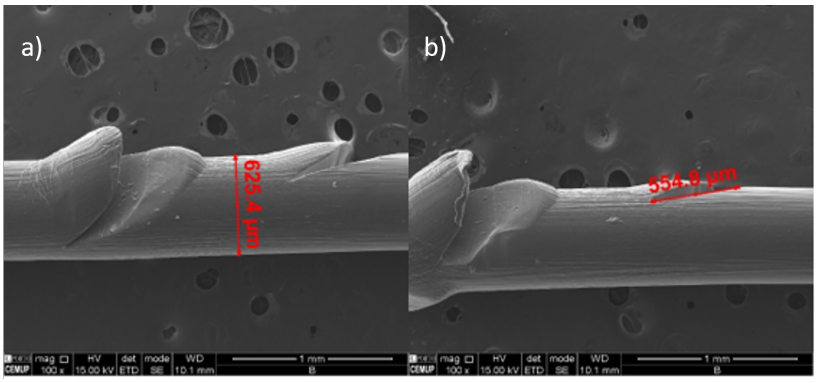

Figure 3.1 PCL cog thread SEM images: a) SEM image with diameter dimension; b) SEM image with cut dimension.

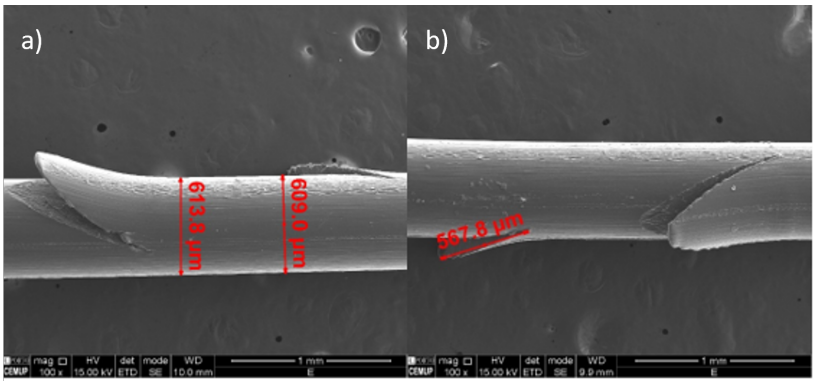

Figure 3.2 PDO cog thread SEM images: a) SEM image with diameter dimension; b) SEM image with cut dimension.

Through the figures obtained, it was possible to take some approximate measurements for future cog suture design. The dimensions taken were thread diameter, cut angle, cut depth, distance between barbs (table 3.2). This dimensions were measured 3 times and the values presented in table 3.2 represent an approximation of the mean of this values.

Table 3.2 PCL and PDO cog thread dimensions from SEM exam.

	PCL	**PDO**
Diameter	$\approx 630\mu m$	$\approx 610\mu m$
Cut angle	$\approx 135^o$	$\approx 155^o$
Cut depth	$\approx 200\mu m$	$\approx 300\mu m$
Distance between barbs	$\approx 1600\mu m$	$\approx 1500\mu m$

Through SEM analysis it was verified that the barbs were offset from each other around the suture by 120 degrees. As will be mentioned in section 3.2, for a first attempt to fabric this type of sutures, it will be chosen to make barbs only on opposite sides of the suture.

3.2 Cog thread manufacturing

As mentioned before, this project aims to develop sutures through MEW, mainly due to the ability of this method to create micrometer filaments. At the same time, it allows the realization of different geometries with the exact diameter dimensions of extruded filaments. Therefore, the laboratory's MEW equipment was utilized to manufacture sutures with the desired final dimensions.

3.2.1 Melt electrowriting device

Over the past two decades, due to an increased interest in electrohydrodynamic processes and the propagation of low cost FDM, new technologies converging AM and electrospinning, such as electrowriting, have been developed [89].

Because the MEW process is not yet fully established and applications are constantly being updated, a substantial number of devices are custom-built in laboratories to fulfil a particular need or application. The MEW prototype used in this project was developed within the "SpinMesh" project [89]. The device was built using an XY moving collecting plate and a Z moving printing head on an aluminium box structure (figure 3.3). The high voltage supply is separated from the equipment, as shown in figure 3.3, with one electrode linked to the collection plate and the other to the nozzle. The equipment design takes all electrostatic discharge (ESD) measures to prevent electrical interference and device malfunction, and all areas isolated from the charged electrode are grounded [89].

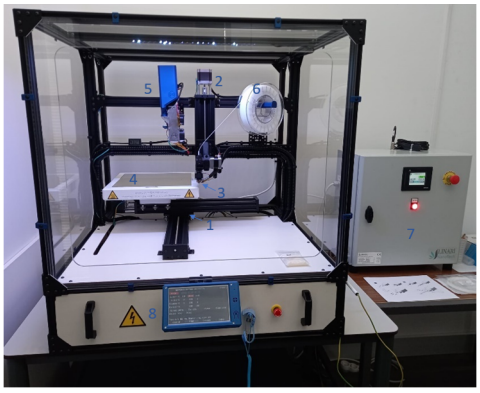

Figure 3.3 MEW prototype:1-XY movement device; 2-Z movement device;3-extrusion and heating devices;4-collector plate;5-pellet support; 6-filament support; 7-high voltage generator; 8-touchscreen LCD.

One of the most crucial components of a MEW device is the controller board responsible for the management of the machine's behaviour by reading inputs (G codes and

status of the equipment) and creating outputs (motion commands for the collector plate, the printing head, the extruder temperature, and position) through electric signals. Of the tens of different controller units available commercially, the *Duet 3D 2.0 Ethernet* is used in this machine. This is a versatile board that allows the use of multiple extruders, a high-performance 32-bit processor, a graphic touchscreen to make the experience more user-friendly, and the ability to monitor the equipment's parameters from a safe distance *via* a computer and heating chamber. When regulating the deposition of fibres on the micron scale, the influence of micro stepping can be substantial. The stepper drivers on the board enable $x256$ micro-stepping, allowing for accurate monitoring of the motor position [89].

Linear actuators powered by stepper motors ensure the motion of the MEW equipment. All the actuators are made of a C-shaped aluminium profile with a stepper motor attached to it that sends motion to a fuse. The collection plate moves in both the X and Y directions since it is mounted on top of each of the linear actuators simultaneously. One of the actuators in a linear actuator system must be moveable. The Y-axis actuator is fixed, while the X-axis actuator is assembled on top of the gantry plate, linked to the Y-axis fuse. This method allows for a clear X-Y movement of the collecting surface. Each actuator has a $500mm$ range of motion. Since the Z axis sole purpose in electrowriting is to establish the tip to collector distance, it is fixed, and the range is narrower, using an actuator of $250mm$ [89].

Analysing the equipment utilized in terms of precision of the movement, a stepper motor (*NEMA 23HM20-0384S*) with 400 steps/revolution is used for each actuator, along with a $2mm$ pitch lead screw with four starting positions. Without considering the interpolations obtained using stepper drivers, the resolution of the movement is $0.02mm$ - $20\mu m$ [89].

One of the requirements for a successful MEW device is the capacity to generate reproducible conditions over time while considering the polymer's uniformity, thus heating and supplying become very important. The installation of a standard polymer extruder on this equipment is owing to the ease of the process. The extrusion is controlled by the same board that controls the movement, and control commands are communicated to the equipment through G-Code. Filament or pellets can be used to power the device. The compatible filament is the standard $1.75mm$ commonly available and is fed by a direct extruder, in this case, the *Bondtech QR* owing to the component's reliability with a dual-gear drive mechanism that decreases the chance of material slipping. Because the material rate directly impacts the amount of material on the Taylor Cone, it is critical that the material volume extruded be meticulously controlled [89].

The heating system comprises a standard FDM hotend set with a heater block heated by a ceramic cartridge. The heating device utilized was an *E3D V6 Hotend*. The dependability and versatility of this specific equipment were important considerations in its selection. The maximum working temperature with the thermistor of 285^oC is one of the

possible limits of the selected item; however, both the board and the heat block are compatible with the installation of a thermocouple or PT100, which enable temperatures up to 400^oC. In order to preserve closeness to traditional FDM devices, this device employs a normal nozzle as a spinneret rather than the typical needles used in MES and MEW systems [89].

The collection surface is a square-shaped aluminium plate with a thickness of $3mm$ and a surface size of $270x270mm$. Because the collecting surface functions as an electrode, it is critical to provide electrical field homogeneity over the whole collection area. Therefore aluminium, a highly electrically conductive metal, was used. An intermediary component with significant electrical resistance was required to provide appropriate insulation between the electrode and the linear actuator that moves the collector. This insulation is especially critical when the collector is charged because it avoids actuator malfunction and user safety. The connection between the moving plate and the intermediate component in the equipment was made possible by a PLA 3D-printed platform screwed to the plate [89].

A $60kV - 150W$ positive high voltage generator serves as the high-voltage source. The device has a minimal output current of $0.01mA$ and communicates with the user *via* a touchscreen LCD or a Web interface. The power supply's safety features include a magnetic switch as an interlock, a grounding dielectric bar, an high voltage "ON" light, a ground distribution bar, and manual input requirements when the machine is turned on. Simultaneously, the grounding wires are attached to various structures to guarantee that the user is not at risk of a high voltage discharge. The high-voltage and grounding connections are suited to the actual mount, but if needed, they may be relocated with minimal modifications, primarily to ensure the electrical insulation on the spinneret [89].

3.2.2 Novel cog thread design

Threads similar to those on the market were manufactured: $120mm$ in length, with a diameter of approximately $600\mu m$. Only $90mm$ of those $120mm$ would have barbs (figure 3.4).

Through the analysis of the existing sutures on the market, it was decided to have a spacing between barbs of $1.5mm$, with the barbs having an offset of 180 degrees. In addition, bidirectional sutures were created, between the two different directions in which the barbs are spaced 10mm apart (figure 3.4).

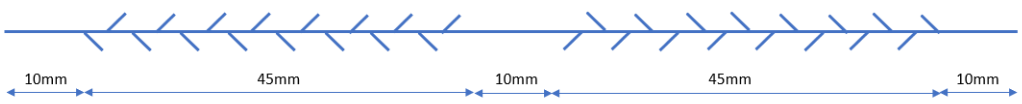

Figure 3.4 Example of the desired geometry.

3.2.3 Suture manufacturing

To print the idealized sutures, it was necessary to develop the specific G Code for the MEW machine to be used and try to improve it, taking into account the results obtained with the previous codes. The first code developed was initially tested in *NCVIEWER* to confirm that it was in agreement with what was initially intended. The result obtained in *NCVIEWER* can be seen in figure 3.5, figure 3.6 and figure 3.7.

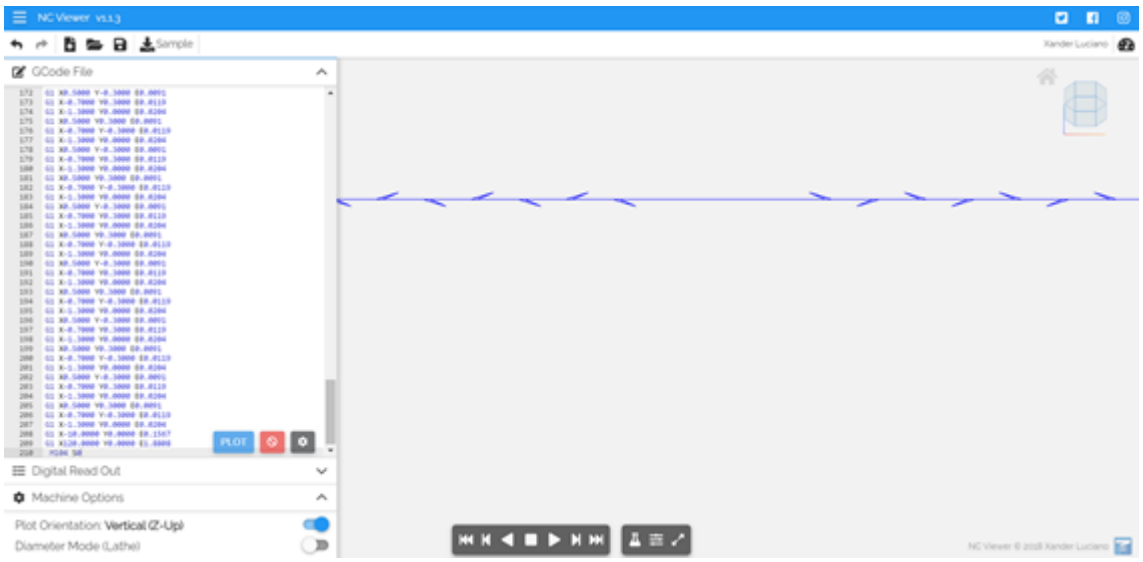

Figure 3.5 *NCVIEWER* G Code simulator 1.

Figure 3.6 *NCVIEWER* G Code simulator 2.

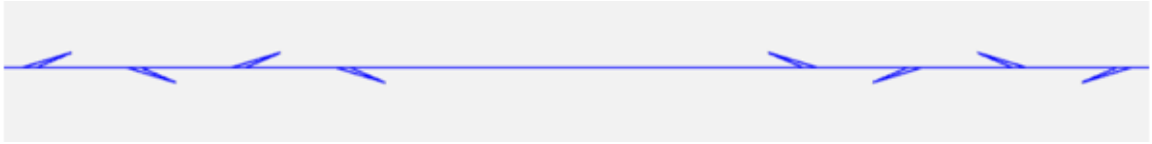

Figure 3.7 *NCVIEWER* G Code simulator 3.

Although the images obtained in *NCVIEWER* seem quite promising, the same did not happen with the first print made with a 400μm nozle. MEW gave rise to several challenges that, despite trying to solve, ended up limiting the manufacture of cog threads. With the

codes performed to create geometries similar to those shown in the previous figures, the printing result can be seen in figure 3.8.

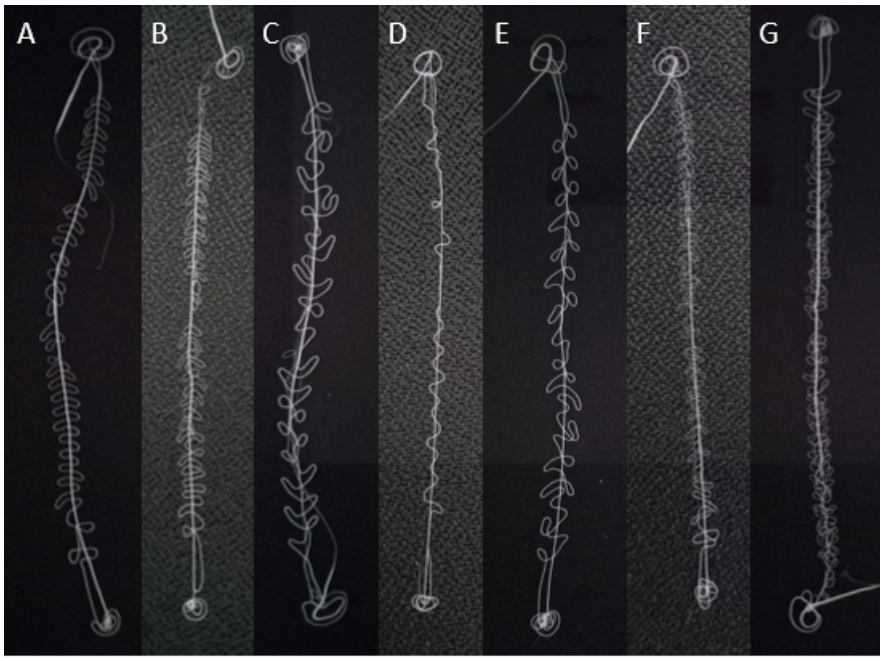

Figure 3.8 Some of the resulting MEW printed sutures: A- suture printed with G code shown in Appendix A; B- suture printed with G code shown in Appendix B; C- suture printed with G code shown in Appendix C; D- suture printed with G code shown in Appendix D; E- suture printed with G code shown in Appendix E; F- suture printed with G code shown in Appendix F; G- suture printed with G code shown in Appendix G.

Although it was impossible to produce the sutures through MEW with the first code developed, as shown in figure 3.8, several attempts were made to change the printing parameters and even the geometry of the sutures to try to obtain something more similar to what was desired [1]. Therefore, changes were made in terms of printing parameters on extrusion temperature, collection plate movement speed, applied tension and amount of extruded material. In terms of geometry, attempts were made to change pitched barbs to horizontal, increase the spacing between barbs, and increase the barbs' size. Although these attempts have been carried out, it has not been possible to obtain sufficiently satisfactory results.

Furthermore, with the same G Code, different geometries were sometimes obtained. These differences may be due to uncontrolled ambient conditions, wrong machine calibration or nozzle displacement accuracy limitation.

[1]The codes used to print the sutures shown in 3.8 can be conferred in appendix A to G.

3.3 Printing and conventional production

As mentioned above, several attempts have been made to produce by MEW the sutures with the desired geometry. Several printing parameters were changed, and the geometry was even altered to test the machine's ability to produce "simpler" sutures.

Since it was not possible to obtain the desired geometries through MEW, the possibility of creating a "suture cutting mechanism" was considered. Thus, the sutures would be printed with the desired diameter through MEW, due to its ability to manufacture microfibers with mixtures of biodegradable materials and for example anti-inflammatory agents, and would then be cut in a created machine.

3.3.1 Continuous filament printing characterization

The machine's nozzle was modified to $600\mu m$ diameter. After placing the $600\mu m$ nozzle, sutures with different parameters were printed in order to try to find the parameters that gave the sutures the best properties and the desired design.

In table 3.3 and figure 3.9 it is possible to see some of the printing parameters and the correspondent printed filaments. The extrusion used is represented in all tables by the *Diameter** since the extrusion was calculated using the equation 3.1 taking in consideration the desired diameter (d) and the length (l) in millimeters.

$$e = \frac{d^2 \cdot l}{1.75^2} \tag{3.1}$$

Table 3.3 Printing parameters 1.

	Sample 1	Sample 2	Sample 3	Sample 4	Sample 5	Sample 6
Diameter* μm	600	575	550	575	550	575
Temperature ^oC	220	220	220	220	220	220
Velocity mm/s	2250	2250	2250	2250	2250	2500
Voltage kV	7.05	7.05	7.05	6.25	6.25	6.25

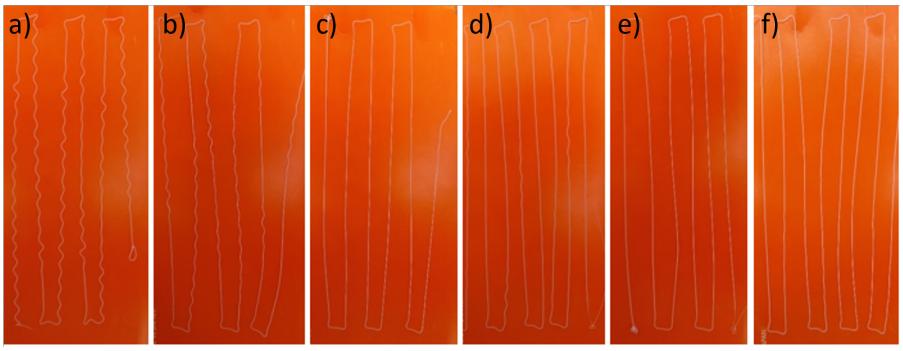

Figure 3.9 Filament printed with different printing parameters: a) sample 1; b) sample 2; c) sample 3; d) sample 4; e) sample 5; f) sample 6

As shown in table 3.3 and figure 3.9, with the parameters initially used it was not possible to obtain filaments with diameters of $575\mu m$ and $600\mu m$. Thus, the parameters were changed in order to understand its influence and to try to obtain filaments with a diameter of $600\mu m$.

Changing only the applied voltage from $7.05kV$ to $6.25kV$, it was not possible to verify the influence of this parameter. Therefore, as can be seen in the last column of table 3.4 and in the last image of figure 3.10, the printing speed was increased from $2250mm/s$ to $2500mm/s$ and it was possible to obtain filaments of $575\mu m$ of diameter with less imperfections. Therefore, the speed was increased again (figure 3.10.

Table 3.4 Printing parameter 2.

	Sample 7	Sample 8	Sample 9	Sample 10	Sample 11
Diameter* μm	500	600	575	600	600
Temperature ^oC	220	220	175	175	175
Velocity mm/s	2750	2750	2750	2750	2750
Voltage kV	6.25	6.25	6.25	6.25	6.25

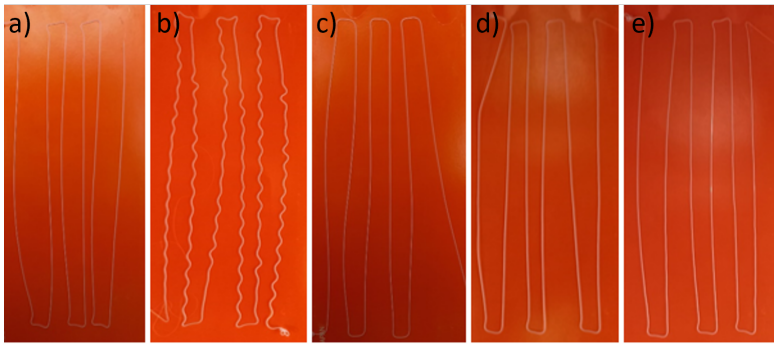

Figure 3.10 Filament printed with different printing parameters: a) sample 7; b) sample 8; c) sample 9; d) sample 10; e) sample 11.

Since it was possible to produce $600\mu m$ diameter fibers, some parameters (voltage, extrusion velocity) were changed again to try to obtain more filaments with the same diameter to test through uniaxial tensile test (TT) to choose the best parameters to print the sutures to be cut later.

From all the filaments printed, the ones from the edges were not used due to the acceleration and deceleration of the printing parameters during the process. The filaments used can be seen in figure 3.11. To assure that the filaments printed had the desired diameter a digital caliper was used and three measurements were done in each filament (one on each side and one on the middle) and similar results to the ones expected were obtained in almost all the printed filaments.

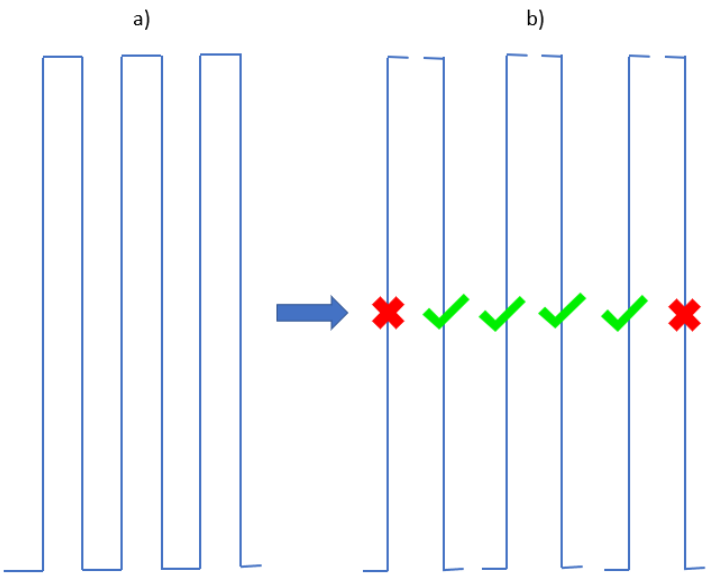

Figure 3.11 Scheme of used filaments: a)Printed filaments; b)used filaments.

Moreover, despite not wanting to create sutures with more than $600\mu m$, it was tried to see the maximum diameter obtained with the $600\mu m$ nozzle and what is the minimum temperature that can be defined so that the printing is viable. After performing some prints during which some printing parameters were changed, it was possible to obtain filaments with $650\mu m$ and the minimum print temperature obtained was 165^oC.

3.3.2 Cutting adaptor

To create the cogs on the threads, it was necessary to develop a filament cutting mechanism. Therefore, the *Multitest 2.5-dV*, already used in this work to perform the uniaxial tensile tests, was adapted to create a cutting machine. The test machine was chosen because it already has an elevating mechanism and a load cell that better monitors the cutting movement without additional costs. Therefore, two fundamental parts were developed to adapt the existing machine: the filament support and the upper part responsible for cutting.

3.3.2.1 Filament support

The idealization of the filament support to carry out the cut started with the fitting part of the filament's support in the *Multitest 2.5-dV*. Therefore, based on the dimensions of the supports of the existing parts in the laboratory, a 3D model was created in *SolidWorks* (figure 3.12). The model was printed to verify if the chosen dimensions allowed the perfect fit.

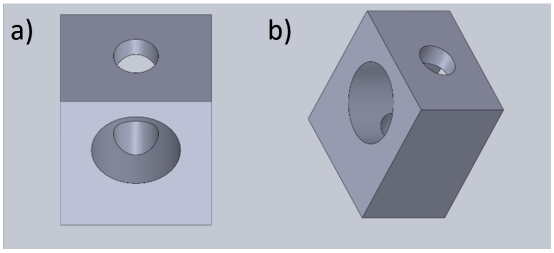

Figure 3.12 Perspective views of cutting machine adaptation *SolidWorks* initial model: a) inclined lateral view; b) inclined top view.

Some corrections were necessary, namely in the support height and holes diameters (mainly due to the uncertainty associated with the 3D printing machine). Therefore, all holes had to be increased by $0.2mm$ in diameter and the final dimensions of the piece are displayed in figure 3.13.

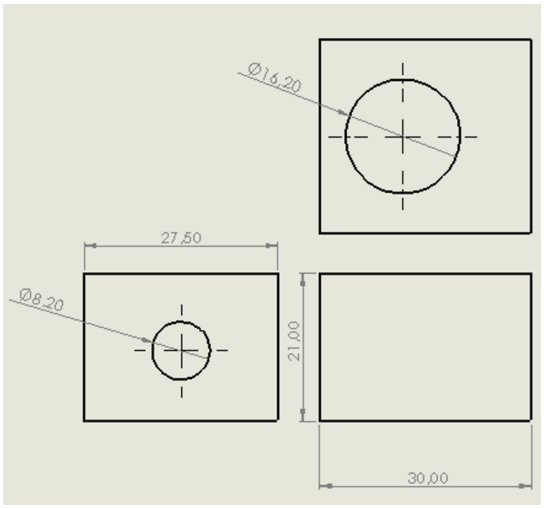

Figure 3.13 Cutting support adaptation final dimensions.

After defining the dimensions of this support, a plate where the filament will rest was added. Since the intention is to obtain 180^o slots in 180^o with a spacing between them of about 1.5mm, the creation of a filament stabilizer was considered to rotate the filament 180^o and to make this undoing of 1.5mm between the grooves on one side with the grooves on the other. The final piece can be seen in figure 3.14.

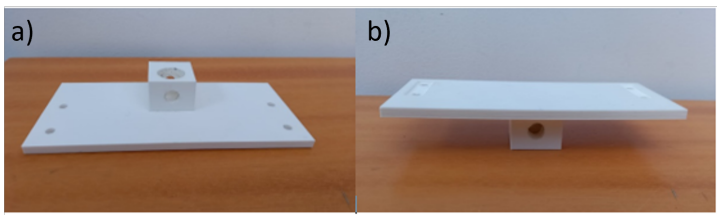

Figure 3.14 Printed final filament support piece: a) inclined top view; b) inclined front view.

Considering the possible use of these printed PLA models to create metal components, it is necessary to think of a way to optimize the material, since if these parts are made through machining, there is a lot of wasted material that could be decreased. Therefore, the connecting piece to the testing machine could be made separately and subsequently screwed to the filament support plate, as long as the placement of the screws does not harm the surface used for supporting and cutting the filament.

In addition, the dimensions of the models created in *SolidWorks* were defined in case the parts were printed on *Prusa* 3D printers existing in the laboratory where this work was carried out.

3.3.2.2 Cutting part

Prototypes of parts were created to put in the machine to carry out the cut. The first attempt had as an idealization the supports of scalpels. In this prototype, the upper plate of the machine was made up of several blade supports equal to those of traditional scalpels. Therefore, the model was composed of a part that connected to the *Multitest 2.5 dV* device, similar to the one created to support the filament; of several small holders for the blades identical to those found in traditional scalpels; and of one part to ensure the joining of the other parts, as shown in Figure 3.15.

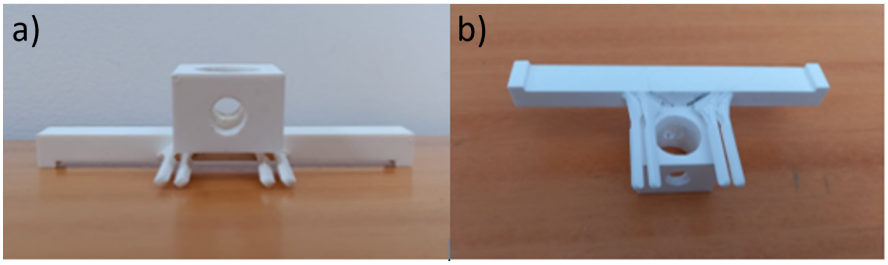

Figure 3.15 First cutting prototype: a) inclined front view; b) inclined top view.

In addition to the difficulty of placing the blades in their places, it would be very challenging to manufacture through machining. In this way, a more practical approach was thought for both the use and the manufacture of this piece. It was then considered the construction of a rigid support with several grooves to place the blades.

Regarding the angles used for the grooves, in addition to the geometry of the cogged threads already commercialized (Table 3.2), some existing research content was also used to decide the best cutting angle. In order to understand the advantages of using an upper or lower cutting inclination, two models were created with different inclinations, one was between 140^o and 175^o (as advised in [53]) and the other did not. The cutting angles were 150^o and 130^o. In figure 3.16 it is possible to visualize one of the created models of the final cutting parts.

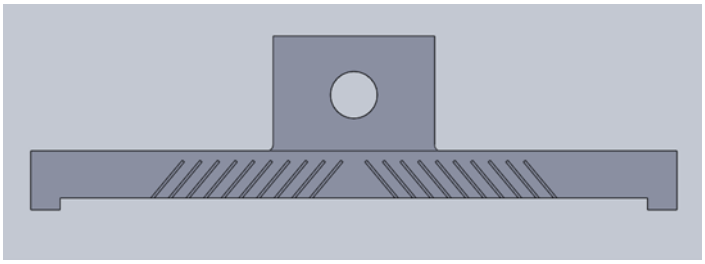

Figure 3.16 *SolidWorks* model of cutting part with 130^o cutting angle.

The *SolidWorks* models were created considering the usual thickness of the blades, the type of support of the piece, and the cutting dimensions that were intended to be obtained, namely cutting distance and cutting angle. To control the path of the blades, a kind of flap was also created (based on the blade dimensions, the desired depth of cut, and the inclination of the blades) to ensure that the depth of cut was the desired one. Both models were printed, and the result is showed in figure 3.17.

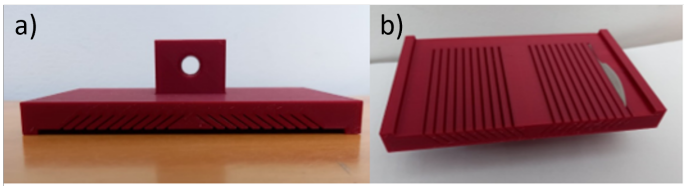

Figure 3.17 Printed final cutting parts: a) front view; b) inclined top view.

3.3.2.3 Cutting device assembly

Placing the printed pieces shown in figure 3.14 and in figure 3.17 in the *Multitest 2.5dV* machine, the final set shown in figure 3.18 was obtained.

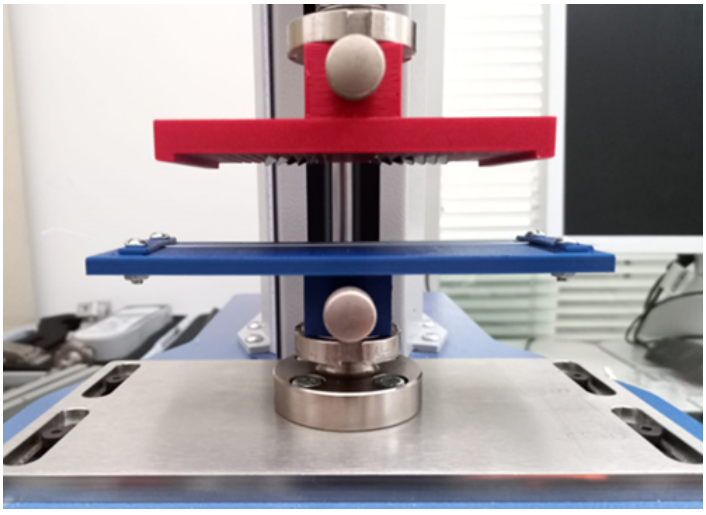

Figure 3.18 Cutting machine prototype.

This first model created has several limitations found while cutting the sutures, some of which could not be solved during this work for various reasons. Those difficulties will be exposed a little later in this report.

3.3.2.4 Cutting procedure

The cutting procedure was changed throughout the cutting attempts made due to some difficulties encountered during the process. One of the main problems faced was the type of blades used. In the first attempts to use the cutting model (figure 3.18), *paragon N.24* scalpel blades were placed. These blades seemed appropriate since they can be purchased in individual sachets and come sterilized. However, their geometry makes the entire cutting process difficult as it presents a curvature in the part that makes the cut. Therefore, blades with a straight geometry were used to simplify the filament placement on the cutting table and ensure that the cut is carried out on it.

The second problem found was due to the flaps. Contrary to what was expected, the flaps did not have the intended function, because the blades were not able to make the cuts with the desired depth when the flaps touched the filament support base. Thereafter, a new problem appeared due to the relative position of the flaps and the place where the displacement/force is applied to the cutting piece. The displacement/force is applied in the center of the cutting piece and the flaps were placed in its corners. Since the part was made of a polymer (easily deformable), when the flaps met the support the cuts in the middle were deeper than the ones in the corners. This problem was solved when the blades were changed, because the rectangular blades were relatively taller than the ones previously used.

Although the flaps had lost their effect, the difference between the cuts from the centre of the plate to the edges continued to be verified. This is due to the relative position of the displacement/force application and the blades. This was one of the problems that remained throughout the entirety of the thesis, as was the need to perform the cuts on the opposite sides at different heights due to the difficulty of ensuring that the blades on both sides were completely levelled. There are several possibilities for the existence of this difficulty: inability to ensure parallelism the upper and lower parts; the uncertainty regarding the impression of the 3D printer; and the difficulty of, with the placement of the blades one by one by hand, ensuring that the blades were all in the same position.

Although this last problem has not been solved, it will be remedied by making the cuts with only one side of the created piece (figure 3.19), forcing to spend more time to make the cuts but ensuring the possibility of cutting one side without breaking the filament on the opposite side.

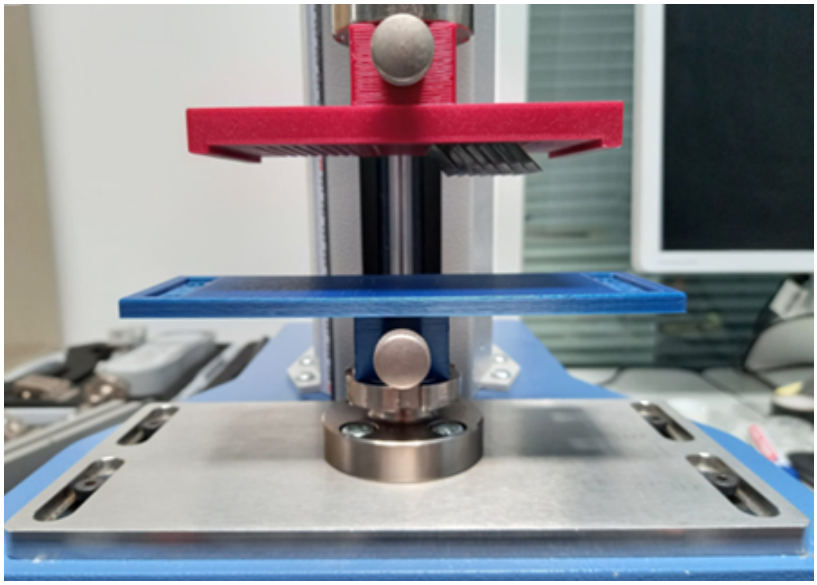

Figure 3.19 Cutting machine with rectangular blades on one side only.

During filament cuttings, the procedure followed the next steps:

1. Place the lower and upper part of the set and ensure that the blades are placed on only one side (figure 3.20).

2. Lower the upper part and with the help of the load cell set the machine's zero position (origin) when both parts come into contact (matter of visualization simplicity) (figure 3.20).

3. Secure the filament, ensuring that the pieces guaranteeing its fixation are both fully introduced to one side (in this case, the right side) and that the filament is fully stretched.

4. Set program parameters (downward direction; descent velocity: 10mm/min) (figure 3.20).

5. Lower the top "by hand" to a distance close to the origin defined in point 2.

6. Start the program and stop it when the desired power is reached ($\approx -25N$).

7. Raise the top piece to a reasonable height that allows the blades or filament to be maneuvered without incident.

8. Rotate the blade holder outwards to ensure the blades are positioned on the opposite side (figure 3.20).

9. Repeat steps 5, 6, and 7 (Figure 28).

10. Rotate and fix the filament by turning the parts that hold it together and ensure that both parts are brought to the opposite side where they were placed in step 3 (left side).
11. Repeat steps 5, 6, 7, 8, and 9.
12. Remove the cut filament.

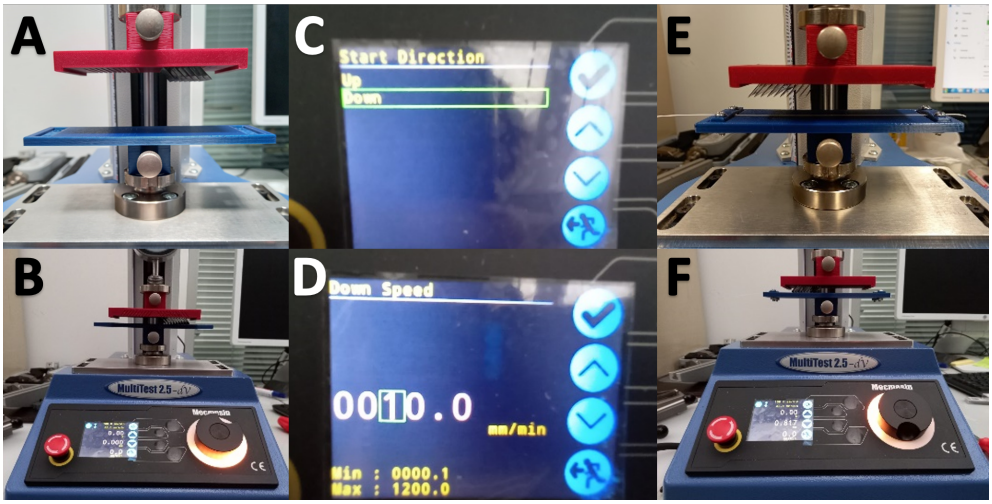

Figure 3.20 Graphic representations of steps: A step 1; B step 2; C step 4; D step 8; E and F step 9.

All parameters presented in the previous steps, namely cutting velocity and stopping force, were defined after carrying out some superficial tests and without great scientific rigor due to the difficulty of accessing the necessary material, so the influence of these parameters should be better analysed. Furthermore, the fixation of the filament to the pieces that ensured the possibility of it controlled rotation was carried out with the aid of a glue to ensure that the filament did not move more than desired. Moreover, it might be necessary to consider using glue or resin to ensure that the blades remain in place.

3.4 Novel cog thread characterization

Having already defined the printing parameters, the prototype of the cutting machine created, and the process of using it carried out, the steps presented in the section 3.3.2.4 were carried out both with the upper support with more cutting inclination and with less and with the printed filaments. The resulting filaments were further analysed.

On a visual level, it was easy to see that the cuts were not successfully done. This can be due to, among other factors, the fact that only the horizontal movement was used to carry out the cut, the cutting velocity was too slow, or also the blades were not sharp enough. Some marks did not seem to be effective cuts but relatively small saliences in the place where the cuts should be.

As the result, it was not what was intended; it was impossible to guarantee the filaments' fixation in tissues through the "barbs" created. Therefore, at the level of tests carried out subsequently, only the TT of the filament was considered, and the others in which the filaments were integrated into animal tissue were not carried out.

3.5 Animal tissue tested

This project involves *ex vivo* studies. The sow' pelvic tissues were acquired at the slaughterhouse *Matadouro Carneiro e Salgueirinho Lda*, NCV D 13, located in Trofa, for research purposes and all the procedures respected the conditions imposed by Regulation (EC) No. 1069/2009 of 21st October.

3.6 Mechanical tests

Understanding the failure properties of the implant material and comparing the mechanical properties of different designs of similar products permits a more knowledgeable decision and allows to find the path towards the development of a better-suited solution. Since vaginal tissue is an anisotropic, biaxial and multiaxial examination of the tissue may offer more specific information on the mechanical behaviour of the tissue. However, due to limited material dimensions, researchers are frequently forced to perform uniaxial testing [98]. In this thesis, it was decided to test the influence of the different sutures when applied on pig's vaginal tissue using TT and ball burst (BB) test.

3.6.1 Uniaxial tensile test

TT is widely accepted as the primary approach for studying material behaviour. To assure quality, tensile characteristics are typically mentioned in material specifications. Finally, tensile characteristics are frequently utilized to anticipate a material's behaviour under more complicated loading circumstances. With uniaxial tensile testing, the filament stiffness is evaluated [99, 100].

The uniaxial tensile tests were performed on the *Multitest 2.5 dV* machine. All the tensile tests were carried out by applying longitudinal axial load. The tested materials were held by the two clamps shown in figure 3.21, and each sample was pre-loaded till $0.1N$ to remove slack from the tissue. To carry out the tests, a $100N$ load cell was used, and a movement velocity of $10mm/min$ was defined [100, 101] (Jones et al., 2009; Rita Rynkevic et al., 2019).

At the beginning of each test, with the clamps leaning against each other on the machine, the machine was reset to place the filament/suture and know its initial length. After extracting this value, the distance marker was reset again to start the test.

Figure 3.21 Machine set up to uniaxial tensile tests.

3.6.2 Pulling test

Although the intended results were not obtained with the printed and cut filaments, the intended tests were continued with the commercial cog threads. In the following tests, only the PCL commercial sutures were used, since they are from the same material as the printed filaments.

For the next tests, sow's vaginal tissue obtained in butchery was used to understand the functioning of cog threads when introduced into the vaginal tissue of an animal. The first test was designed to determine how much pressure was required to completely loosen the thread if it were inserted into the sow's vaginal tissue. Thus, three sutures were placed in the pig's vaginal tissue using a needle and a proper cannula, leaving one end of the tissue unstitched. In these studies, the animal tissue was connected to the superior clamp, while the threads were clamped to the inferior one (figure 3.22).

Figure 3.22 Ex vivo uniaxial tensile testing set up.

The starting length was not measured in this sort of test. As previously stated, the velocity utilized was $10mm/min$, and the experiments were ended when the thread was fully removed from the animal tissue.

3.6.3 Ball burst test

In contrast to the TT, where the load or deformation is applied in-plane to the specimen, in the BB test an orthogonal load is applied to the central portion of the tissue specimen (figure 3.23). Therefore, while the TT provides valuable data about the directional mechanical properties of the tested tissue, the BB test can provide data about the multiaxial mechanical properties of the whole tissue structure [98].

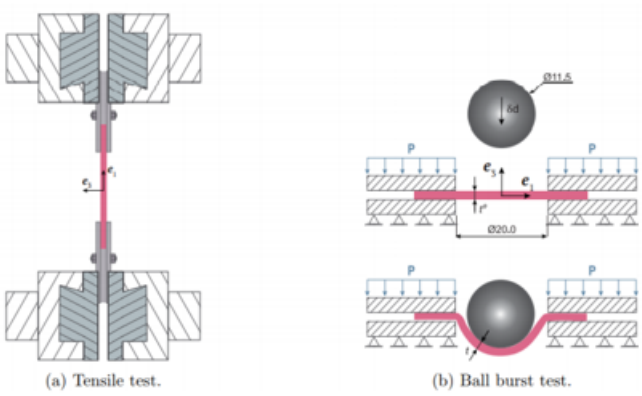

(a) Tensile test. (b) Ball burst test.

Figure 3.23 TT and BB experimental set up [98].

Spherical indentation (BB) test, typically used in the textile industry, is performed to discover the busting strength (the force or pressure needed to rupture the specimen by distending it with force applied at right angles to the plane of the specimen under stipulated conditions) of tissues [102].

The BB test determines the failure properties of a material when subjected to biaxial loads. Therefore it has been used to characterize the multi-axial material properties [102]. With this test, it is possible to obtain force *vs.* displacement curves, but, by itself, it does not provide any information on the intrinsic properties (properties that provide a complete characterization of the material's mechanical properties that are necessary for design and strength analysis purposes) of the test specimen [102].

Although the BB test due to bending and finite thickness effects does not allow the characterization of stress, it gives an indirect measurement of the material strength that will be used to compare the different sutures analysed in this report [98].

3.6.3.1 Ball burst device

As there is no laboratory access to a BB machine, it was decided to develop at least one prototype in which it would be possible to develop the idealized tests. Therefore, applying

some concepts shown in the existing literature, a prototype of a BB machine was designed and printed. The design of the developed parts was very similar to some designs found in the literature, as shown in figure 3.24; however, some parts were modified in order to simplify geometries and ensure that it was possible to carry out the tests with the model printed in PLA [103].

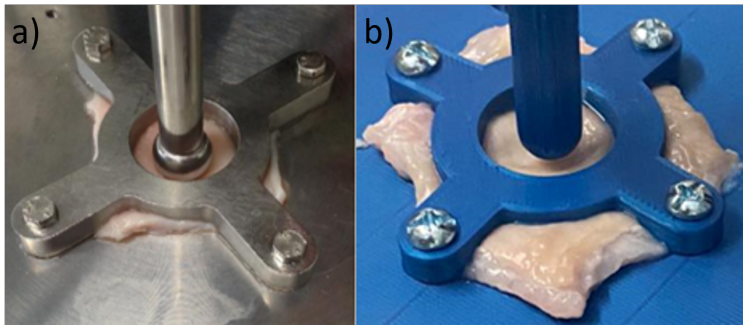

Figure 3.24 BB machine found in literature and BB developed prototype [103].

This new support started by developing a method of fixing the ball burst support parts to the *Mutitest 2.5 dV* machine. Therefore, the support created in the cutting machine section was adapted for the upper part of the mechanism (figure 3.25). The dimensions used for the column's height and diameter were based on the dimensions and distances made in previous studies [103, 98]. Therefore, the chosen diameter for the tip was $9.5mm$ and the height was $50mm$.

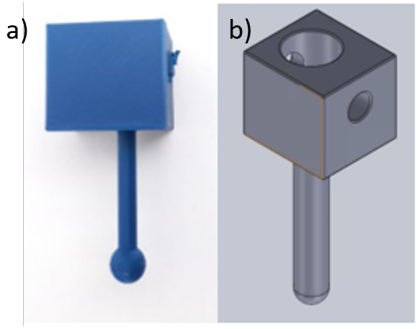

Figure 3.25 Superior part of BB test machine prototypes: a) first printed prototype; b) second *SolidWorks model* prototype.

As shown in figure 3.25, first a piece was created, like the one previously seen in the literature, but due to its fragility, it was adapted so that the test would not be compromised, but if it could guarantee the integrity of the part [103].

For the lower part, to ensure greater stability, it was preferred to create a part that would contact the base of the machine *Mutites 2.5 dV*, as shown in figure 3.26.

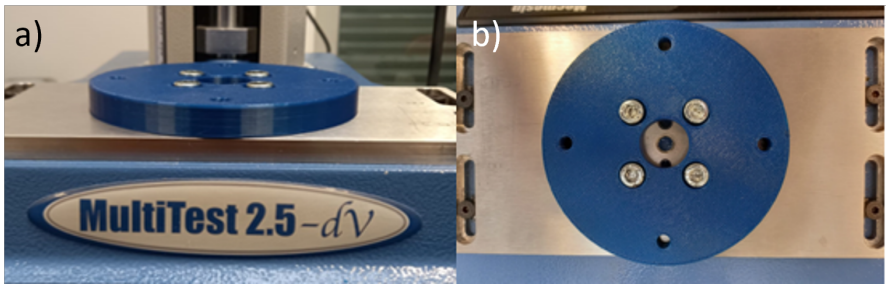

Figure 3.26 BB machine inferior support: a) inclined front view; b) top view.

Although the upper platform has a similar geometry to the lower one, a recess had to be added to aid a smaller piece (figure 3.29) to ensure that the tissue tested remains completely tied in. Therefore, the geometry of the upper platform can be seen in figure 3.27.

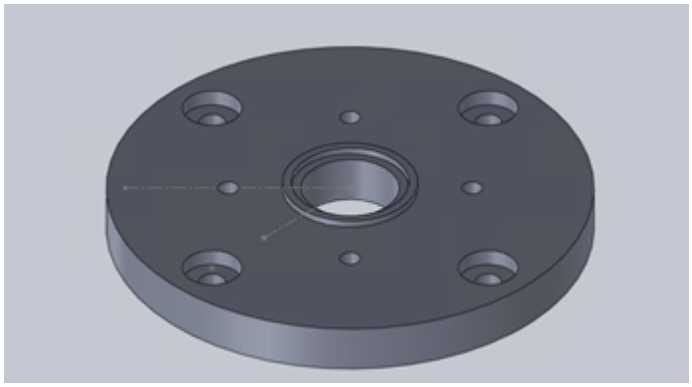

Figure 3.27 *SolidWorks* model of superior platform.

To connect the two platforms, four cylindrical supports with $50mm$ height and $15mm$ of diameter (figure 3.28) were created. These dimensions were established to ensure stiffness and the possibility of carrying out tests where $50mm$ in distance is achieved. To secure all these parts, M5 screws were used.

Figure 3.28 *SolidWorks* model of cylindrical supports.

All dimensions of the part that holds the specimens shown in figure 3.29 were approximations of dimensions taken from images of BB supports.

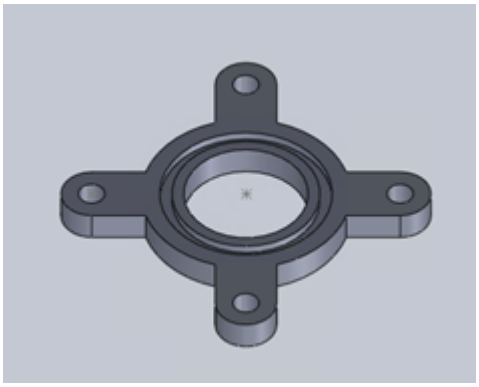

Figure 3.29 *SolidWorks* model of tissue holder.

After creating the *SolidWorks* model of all parts, they were printed on the *Prusa 3D* printer, and the set shown in figure 3.18 was obtained.

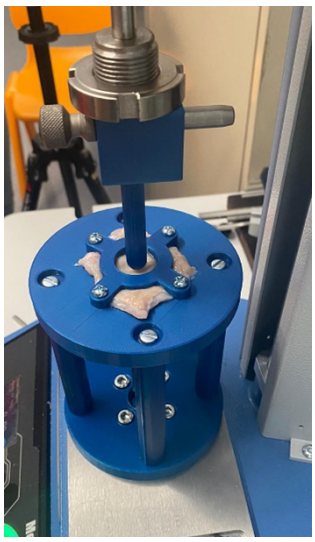

Figure 3.30 BB machine assembly.

As mentioned before, some parts' dimensions were increased in order to make the machine more robust since PLA is not as resistant as metal. For example, if metal parts were to be used, cylindrical supports could be less in number and thinner, and M3 screws could be easily used. In case to make this prototype real, some changes in dimensions must be carried out.

3.6.3.2 Ball burst method

The BB machine model created in *SolidWorks* and printed in PLA was used to perform this test. The parts relating to the set were assembled on the machine (figure 3.31) and a program with a descending speed of $10mm/min$ was defined.

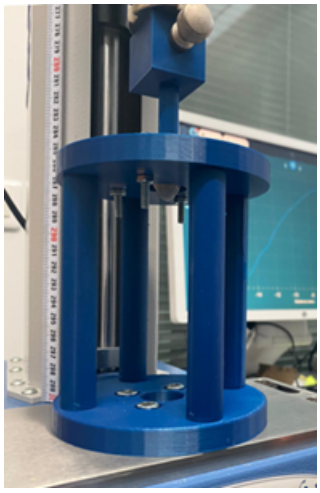

Figure 3.31 BB set up.

Since this vaginal canal might be 100mm long and its characteristics vary throughout that length, it was required to evaluate the performance of animal tissue with and without sutures in the same depth zone of the vaginal canal. As a result, each sample with a suture corresponds to a sample without a suture collected from the same region of the sow's vaginal canal. The threads were inserted into the vaginal tissue using a suitable needle and cannula. Because the goal of the BB test is to perform a multiaxial test, two threads were inserted at an angle of about 90 degrees between them in each sample with the thread examined (figure 3.32). Furthermore, it was ensured that all samples were properly secured, and the samples with threads were placed with the crossover point of the threads in the centre of the testing machine.

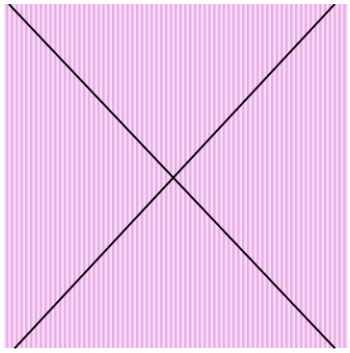

Figure 3.32 Example of insertion of sutures in samples with thread.

This page was intentionally left blank.

Chapter 4

Results and Discussion

This chapter describes the preparations for all of the tests done (TT, pulling test and BB test) as well as the data collected, along with brief comments on them.

4.1 Uniaxial tensile test

4.1.1 Commercial cog thread

The uniaxial tensile test was performed to analyse the mechanical properties of the commercial cogged threads. Four specimens of each suture type were used. The commercial suture was placed in the test machine to carry out the test, and each clamp held each end of the suture. Figure 4.1 shows the sutures correctly placed in the tensile testing machine before (a and b) and after (c and d) their rupture.

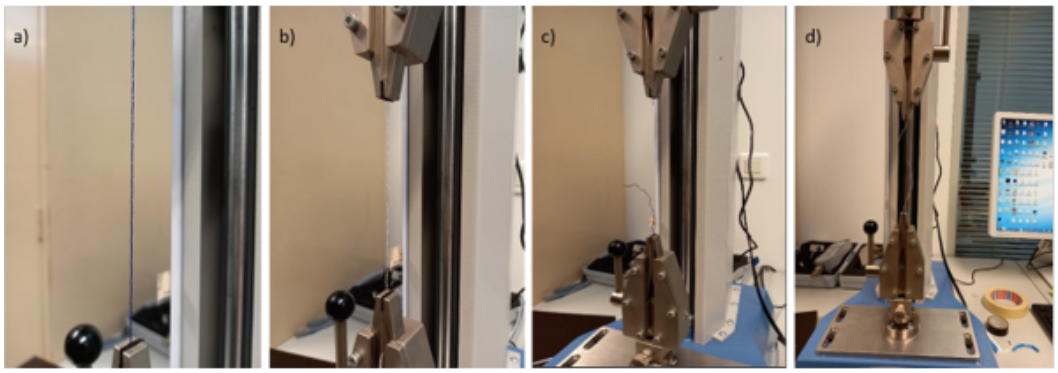

Figure 4.1 Sutures placed in Tensile Test machine: a) PDO before rupture; b) PCL before rupture; c) PDO after rupture; d) PCL after rupture.

As previously mentioned, the velocity used was $10mm/min$ in these tests, and the test was stopped when the cogged thread broke. Each sample's initial length was measured, and the load vs. relative elongation curve (length variation divided by the initial length) was drawn and analysed, as can be seen in figure 4.2.

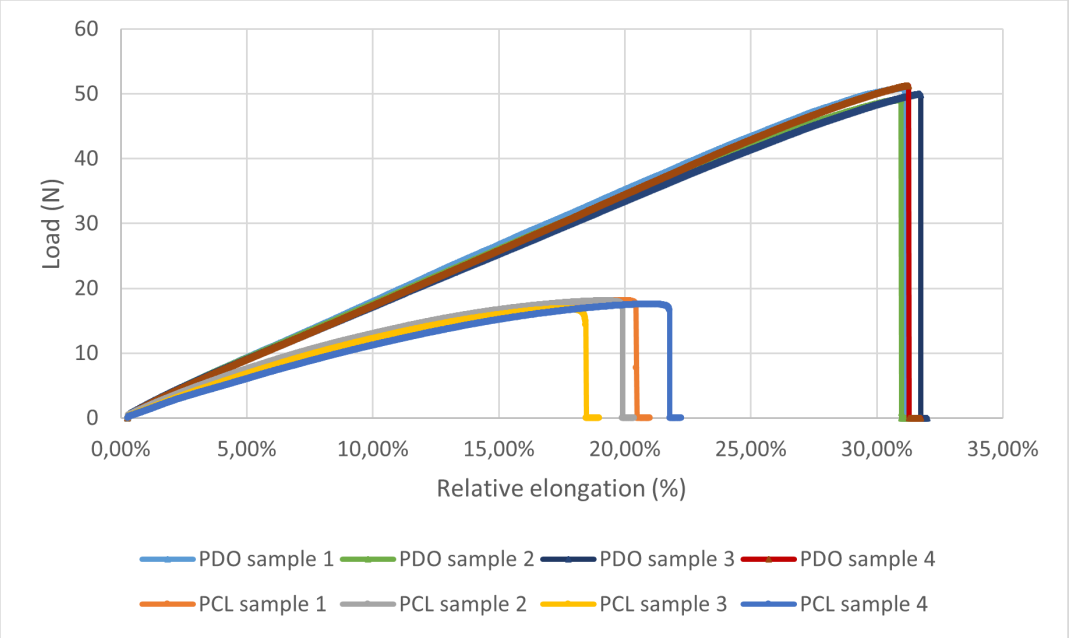

Figure 4.2 Load vs relative elongation of PCL and PDO cog thread samples – TT.

As shown in figure 4.2, PDO threads are more resistant to deformation imposed on them (approximately 30% maximum relative elongation for a load of approximately $20N$) than PCL threads (approximately 20% maximum relative elongation for a load of approximately $50N$). It is also observed that before the samples broke, there was a short period of plastic deformation, so most of the deformation that occurred appears to be elastic (restorable). Figure 4.3 shows some of the permanent defects that the PCL (figure 4.3 A) and PDO (figure 4.3 B) cog threads had after the TT. These images were obtained through do SEM exam.

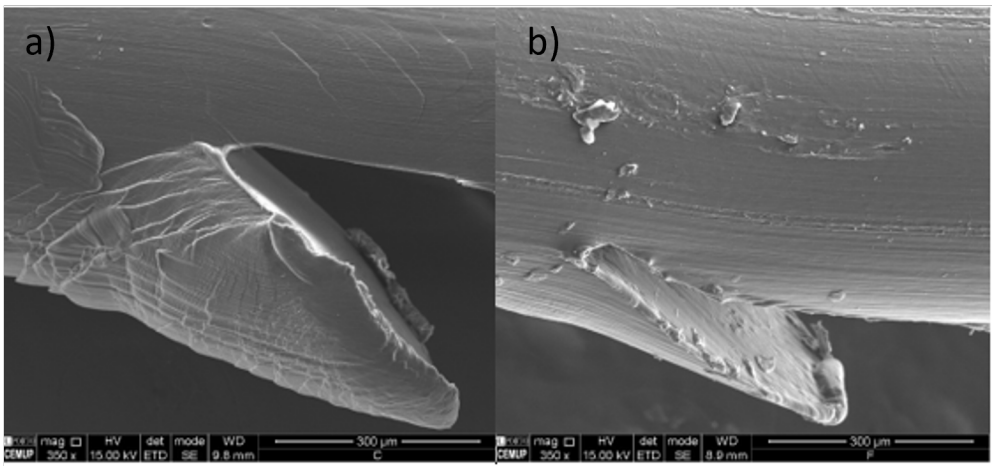

Figure 4.3 PCL and PDO cogged thread TT permanent defects - SEM exam: a) PCL; b) PDO.

4.1.2 Printed filament

It was chosen to examine the effects of table movement velocity, applied tension, and extrusion temperature using the printed filaments. As a result, four samples were subjected to uniaxial tensile testing for each combination of printing settings. The diameter of the tested filaments was $600\mu m$. Parameter combinations are shown in table 4.1 to simplify naming throughout the report. The filament was placed in the test machine to carry out the test, like in the commercial cogged thread tests. In these tests the velocity used was $10mm/min$, as previously mentioned, and the tests were stopped when length variation reached out $100mm$. The tests were stopped at this point because it seemed like an adequate distance as the average linear length of the vagina was $62.7mm$ with a relatively large range (40.8–$95mm$) [104].

Table 4.1 Filament printing parameter combinations.

	Velocity (mm/min)	**Temperature (^oC)**	**Voltage (kV)**
Combination 1	2250	175	6.25
Combination 2	2250	175	7.05
Combination 3	2750	175	6.25
Combination 4	2750	175	7.05
Combination 5	2750	200	6.25
Combination 6	2750	200	7.05

Each sample's initial length was measured and the load vs. relative elongation curve was also drawn and analysed in this case, as it can be seen in figure 4.4 to figure 4.9.

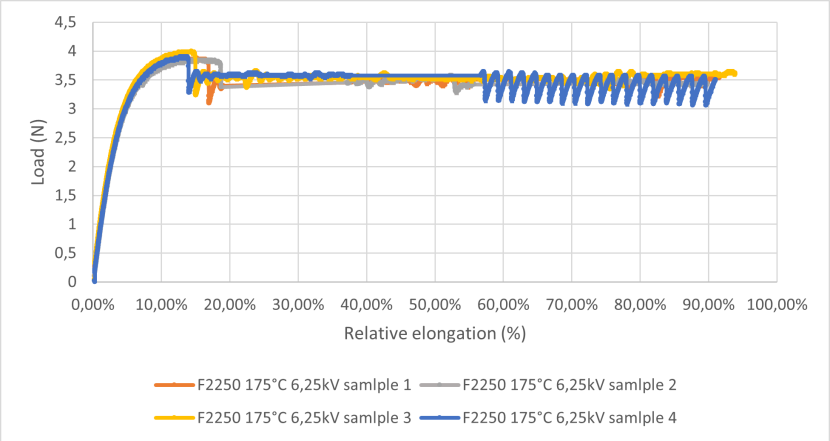

Figure 4.4 Load vs relative elongation of PCL printed filaments combination 1 – TT.

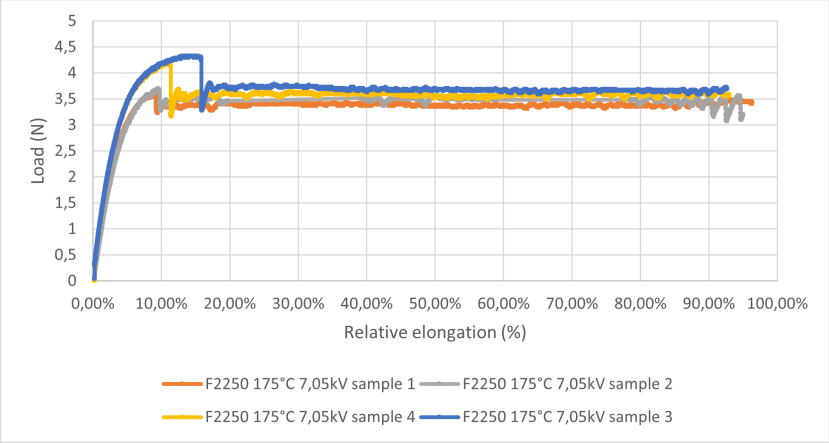

Figure 4.5 Load vs relative elongation of PCL printed filaments combination 2 – TT.

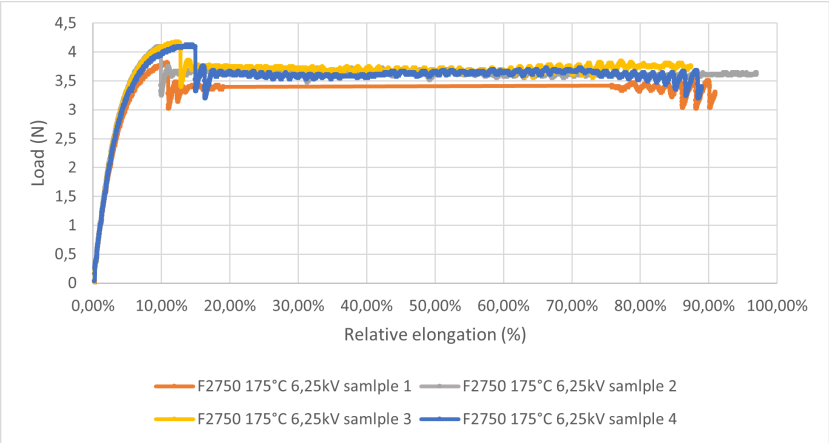

Figure 4.6 Load vs relative elongation of PCL printed filaments combination 3 – TT.

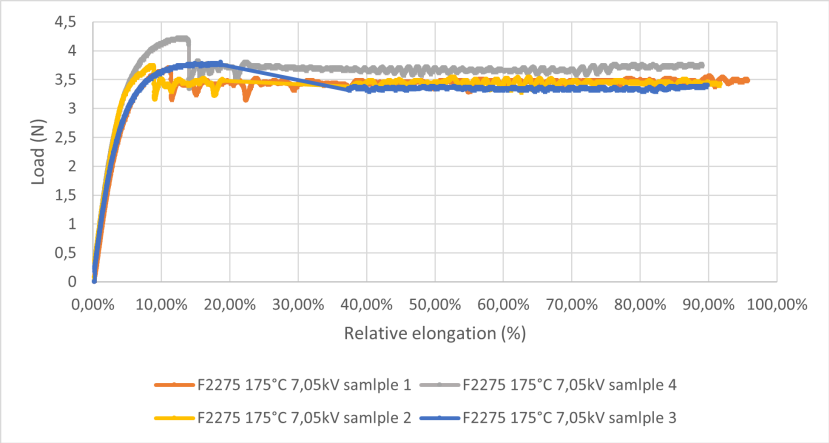

Figure 4.7 Load vs relative elongation of PCL printed filaments combination 4 – TT.

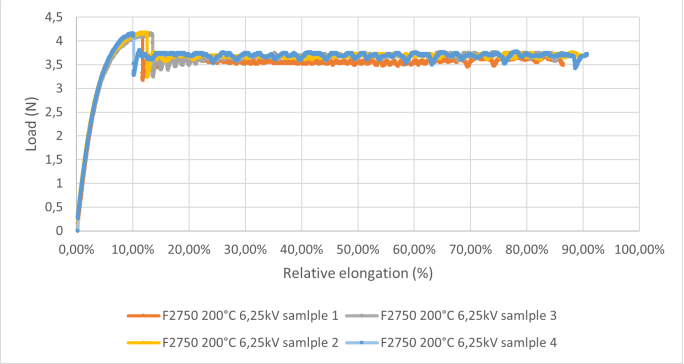

Figure 4.8 Load vs relative elongation of PCL printed filaments combination 5 – TT.

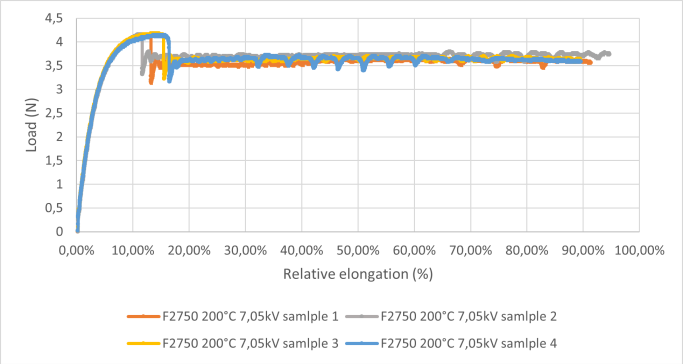

Figure 4.9 Load vs relative elongation of PCL printed filaments combination 6 – TT.

Analysis of the curves, drawn from the data obtained during the TT, showed that there is a first break in the applied load in all curves followed by a few more minor breaks until reaching $100mm$ of elongation. This first break is related to the effect that can be seen in figure 4.10. In other words, when this load reduction was graphically visualized, the alteration in the filament presented in figure 4.10 was also visible.

Figure 4.10 PCL printed filament response to uniaxial tensile test.

Furthermore, it is necessary to bear in mind that the findings obtained have a slight reliance on the time elapsed between printing the filaments and doing experiments with them. It was feasible to verify this since some samples were analysed on the day of printing while others were only analysed the next day (table 4.2), and it was graphically demonstrated that there is a slight variation in the findings obtained. If the uniaxial test is performed on the day after the filament is printed, the maximum load supported by it is greater than if the test is performed on printing day.

Table 4.2 Association of samples with their testing day.

Print day	Comb.1 All samples	Comb.2 Sample 1, 2	Comb.3 Sample 1	Comb.4 Sample 1, 2, 3	
Next day	Comb.2 Sample 3, 4	Comb.3 Sample 2, 3, 4	Comb.4 Sample 4	Comb.5 All samples	Comb.6 All samples

To make the study of the data easier, the visuals produced from the samples tested under identical conditions were compared. As there are many samples for each day and the results observed with samples of the same combination with tests performed under the same conditions are very similar, just one sample of each combination with a given test condition was used to create the graphics. The graphs obtained can be seen in figure 4.11 and figure 4.12, printing day and day after printing day, respectively.

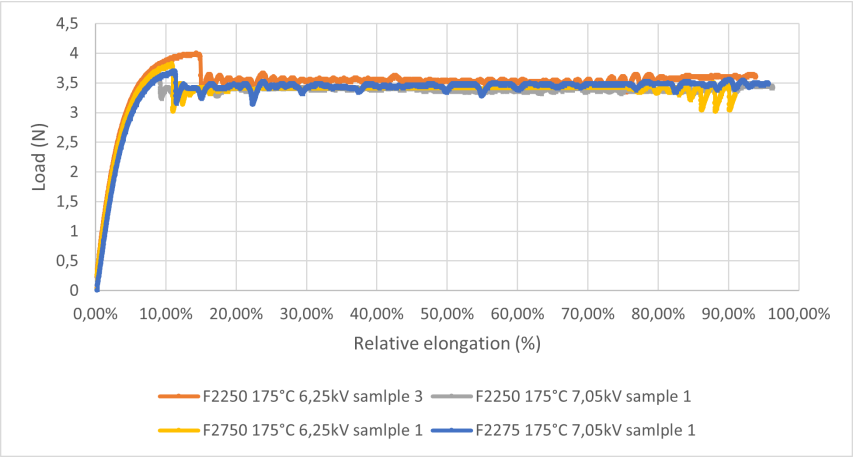

Figure 4.11 Load vs relative elongation of PCL printed filaments tested on the printing day – uniaxial tensile test.

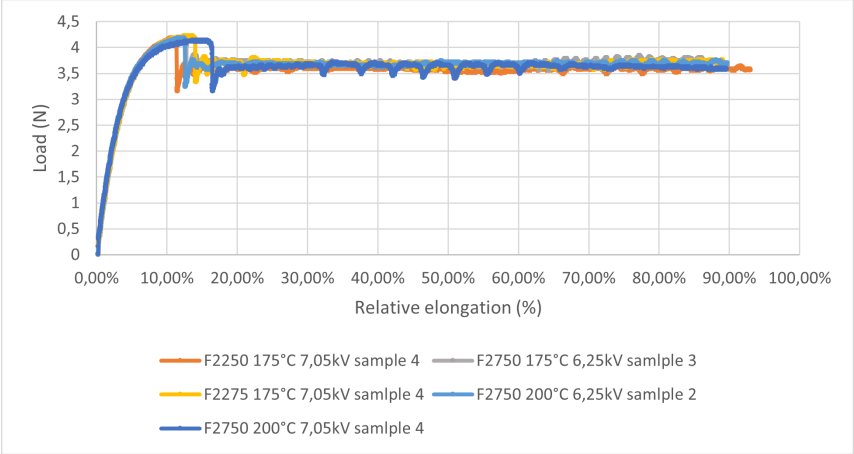

Figure 4.12 Load vs relative elongation of PCL printed filaments tested on the day after the printing day – uniaxial tensile test.

Due to the results presented in figure 4.11 and figure 4.12, it was considered that $6.25kV$ would be an adequate voltage to create filaments with better mechanical properties, as some literature suggested [89]. Furthermore, it was chosen to utilize a temperature of 175^oC since 200^oC is quite near the thermal degradation temperature of PCL, which might indicate adverse changes in the material's characteristics. Regarding the collecting table speed, it was decided to keep testing both velocities (2250 and $2750mm/min$) because no significant difference was detected in filaments with both velocities.

4.1.3 Printed and cut filament

Considering the results obtained in the previous subsection, several $600\mu m$ diameter filaments were printed, with an extrusion temperature of 175^oC and an apex voltage of $6.25kV$. Following that, these filaments were cut using the methods outlined in the cutting machine section, and additional TT were performed to understand the cuts' impact and the cutting angles (130^o or 150^o) made, as well as the capacity to do them carefully.

Four samples were subjected to uniaxial tensile testing for each cutting angle and velocity combination. The cut filament was inserted in the test machine, the same as the commercial cog thread and printed filament testing. As previously stated, the velocity utilized in these experiments was 10mm/min, and the tests were ended when the length variation reached $100mm$, or the filament broke. In this example, the starting length of each sample was determined, and the load vs. relative elongation curve was also drawn and analysed, as shown in figure 4.13 and figure 4.14.

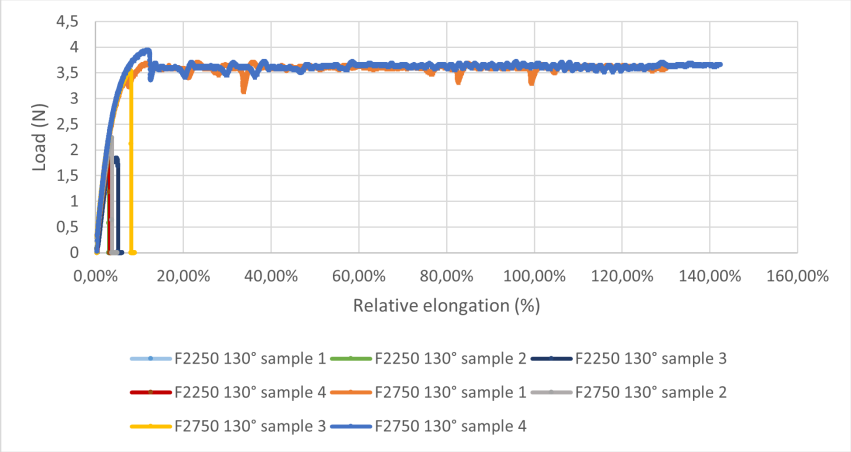

Figure 4.13 Load vs relative elongation of PCL cut filaments with 130^o - uniaxial tensile test.

Figure 4.14 Load vs relative elongation of PCL cut filaments with 150^o - uniaxial tensile test.

The curves produced in these tests appear to be a mix of commercial cogged thread and cut filament behaviour. This is due to the fact that certain filaments have deeper cuts than others, resulting in a mix of behaviours. The sutures broke relatively early in the filaments with larger incisions, demonstrating an unwanted vulnerability in the type of sutures designed. In the case in which the cuts were not as deep, the threads presented a behaviour similar to that shown in figure 4.10, with the tightening beginning in one of the cut locations.

The results show that, in addition to not being able to duplicate the necessary geometry in the best way possible, the cutting process employed is also not precise enough to be used in the fabric of cog threads and marked the sutures instead of cutting them (figure 4.15. New solutions must be created and researched.

Figure 4.15 Optical microscope image of printed and cut thread 130^o.

4.2 Ex vivo pulling test

For all three samples, the load vs. distance curve was drawn and analysed. The curves are shown in figure 4.16.

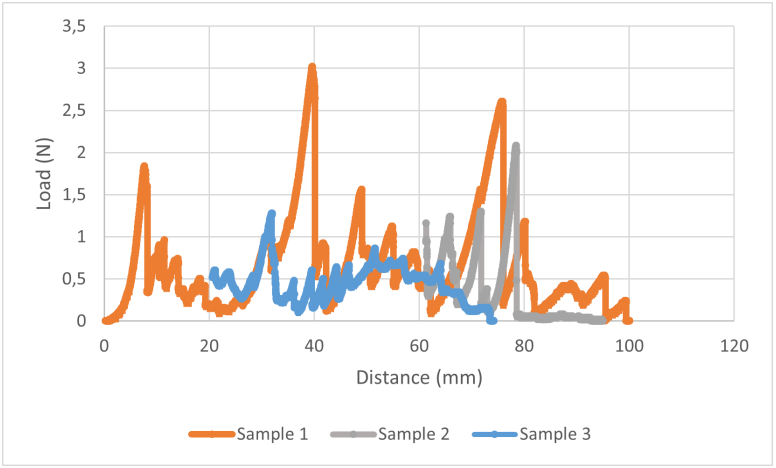

Figure 4.16 Load vs distance curve PCL commercial cog threads – ex vivo pulling test.

There was a problem in recording the results, so it was not possible to present the complete curve of the three samples. Therefore, as shown in figure 4.16, we only have the complete information of the test performed on the first sample. Based on the data gathered, it is reasonable to conclude that the barbs in the threads can provide some resistance to undesired movement. The best resistance was approximately $3N$, which equates to a capacity of around 300 grams.

4.3 Ex vivo ball burst test

The tests of all samples were conducted until there was complete rupture of the vaginal tissue and in some cases of the threads. The load vs distance curve of every sample was drawn and analysed (figure 4.17). For this test was necessary to use a $1000N$ load cell.

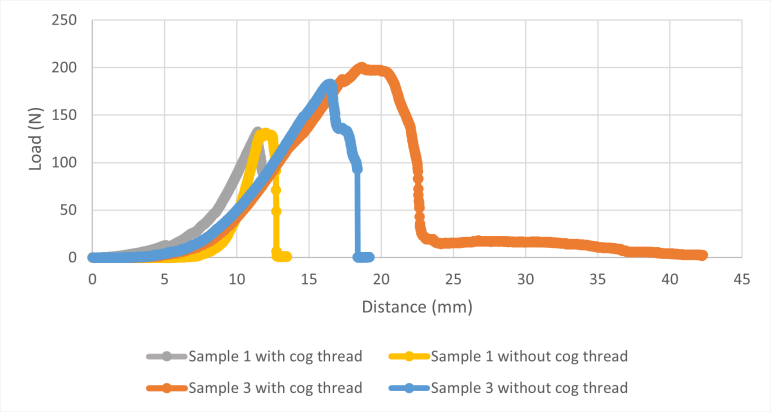

Figure 4.17 Load vs distance PCL commercial cog thread - ex vivo BB test.

Although we used three samples with and without threads, in figure 4.17 only four curves are shown because, during the test performed on the second sample with thread, there was an error in recording the data, so it is not possible to draw the complete curve (figure 4.18).

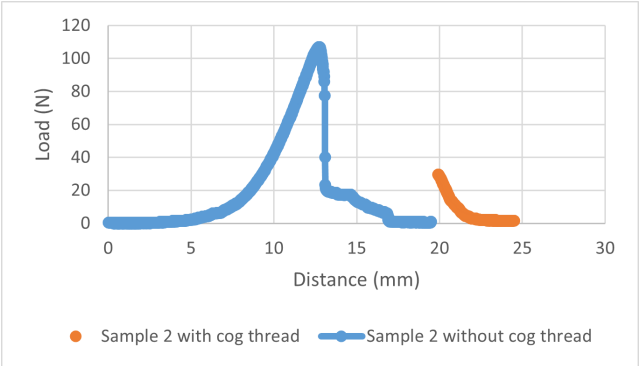

Figure 4.18 Load vs distance PCL commercial cog thread sample 2 - ex vivo BB test.

With the data that was possible to save from the tests is possible to see that the cogged threads can offer additional strength to the vaginal tissue; however, since not all the data was saved and the results saved reflect different behaviours it is not possible to define with certainty the benefits of inserting the threads into the vaginal tissue.

Chapter 5

Conclusions and Future Work

The execution of this thesis was characterized by several difficulties, beginning with Coronavirus and concluding with difficulty to generate viable cog threads by MEW and cutting. Not everything, however, was negative. Commercial cog threads were visually analysed using SEM and tested using a TT; the findings may still be compared in the future with the results of similar tests performed with the novel solutions developed. Furthermore, commercial cog threads were implanted in sow's vaginal tissue, and it was determined that their use can improve the mechanical characteristics evaluated. Nevertheless, new studies must be done in order to better evaluate the influence of these threads. In the future, ball burst tests should be carried out in a similar way to the ones performed, but using all samples from the same area of the vaginal canal, even from different sows with similar ages and physiognomies, due to the variation in properties along the canal.

Additionally, although MEW could not be used to print threads with the appropriate geometry, several printing parameters, particularly temperature (175^oC) and applied tension ($6.25kV$), were defined as the most efficient in terms of the evaluated mechanical characteristics and thermal deterioration of the material.

Furthermore, a cutting machine prototype was constructed to generate cog threads even if they were not fully developed by MEW. Despite the inability to properly cut the printed filaments, it allowed us to rule out a cutting method in the future.

During this thesis, some attempts were made to cut filaments with objects that we usually use in our daily lives (razor blade, potato peelers, ...) find a new approach future work possibly. It is worth noting that with the help of a razor blade, it was possible to make more satisfactory cuts than those made with the prototype, so it would be worthwhile to consider a cutting mechanism that performed horizontal movement rather than vertical movement or even a combination of both.

Also, another approach that could work is the one that Harry J. Buncke presented to the world in 1997, where two wheels, with blades that spin and keep contact with the filament generating barbs throughout its length, carried out the cutting of the sutures [51].

Still, in terms of future work, both the created and commercialized threads could

be tested and compared for degradation. This type of test was previously done with electrospun filaments and the results were presented in the abstract submitted in the Doctoral Congress of Engineering (DCE) 2021, as shown in Appendix H. Moreover, MEW printing with mixtures of biodegradable materials and anti-inflammatory agents or other materials could be better developed and studied, both at the mechanical property level and the effect of temperature on the agents and materials used.

References

[1] Steven Swift, Patrick Woodman, Amy O'Boyle, Margie Kahn, Michael Valley, Deirdre Bland, Wei Wang, and Joe Schaffer. Pelvic Organ Support Study (POSST): The distribution, clinical definition, and epidemiologic condition of pelvic organ support defects. *American Journal of Obstetrics and Gynecology*, 192(3):795–806, 2005.

[2] Food and Drug Administration. pelvic-organ-prolapse-pop @ www.fda.gov, 2019.

[3] E. J.M. Lensen, M. I.J. Withagen, K. B. Kluivers, A. L. Milani, and M. E. Vierhout. Surgical treatment of pelvic organ prolapse: A historical review with emphasis on the anterior compartment. *International Urogynecology Journal*, 24(10):1593–1602, 2013.

[4] Zara-louise Farmer, Juan Domínguez-robles, Caterina Mancinelli, and Eneko Larrañeta. Urogynecological surgical mesh implants : New trends in materials , manufacturing and therapeutic approaches. *International Journal of Pharmaceutics*, 585(June):119512, 2020.

[5] Patrick Dällenbach. To mesh or not to mesh: A review of pelvic organ reconstructive surgery. *International Journal of Women's Health*, 7:331–343, 2015.

[6] Saman Naghieh, Ehsan Foroozmehr, Mohsen Badrossamay, and Mahshid Kharaziha. Combinational processing of 3D printing and electrospinning of hierarchical poly(lactic acid)/gelatin-forsterite scaffolds as a biocomposite: Mechanical and biological assessment. *Materials and Design*, 133, 2017.

[7] Ann Yates. Female pelvic floor 1: anatomy and pathophysiology | Nursing Times. *Nursing Times*, 115(5):18–21, 2019.

[8] M. Alperin. *What Biomechanics Has to do With the Female Pelvic Floor - A Historical Perspective*. Elsevier Inc., 2016.

[9] John O.L. DeLancey. *Pelvic Floor Anatomy and Pathology*. Elsevier Inc., 2016.

[10] Richard C Bump and Peggy A Norton. EPIDEMIOLOGY AND NATURAL HISTORY OF PELVIC FLOOR DYSFUNCTION. *Obstetrics and Gynecology Clinics of North America*, 25(4):723–746, 1998.

[11] S. Todros, P. G. Pavan, and A. N. Natali. Biomechanical properties of synthetic surgical meshes for pelvic prolapse repair. *Journal of the Mechanical Behavior of Biomedical Materials*, 55:271–285, 2016.

[12] Matthew D. Barber and Christopher Maher. Epidemiology and outcome assessment of pelvic organ prolapse. *International Urogynecology Journal and Pelvic Floor Dysfunction*, 24(11):1783–1790, 2013.

[13] Cheryl B. Iglesia and Katelyn R. Smithling. Pelvic Organ Prolapse. *American family physician*, 96(3):179–185, 2017.

[14] J. Eric Jelovsek, Christopher Maher, and Matthew D. Barber. Pelvic organ prolapse. *Lancet*, 369(9566):1027–1038, 2007.

[15] Instituto Nacional de Estatística. População residente em Portugal poderá passar dos atuais 10,3 milhões para 8,2 milhões em 2080. Contudo, na Área Metropolitana de Lisboa e no Algarve a população residente poderá aumentar - 2018 - 2080, 2020.

[16] Teresa Mascarenhas, Miguel Mascarenhas-Saraiva, Amélia Ricon-Ferraz, Paula Nogueira, Fernando Lopes, and Alberto Freitas. Pelvic organ prolapse surgical management in Portugal and FDA safety communication have an impact on vaginal mesh. *International Urogynecology Journal*, 26(1):113–122, 2015.

[17] Jennifer M. Wu, Andrew F. Hundley, Rebekah G. Fulton, and Evan R. Myers. Forecasting the prevalence of pelvic floor disorders in U.S. women: 2010 to 2050. *Obstetrics and Gynecology*, 114(6):1278–1283, 2009.

[18] Dhinagar Subramanian, Karine Szwarcensztein, Josephine A Mauskopf, and Mark C Slack. Rate, type, and cost of pelvic organ prolapse surgery in Germany, France, and England. *European journal of obstetrics, gynecology, and reproductive biology*, 144(2):177–181, jun 2009.

[19] L L Subak, L E Waetjen, S van den Eeden, D H Thom, E Vittinghoff, and J S Brown. Cost of pelvic organ prolapse surgery in the United States. *Obstetrics and gynecology*, 98(4):646–651, oct 2001.

[20] Food and Drug Administration. Urogynecologic Surgical Mesh: Update on the Safety and Effectiveness of Transvaginal Placement for Pelvic Organ Prolapse. *FDA safety communication*, (July):July 1–15, 2011.

[21] Renée M. Ward, Digna R. Velez Edwards, Todd Edwards, Ayush Giri, Rebecca N. Jerome, and Jennifer M. Wu. Genetic epidemiology of pelvic organ prolapse: A systematic review. *American Journal of Obstetrics and Gynecology*, 211(4):326–335, 2014.

[22] Susan L. Hendrix, Amanda Clark, Ingrid Nygaard, Aaron Aragaki, Vanessa Barnabei, and Anne McTiernan. Pelvic organ prolapse in the Women's Health Initiative: Gravity and gravidity. *American Journal of Obstetrics and Gynecology*, 186(6):1160–1166, 2002.

[23] Toby D. Brown, Paul D. Dalton, and Dietmar W. Hutmacher. Melt electrospinning today: An opportune time for an emerging polymer process. *Progress in Polymer Science*, 56:116–166, 2016.

[24] Ann Yates. Female pelvic floor 2: assessment and rehabilitation. *Nursing Times*, 115(6):30–33, 2019.

[25] Cleaveland Clinic Medical Professsional. Surgical Mesh: Use and Complications in Women, 2020.

[26] Stergios K. Doumouchtsis and Eleftheria L. Chrysanthopoulou. Urogenital consequences in ageing women. *Best Practice and Research: Clinical Obstetrics and Gynaecology*, 27(5):699–714, 2013.

[27] Chahin Achtari and Peter L. Dwyer. Sexual function and pelvic floor disorders. *Best Practice and Research: Clinical Obstetrics and Gynaecology*, 19(6):993–1008, 2005.

[28] Mahshid Vashaghian, Alejandra M. Ruiz-Zapata, Manon H. Kerkhof, Behrouz Zandieh-Doulabi, Arie Werner, Jan Paul Roovers, and Theo H. Smit. Toward a New Generation of Pelvic Floor Implants With Electrospun Nanofibrous Matrices: A Feasibility Study. *Neurourology and Urodynamics*, 36(February 2016):565–573, 2015.

[29] Food and Drug Administration. Urogynecologic surgical mesh, 2019.

[30] Kim Keltie, Sohier Elneil, Ashwani Monga, Hannah Patrick, John Powell, Bruce Campbell, and Andrew J. Sims. Complications following vaginal mesh procedures for stress urinary incontinence: An 8 year study of 92,246 women. *Scientific Reports*, 7(1), 2017.

[31] xenogenous @ medical-dictionary.thefreedictionary.com.

[32] Jan Deprest, Fang Zheng, Maja Konstantinovic, Federico Spelzini, Filip Claerhout, Anneke Steensma, Yves Ozog, and Dirk De Ridder. The biology behind fascial defects and the use of implants in pelvic organ prolapse repair. *International Urogynecology Journal*, 17(SUPPL. 7):16–25, 2006.

[33] Jei Won Moon and Hee Dong Chae. Vaginal approaches using synthetic mesh to treat pelvic organ prolapse. *Annals of Coloproctology*, 32(1):7–11, 2016.

[34] Ea Løwenstein, Lars Alling Møller, Jennie Laigaard, and Helga Gimbel. Reoperation for pelvic organ prolapse : a Danish cohort study. pages 119–124, 2018.

[35] Natalia Price, Alex Slack, Eman Jwarah, and Simon Jackson. The incidence of reoperation for surgically treated pelvic organ prolapse: an 11-year experience. *Menopause International*, 14(4):145–148, 2008.

[36] Lannah L Lua, Erika D Vicente, Prathamesh Pathak, and Daniel Lybbert. Comparative analysis of overall cost and rate of healthcare utilization among apical prolapse procedures. pages 1481–1488, 2017.

[37] Cecilia Cheon and Christopher Maher. Economics of pelvic organ prolapse surgery. pages 1873–1876, 2013.

[38] Lei Xie, Longjiang Shen, and Bingyan Jiang. *Modelling and Simulation for Micro Injection Molding Process*. 2011.

[39] Pouyan Ahangar, Megan E Cooke, Michael H Weber, and Derek H Rosenzweig. Current Biomedical Applications of 3D Printing and Additive Manufacturing. *Applied Sciences*, 9(8), 2019.

[40] Lucie Hympanova, Marina Gabriela Monteiro Carvalho Mori da Cunha, Rita Rynkevic, Radoslaw A. Wach, Alicja K. Olejnik, Patricia Y.W. Dankers, Boris Arts, Tristan Mes, Anton W. Bosman, Maarten Albersen, and Jan Deprest. Experimental reconstruction of an abdominal wall defect with electrospun polycaprolactone-ureidopyrimidinone mesh conserves compliance yet may have insufficient strength. *Journal of the Mechanical Behavior of Biomedical Materials*, 88, 2018.

[41] Anna Bachs-Herrera, Omid Yousefzade, Luis J del Valle, and Jordi Puiggali. Melt Electrospinning of Polymers: Blends, Nanocomposites, Additives and Applications. *Applied Sciences*, 11(4), 2021.

[42] Yujin Myung and Chinkoo Jung. Mini-midface Lift Using Polydioxanone Cog Threads. *Plastic and Reconstructive Surgery - Global Open*, (January 2017):1–5, 2020.

[43] Chang Gun Lee, Jaeyun Jung, Samnoh Hwang, Chan Oh Park, Soonjae Hwang, Minjeong Jo, Min Hi Sin, Hyun Ho Kim, and Ki-Jong Rhee. Histological Evaluation of Bioresorbable Threads in Rats. *The Korean Journal of Clinical Laboratory Science*, 50(3):217–224, 2018.

[44] Vincent Wong. Hanging by a Thread: Choosing the Right Thread for the Right Patient. *Journal of Dermatology & Cosmetology*, 1(4):86–88, 2017.

[45] Rakesh Kalra. Use of barbed threads in facial rejuvenation. *Indian Journal of Plastic Surgery*, 41(3 SUPPL.), 2008.

[46] James a Greenberg and Randi H Goldman. Barbed Suture : A Review of the Obstetrics and Gynecology. *Reviews in Obstetrics & Gynecology*, 6(3):107–115, 2013.

[47] N. P. Ingle, H. Cong, and M. W. King. *Barbed suture technology.* Woodhead Publishing Limited, 2013.

[48] Hui Cong, Simon Roe, Peter Mente, Gregory Ruff, and W. Martin King. Fabrication and tissue anchoring performance of nylon and polypropylene barbed surgical sutures. *Journal of Donghua University (English Edition)*, 30(5):391–393, 2013.

[49] Nathaniel A. Matlin. Wool-like artificial fibers, U.S. Patent 2 866 256, Dec. 1958.

[50] John H. Alcamo. Surgecal suture, U.S. Patent 3 123 077, Mar. 1964.

[51] John H. Alcamo. Surgical methods using one-way suture, U.S. Patent 5 931 855, Aug. 1999.

[52] Donald Kress. The history of barbed suture suspension: Applications, and visions for the future. *Simplified Facial Rejuvenation*, pages 247–256, 2008.

[53] Jeffrey C. Leung, Gregory L. Ruff, and Matthew A. Megaro. Barbed sutures, U.S. Patent 8 795 332 B2, Aug. 2014.

[54] Malcolm D. Paul. Barbed sutures in aesthetic plastic surgery: evolution of thought and process. *Aesthetic surgery journal / the American Society for Aesthetic Plastic surgery*, 33(3 Suppl):17–31, 2013.

[55] Gregory L. Ruff. The history of barbed sutures. *Aesthetic surgery journal / the American Society for Aesthetic Plastic surgery*, 33(3 Suppl):12–16, 2013.

[56] Jeffrey Zaruby, Kristen Gingras, Jack Taylor, and Don Maul. An in vivo comparison of barbed suture devices and conventional monofilament sutures for cosmetic skin closure: biomechanical wound strength and histology. *Aesthetic surgery journal*, 31(2):232–240, feb 2011.

[57] V-loc™ wound closure device - product catalog. 555 Long Wharf Drive New Haven, CT 06511, 800.962.9888, 2021.

[58] Aman Dua and Bhawna Bhardwaj. A case report on use of cog threads and dermal fillers for facial-lifting in facioscapulohumeral muscular dystrophy. *Journal of Cutaneous and Aesthetic Surgery*, 12(1), 2019.

[59] CBB Medical Training Pte Ltd . Mold cutting threads – the new innovation from korean thread lifting, 2021.

[60] Amit Bandyopadhyay, Susmita Bose, and Suman Das. 3D printing of biomaterials. *MRS Bulletin*, 40(2):108–114, 2015.

[61] Sanjita Wasti and Sushil Adhikari. Use of Biomaterials for 3D Printing by Fused Deposition Modeling Technique: A Review. *Frontiers in Chemistry*, 8(May):1–14, 2020.

[62] Karthik Tappa and Udayabhanu Jammalamadaka. Novel biomaterials used in medical 3D printing techniques. *Journal of Functional Biomaterials*, 9(1), 2018.

[63] Sarwar Beg, Waleed H Almalki, Arshi Malik, Mohd Farhan, Mohammad Aatif, Ziyaur Rahman, Nabil K Alruwaili, Majed Alrobaian, Mohammed Tarique, and Mahfoozur Rahman. 3D printing for drug delivery and biomedical applications. *Drug Discovery Today*, 25(9):1668–1681, 2020.

[64] Beata Grabowska, Karolina Kaczmarska, Sylwia Cukrowicz, Elżbieta Mączka, and Artur Bobrowski. Polylactide Used as Filment in 3D Printing – Part 1 : FTIR , DRIFT and TG-DTG Studies. *Journal of Casting & Materials Engineering*, 4(3):48–52, 2020.

[65] Helena N. Chia and Benjamin M. Wu. Recent advances in 3D printing of biomaterials. *Journal of Biological Engineering*, 9(1):1–14, 2015.

[66] Udayabhanu Jammalamadaka and Karthik Tappa. Recent advances in biomaterials for 3D printing and tissue engineering. *Journal of Functional Biomaterials*, 9(1), 2018.

[67] Ngoc-Hien Tran, Van Chie Nguyen, Anhhuy Ngo, and Van-Cuong Nguyen. Study on the Effect of Fused Deposition Modeling (FDM) Process Parameters on the Printed Part Quality. 2017.

[68] Caroline Bonnans, Jonathan Chou, and Zena Werb. Remodelling the extracellular matrix in development and disease, 2014.

[69] Nandana Bhardwaj and Subhas C. Kundu. Electrospinning: A fascinating fiber fabrication technique. *Biotechnology Advances*, 28(3):325–347, 2010.

[70] Eugene D. Boland, Branch D. Coleman, Catherine P. Barnes, David G. Simpson, Gary E. Wnek, and Gary L. Bowlin. Electrospinning polydioxanone for biomedical applications, 2005.

[71] Seema Agarwal, Joachim H. Wendorff, and Andreas Greiner. Use of electrospinning technique for biomedical applications. *Polymer*, 49(26):5603–5621, 2008.

[72] Jason Lyons, Christopher Li, and Frank Ko. Melt-electrospinning part I: Processing parameters and geometric properties. *Polymer*, 45(22):7597–7603, 2004.

[73] M. Mohammadian and A. K. Haghi. Systematic parameter study for nano-fiber fabrication via electrospinning process. *Bulgarian Chemical Communications*, 46(3):545–555, 2014.

[74] W. E. Teo and S. Ramakrishna. A review on electrospinning design and nanofibre assemblies. *Nanotechnology*, 17(14), 2006.

[75] Felix M. Wunner, Marie Luise Wille, Thomas G. Noonan, Onur Bas, Paul D. Dalton, Elena M. De-Juan-Pardo, and Dietmar W. Hutmacher. Melt Electrospinning Writing of Highly Ordered Large Volume Scaffold Architectures. *Advanced Materials*, 30(20):1–6, 2018.

[76] William E. King, Yvonne Gillespie, Keaton Gilbert, and Gary L. Bowlin. Characterization of polydioxanone in near-field electrospinning. *Polymers*, 12(1), 2020.

[77] Matthew Lanaro, Larnii Booth, Sean K. Powell, and Maria A. Woodruff. *Electrofluidodynamic technologies for biomaterials and medical devices: Melt electrospinning.* Elsevier Ltd, 2018.

[78] R. P.A. Hartman, D. J. Brunner, D. M.A. Camelot, J. C.M. Marijnissen, and B. Scarlett. Electrohydrodynamic atomization in the cone-jet mode physical modeling of the liquid cone and jet. *Journal of Aerosol Science*, 30(7):823–849, 1999.

[79] M Komarek and L Martinova. Design and evaluation of melt-electrospinning electrodes. *Proceedings of the 2nd Nanocon*, pages 10–15, 2010.

[80] Dietmar W. Hutmacher and Paul D. Dalton. Melt electrospinning. *Chemistry - An Asian Journal*, 6(1):44–56, 2011.

[81] Felix Wunner, Sammy Florczak, Pawel Mieszczanek, Onur Bas, Elena Juan Pardo, and Dietmar Hutmacher. Electrospinning with polymer melts - state of the art and future perspectives. In K Healy, P Ducheyne, D W Grainger, D E Hutmacher, and C J Kirkpatrick, editors, *Comprehensive Biomaterials II (Reference Module in Materials Science and Materials Engineering)*, pages 217–235. Elsevier, The Netherlands, 2017.

[82] Toby David Brown. *Melt electrospinning writing.* PhD thesis, Queensland University of Technology, 2015.

[83] Paul D Dalton. Melt electrowriting with additive manufacturing principles. *Current Opinion in Biomedical Engineering*, 2:49–57, 2017.

[84] Toby D Brown, Paul D Dalton, and Dietmar W Hutmacher. Direct Writing By Way of Melt Electrospinning. *Advanced Materials*, 23(47):5651–5657, 2011.

[85] Felix M Wunner, Sebastian Eggert, Joachim Maartens, Onur Bas, Paul D Dalton, Elena M De-Juan-Pardo, and Dietmar W Hutmacher. Design and Development of a Three-Dimensional Printing High-Throughput Melt Electrowriting Technology Platform. *3D Printing and Additive Manufacturing*, 6(2):82–90, 2019.

[86] Ferdows Afghah, Caner Dikyol, Mine Altunbek, and Bahattin Koc. Biomimicry in Bio-Manufacturing: Developments in Melt Electrospinning Writing Technology Towards Hybrid Biomanufacturing. *Applied Sciences*, 9(17), 2019.

[87] Gernot Hochleitner, Julia Franziska Hümmer, Robert Luxenhofer, and Jürgen Groll. High definition fibrous poly(2-ethyl-2-oxazoline) scaffolds through melt electrospinning writing. *Polymer*, 55(20):5017–5023, 2014.

[88] Paul Dalton, M Muerza-Cascante, and Dietmar Hutmacher. Design and fabrication of scaffolds via melt electrospinning for applications in tissue engineering. *RSC Polymer Chemistry Series*, 2015:100–120, 2015.

[89] Miguel Nuno Barbosa Cunha. Optimisation of a MEW prototype for mesh implants fabrication. 2020.

[90] Toby D Brown, Fredrik Edin, Nicola Detta, Anthony D Skelton, Dietmar W Hutmacher, and Paul D Dalton. Melt electrospinning of poly(ϵ-caprolactone) scaffolds: Phenomenological observations associated with collection and direct writing. *Materials Science and Engineering: C*, 45:698–708, 2014.

[91] Ibrahim Hassounah. Melt Electrospinning of Thermoplastic Polymers. page 254, 2012.

[92] Jodie N Haigh, Tim R Dargaville, and Paul D Dalton. Additive manufacturing with polypropylene microfibers. *Materials Science and Engineering: C*, 77:883–887, 2017.

[93] M. S. Singhvi, S. S. Zinjarde, and D. V. Gokhale. Polylactic acid: synthesis and biomedical applications. *Journal of Applied Microbiology*, 127(6):1612–1626, 2019.

[94] Gustavo F Brito, Pankaj Agrawal, and Tomás J A Mélo. Mechanical and Morphological Properties of PLA/BioPE Blend Compatibilized with E-GMA and EMA-GMA Copolymers. *Macromolecular Symposia*, 367(1):176–182, 2016.

[95] Bahareh Azimi, Parviz Nourpanah, Mohammad Rabiee, and Shahram Arbab. Poly (-caprolactone) Fiber: An Overview. *Journal of engineered fibers and fabrics*, 9:74–90, 2014.

[96] Vincenzo Guarino, Gennaro Gentile, Luigi Sorrentino, and Luigi Ambrosio. *Polycaprolactone: Synthesis, Properties, and Applications*, pages 1–36. American Cancer Society, 2017.

[97] Matthew L. Bedell, Adam M. Navara, Yingying Du, Shengmin Zhang, and Antonios G. Mikos. Polymeric Systems for Bioprinting, oct 2020.

[98] João P.S. Ferreira, Rita Rynkevic, Pedro A.L.S. Martins, Marco P.L. Parente, Nele M. Famaey, Jan Deprest, and António A. Fernandes. Predicting the mechanical response of the vaginal wall in ball burst tests based on histology. *Journal of Biomedical Materials Research - Part B Applied Biomaterials*, 108(5):1925–1933, 2020.

[99] J S Afonso, P A L S Martins, M J B C Girao, R M Natal Jorge, A J M Ferreira, T Mascarenhas, A A Fernandes, J Bernardes, E C Baracat, G Rodrigues de Lima, and B Patricio. Mechanical properties of polypropylene mesh used in pelvic floor repair. *International Urogynecology Journal*, 19(3):375–380, 2008.

[100] Keisha A Jones, Andrew Feola, Leslie Meyn, Steven D Abramowitch, and Pamela A Moalli. Tensile properties of commonly used prolapse meshes. *International Urogynecology Journal*, 20(7):847–853, 2009.

[101] Rita Rynkevic, P. Martins, Antonio Fernandes, J. Vange, Monica R. Gallego, Radoslaw A. Wach, Tristan Mes, Anton W. Bosman, and Jan Deprest. In vitro simulation of in vivo degradation and cyclic loading of novel degradable electrospun meshes for prolapse repair. *Polymer Testing*, 78(May):105957, 2019.

[102] Donald O. Freytes, Ann E. Rundell, Jonathan Vande Geest, David A. Vorp, Thomas J. Webster, and Stephen F. Badylak. Analytically derived material properties of multilaminated extracellular matrix devices using the ball-burst test. *Biomaterials*, 26(27):5518–5531, 2005.

[103] R. Rynkevic. *In Vivo Models and in Silico Simulations of Mesh Augmented Prolapse Repair*. 2019.

[104] Kurt T. Barnhart, Adriana Izquierdo, E. Scott Pretorius, David M. Shera, Mayadah Shabbout, and Alka Shaunik. Baseline dimensions of the human vagina. *Human Reproduction*, 21(6):1618–1622, 2006.

Appendices

Appendix A

G Code for first barbed suture printed

NOTE: The applied voltage was $6.25kV$.

M107
M104 S220.0000
G28
G21
G90
M83
M109 S220.0000
G1 Z0
G1 X175 Y75 F3000
G91
G1 X125 E0.4
G1 Y200 E0.8
G1 X-250 E0.8
G1 Y-200 E0.8
G1 X125 E0.4
G1 Y5
G1 X-42.0000 Y30 E2 F3000
G4 S2
G1 F2250.0000
G1 X120.0000 Y0.0000 E1.8808
G1 X-12.0000 Y0.0000 E0.1881
G1 X-0.7000 Y-0.3000 E0.0119
G1 X0.7000 Y0.3000 E0.0119
G1 X-1.5000 Y0.0000 E0.0235
G1 X-0.7000 Y0.3000 E0.0119

```
G1 X0.7000 Y-0.3000 E0.0119
G1 X-1.5000 Y0.0000 E0.0235
G1 X-0.7000 Y-0.3000 E0.0119
G1 X0.7000 Y0.3000 E0.0119
G1 X-1.5000 Y0.0000 E0.0235
G1 X-0.7000 Y0.3000 E0.0119
G1 X0.7000 Y-0.3000 E0.0119
G1 X-1.5000 Y0.0000 E0.0235
G1 X-0.7000 Y-0.3000 E0.0119
G1 X0.7000 Y0.3000 E0.0119
G1 X-1.5000 Y0.0000 E0.0235
G1 X-0.7000 Y0.3000 E0.0119
G1 X0.7000 Y-0.3000 E0.0119
G1 X-1.5000 Y0.0000 E0.0235
G1 X-0.7000 Y-0.3000 E0.0119
G1 X0.7000 Y0.3000 E0.0119
G1 X-1.5000 Y0.0000 E0.0235
G1 X-0.7000 Y0.3000 E0.0119
G1 X0.7000 Y-0.3000 E0.0119
G1 X-1.5000 Y0.0000 E0.0235
G1 X-0.7000 Y-0.3000 E0.0119
G1 X0.7000 Y0.3000 E0.0119
G1 X-1.5000 Y0.0000 E0.0235
G1 X-0.7000 Y0.3000 E0.0119
G1 X0.7000 Y-0.3000 E0.0119
G1 X-1.5000 Y0.0000 E0.0235
G1 X-0.7000 Y-0.3000 E0.0119
G1 X0.7000 Y0.3000 E0.0119
G1 X-1.5000 Y0.0000 E0.0235
G1 X-0.7000 Y0.3000 E0.0119
G1 X0.7000 Y-0.3000 E0.0119
G1 X-1.5000 Y0.0000 E0.0235
G1 X-0.7000 Y-0.3000 E0.0119
G1 X0.7000 Y0.3000 E0.0119
G1 X-1.5000 Y0.0000 E0.0235
G1 X-0.7000 Y0.3000 E0.0119
G1 X0.7000 Y-0.3000 E0.0119
G1 X-1.5000 Y0.0000 E0.0235
G1 X-0.7000 Y-0.3000 E0.0119
G1 X0.7000 Y0.3000 E0.0119
```

G1 X-1.5000 Y0.0000 E0.0235
G1 X-0.7000 Y0.3000 E0.0119
G1 X0.7000 Y-0.3000 E0.0119
G1 X-1.5000 Y0.0000 E0.0235
G1 X-0.7000 Y-0.3000 E0.0119
G1 X0.7000 Y0.3000 E0.0119
G1 X-1.5000 Y0.0000 E0.0235
G1 X-0.7000 Y0.3000 E0.0119
G1 X0.7000 Y-0.3000 E0.0119
G1 X-1.5000 Y0.0000 E0.0235
G1 X-0.7000 Y-0.3000 E0.0119
G1 X0.7000 Y0.3000 E0.0119
G1 X-1.5000 Y0.0000 E0.0235
G1 X-0.7000 Y0.3000 E0.0119
G1 X0.7000 Y-0.3000 E0.0119
G1 X-1.5000 Y0.0000 E0.0235
G1 X-0.7000 Y-0.3000 E0.0119
G1 X0.7000 Y0.3000 E0.0119
G1 X-1.5000 Y0.0000 E0.0235
G1 X-0.7000 Y0.3000 E0.0119
G1 X0.7000 Y-0.3000 E0.0119
G1 X-1.5000 Y0.0000 E0.0235
G1 X-0.7000 Y-0.3000 E0.0119
G1 X0.7000 Y0.3000 E0.0119
G1 X-1.5000 Y0.0000 E0.0235
G1 X-0.7000 Y0.3000 E0.0119
G1 X0.7000 Y-0.3000 E0.0119
G1 X-1.5000 Y0.0000 E0.0235
G1 X-0.7000 Y-0.3000 E0.0119
G1 X0.7000 Y0.3000 E0.0119
G1 X-1.5000 Y0.0000 E0.0235
G1 X-0.7000 Y0.3000 E0.0119
G1 X0.7000 Y-0.3000 E0.0119
G1 X-1.5000 Y0.0000 E0.0235
G1 X-0.7000 Y-0.3000 E0.0119
G1 X0.7000 Y0.3000 E0.0119
G1 X-1.5000 Y0.0000 E0.0235
G1 X-0.7000 Y0.3000 E0.0119
G1 X0.7000 Y-0.3000 E0.0119
G1 X-1.5000 Y0.0000 E0.0235

```
G1 X-0.7000 Y-0.3000 E0.0119
G1 X0.7000 Y0.3000 E0.0119
G1 X-1.5000 Y0.0000 E0.0235
G1 X-0.7000 Y0.3000 E0.0119
G1 X0.7000 Y-0.3000 E0.0119
G1 X-1.5000 Y0.0000 E0.0235
G1 X-0.7000 Y-0.3000 E0.0119
G1 X0.7000 Y0.3000 E0.00119
G1 X-1.5000 Y0.0000 E0.0235
G1 X-0.7000 Y0.3000 E0.0119
G1 X0.7000 Y-0.3000 E0.0119
G1 X-6.5000 Y0.0000 E0.1019
G1 X0.7000 Y-0.3000 E0.0119
G1 X-0.7000 Y0.3000 E0.0119
G1 X-1.5000 Y0.0000 E0.0235
G1 X0.7000 Y0.3000 E0.0119
G1 X-0.7000 Y-0.3000 E0.0119
G1 X-1.5000 Y0.0000 E0.0235
G1 X0.7000 Y-0.3000 E0.0119
G1 X-0.7000 Y0.3000 E0.0119
G1 X-1.5000 Y0.0000 E0.0235
G1 X0.7000 Y0.3000 E0.0119
G1 X-0.7000 Y-0.3000 E0.0119
G1 X-1.5000 Y0.0000 E0.0235
G1 X0.7000 Y-0.3000 E0.0119
G1 X-0.7000 Y0.3000 E0.0119
G1 X-1.5000 Y0.0000 E0.0235
G1 X0.7000 Y0.3000 E0.0119
G1 X-0.7000 Y-0.3000 E0.0119
G1 X-1.5000 Y0.0000 E0.0235
G1 X0.7000 Y-0.3000 E0.0119
G1 X-0.7000 Y0.3000 E0.0119
G1 X-1.5000 Y0.0000 E0.0235
G1 X0.7000 Y0.3000 E0.0119
G1 X-0.7000 Y-0.3000 E0.0119
G1 X-1.5000 Y0.0000 E0.0235
G1 X0.7000 Y-0.3000 E0.0119
G1 X-0.7000 Y0.3000 E0.0119
G1 X-1.5000 Y0.0000 E0.0235
G1 X0.7000 Y0.3000 E0.0119
```

```
G1 X-0.7000 Y-0.3000 E0.0119
G1 X-1.5000 Y0.0000 E0.0235
G1 X0.7000 Y-0.3000 E0.0119
G1 X-0.7000 Y0.3000 E0.0119
G1 X-1.5000 Y0.0000 E0.0235
G1 X0.7000 Y0.3000 E0.0119
G1 X-0.7000 Y-0.3000 E0.0119
G1 X-1.5000 Y0.0000 E0.0235
G1 X0.7000 Y-0.3000 E0.0119
G1 X-0.7000 Y0.3000 E0.0119
G1 X-1.5000 Y0.0000 E0.0235
G1 X0.7000 Y0.3000 E0.0119
G1 X-0.7000 Y-0.3000 E0.0119
G1 X-1.5000 Y0.0000 E0.0235
G1 X0.7000 Y-0.3000 E0.0119
G1 X-0.7000 Y0.3000 E0.0119
G1 X-1.5000 Y0.0000 E0.0235
G1 X0.7000 Y0.3000 E0.0119
G1 X-0.7000 Y-0.3000 E0.0119
G1 X-1.5000 Y0.0000 E0.0235
G1 X0.7000 Y-0.3000 E0.0119
G1 X-0.7000 Y0.3000 E0.0119
G1 X-1.5000 Y0.0000 E0.0235
G1 X0.7000 Y0.3000 E0.0119
G1 X-0.7000 Y-0.3000 E0.0119
G1 X-1.5000 Y0.0000 E0.0235
G1 X0.7000 Y-0.3000 E0.0119
G1 X-0.7000 Y0.3000 E0.0119
G1 X-1.5000 Y0.0000 E0.0235
G1 X0.7000 Y0.3000 E0.0119
G1 X-0.7000 Y-0.3000 E0.0119
G1 X-1.5000 Y0.0000 E0.0235
G1 X0.7000 Y-0.3000 E0.0119
G1 X-0.7000 Y0.3000 E0.0119
G1 X-1.5000 Y0.0000 E0.0235
G1 X0.7000 Y0.3000 E0.0119
G1 X-0.7000 Y-0.3000 E0.0119
G1 X-1.5000 Y0.0000 E0.0235
G1 X0.7000 Y-0.3000 E0.0119
G1 X-0.7000 Y0.3000 E0.0119
```

```
G1 X-1.5000 Y0.0000 E0.0235
G1 X0.7000 Y0.3000 E0.0119
G1 X-0.7000 Y-0.3000 E0.0119
G1 X-1.5000 Y0.0000 E0.0235
G1 X0.7000 Y-0.3000 E0.0119
G1 X-0.7000 Y0.3000 E0.0119
G1 X-1.5000 Y0.0000 E0.0235
G1 X0.7000 Y0.3000 E0.0119
G1 X-0.7000 Y-0.3000 E0.0119
G1 X-1.5000 Y0.0000 E0.0235
G1 X0.7000 Y-0.3000 E0.0119
G1 X-0.7000 Y0.3000 E0.0119
G1 X-1.5000 Y0.0000 E0.0235
G1 X0.7000 Y0.3000 E0.0119
G1 X-0.7000 Y-0.3000 E0.0119
G1 X-1.5000 Y0.0000 E0.0235
G1 X0.7000 Y-0.3000 E0.0119
G1 X-0.7000 Y0.3000 E0.0119
G1 X-1.5000 Y0.0000 E0.0235
G1 X0.7000 Y0.3000 E0.0119
G1 X-0.7000 Y-0.3000 E0.0119
G1 X-1.3000 Y0.0000 E0.0235
G1 X-10.0000 Y0.0000 E0.1567
G1 X120.0000 Y0.0000 E1.8808
M104 S0
```

Appendix B

G Code for second barbed suture printed

NOTE: The applied voltage was $6.25kV$.

M107
M104 S220.0000
G28
G21
G90
M83
M109 S220.0000
G1 Z0
G1 X175 Y75 F3000
G91
G1 X125 E0.4
G1 Y200 E0.8
G1 X-250 E0.8
G1 Y-200 E0.8
G1 X125 E0.4
G1 Y5
G1 X-42.0000 Y30 E2 F3000
G4 S2
G1 F2250.0000
G1 X120.0000 Y0.0000 E1.8808
G1 X-12.0000 Y0.0000 E0.1881
G1 F500
G1 X-0.7000 Y-0.3000 E0.0119
G1 X0.7000 Y0.3000 E0.0119
G1 X-1.5000 Y0.0000 E0.0235

G1 X-0.7000 Y0.3000 E0.0119
G1 X0.7000 Y-0.3000 E0.0119
G1 X-1.5000 Y0.0000 E0.0235
G1 X-0.7000 Y-0.3000 E0.0119
G1 X0.7000 Y0.3000 E0.0119
G1 X-1.5000 Y0.0000 E0.0235
G1 X-0.7000 Y0.3000 E0.0119
G1 X0.7000 Y-0.3000 E0.0119
G1 X-1.5000 Y0.0000 E0.0235
G1 X-0.7000 Y-0.3000 E0.0119
G1 X0.7000 Y0.3000 E0.0119
G1 X-1.5000 Y0.0000 E0.0235
G1 X-0.7000 Y0.3000 E0.0119
G1 X0.7000 Y-0.3000 E0.0119
G1 X-1.5000 Y0.0000 E0.0235
G1 X-0.7000 Y-0.3000 E0.0119
G1 X0.7000 Y0.3000 E0.0119
G1 X-1.5000 Y0.0000 E0.0235
G1 X-0.7000 Y0.3000 E0.0119
G1 X0.7000 Y-0.3000 E0.0119
G1 X-1.5000 Y0.0000 E0.0235
G1 X-0.7000 Y-0.3000 E0.0119
G1 X0.7000 Y0.3000 E0.0119
G1 X-1.5000 Y0.0000 E0.0235
G1 X-0.7000 Y0.3000 E0.0119
G1 X0.7000 Y-0.3000 E0.0119
G1 X-1.5000 Y0.0000 E0.0235
G1 X-0.7000 Y-0.3000 E0.0119
G1 X0.7000 Y0.3000 E0.0119
G1 X-1.5000 Y0.0000 E0.0235
G1 X-0.7000 Y0.3000 E0.0119
G1 X0.7000 Y-0.3000 E0.0119
G1 X-1.5000 Y0.0000 E0.0235
G1 X-0.7000 Y-0.3000 E0.0119
G1 X0.7000 Y0.3000 E0.0119
G1 X-1.5000 Y0.0000 E0.0235
G1 X-0.7000 Y0.3000 E0.0119
G1 X0.7000 Y-0.3000 E0.0119
G1 X-1.5000 Y0.0000 E0.0235
G1 X-0.7000 Y-0.3000 E0.0119

```
G1 X0.7000 Y0.3000 E0.0119
G1 X-1.5000 Y0.0000 E0.0235
G1 X-0.7000 Y0.3000 E0.0119
G1 X0.7000 Y-0.3000 E0.0119
G1 X-1.5000 Y0.0000 E0.0235
G1 X-0.7000 Y-0.3000 E0.0119
G1 X0.7000 Y0.3000 E0.0119
G1 X-1.5000 Y0.0000 E0.0235
G1 X-0.7000 Y0.3000 E0.0119
G1 X0.7000 Y-0.3000 E0.0119
G1 X-1.5000 Y0.0000 E0.0235
G1 X-0.7000 Y-0.3000 E0.0119
G1 X0.7000 Y0.3000 E0.0119
G1 X-1.5000 Y0.0000 E0.0235
G1 X-0.7000 Y0.3000 E0.0119
G1 X0.7000 Y-0.3000 E0.0119
G1 X-1.5000 Y0.0000 E0.0235
G1 X-0.7000 Y-0.3000 E0.0119
G1 X0.7000 Y0.3000 E0.0119
G1 X-1.5000 Y0.0000 E0.0235
G1 X-0.7000 Y0.3000 E0.0119
G1 X0.7000 Y-0.3000 E0.0119
G1 X-1.5000 Y0.0000 E0.0235
G1 X-0.7000 Y-0.3000 E0.0119
G1 X0.7000 Y0.3000 E0.0119
G1 X-1.5000 Y0.0000 E0.0235
G1 X-0.7000 Y0.3000 E0.0119
G1 X0.7000 Y-0.3000 E0.0119
G1 X-1.5000 Y0.0000 E0.0235
G1 X-0.7000 Y-0.3000 E0.0119
G1 X0.7000 Y0.3000 E0.0119
G1 X-1.5000 Y0.0000 E0.0235
G1 X-0.7000 Y0.3000 E0.0119
G1 X0.7000 Y-0.3000 E0.0119
G1 X-1.5000 Y0.0000 E0.0235
G1 X-0.7000 Y-0.3000 E0.0119
G1 X0.7000 Y0.3000 E0.0119
G1 X-1.5000 Y0.0000 E0.0235
G1 X-0.7000 Y0.3000 E0.0119
G1 X0.7000 Y-0.3000 E0.0119
```

```
G1 X-1.5000 Y0.0000 E0.0235
G1 X-0.7000 Y-0.3000 E0.0119
G1 X0.7000 Y0.3000 E0.0119
G1 X-1.5000 Y0.0000 E0.0235
G1 X-0.7000 Y0.3000 E0.0119
G1 X0.7000 Y-0.3000 E0.0119
G1 X-1.5000 Y0.0000 E0.0235
G1 X-0.7000 Y-0.3000 E0.0119
G1 X0.7000 Y0.3000 E0.00119
G1 X-1.5000 Y0.0000 E0.0235
G1 X-0.7000 Y0.3000 E0.0119
G1 X0.7000 Y-0.3000 E0.0119
G1 X-6.5000 Y0.0000 E0.1019
G1 X0.7000 Y-0.3000 E0.0119
G1 X-0.7000 Y0.3000 E0.0119
G1 X-1.5000 Y0.0000 E0.0235
G1 X0.7000 Y0.3000 E0.0119
G1 X-0.7000 Y-0.3000 E0.0119
G1 X-1.5000 Y0.0000 E0.0235
G1 X0.7000 Y-0.3000 E0.0119
G1 X-0.7000 Y0.3000 E0.0119
G1 X-1.5000 Y0.0000 E0.0235
G1 X0.7000 Y0.3000 E0.0119
G1 X-0.7000 Y-0.3000 E0.0119
G1 X-1.5000 Y0.0000 E0.0235
G1 X0.7000 Y-0.3000 E0.0119
G1 X-0.7000 Y0.3000 E0.0119
G1 X-1.5000 Y0.0000 E0.0235
G1 X0.7000 Y0.3000 E0.0119
G1 X-0.7000 Y-0.3000 E0.0119
G1 X-1.5000 Y0.0000 E0.0235
G1 X0.7000 Y-0.3000 E0.0119
G1 X-0.7000 Y0.3000 E0.0119
G1 X-1.5000 Y0.0000 E0.0235
G1 X0.7000 Y0.3000 E0.0119
G1 X-0.7000 Y-0.3000 E0.0119
G1 X-1.5000 Y0.0000 E0.0235
G1 X0.7000 Y-0.3000 E0.0119
G1 X-0.7000 Y0.3000 E0.0119
G1 X-1.5000 Y0.0000 E0.0235
```

```
G1 X0.7000 Y0.3000 E0.0119
G1 X-0.7000 Y-0.3000 E0.0119
G1 X-1.5000 Y0.0000 E0.0235
G1 X0.7000 Y-0.3000 E0.0119
G1 X-0.7000 Y0.3000 E0.0119
G1 X-1.5000 Y0.0000 E0.0235
G1 X0.7000 Y0.3000 E0.0119
G1 X-0.7000 Y-0.3000 E0.0119
G1 X-1.5000 Y0.0000 E0.0235
G1 X0.7000 Y-0.3000 E0.0119
G1 X-0.7000 Y0.3000 E0.0119
G1 X-1.5000 Y0.0000 E0.0235
G1 X0.7000 Y0.3000 E0.0119
G1 X-0.7000 Y-0.3000 E0.0119
G1 X-1.5000 Y0.0000 E0.0235
G1 X0.7000 Y-0.3000 E0.0119
G1 X-0.7000 Y0.3000 E0.0119
G1 X-1.5000 Y0.0000 E0.0235
G1 X0.7000 Y0.3000 E0.0119
G1 X-0.7000 Y-0.3000 E0.0119
G1 X-1.5000 Y0.0000 E0.0235
G1 X0.7000 Y-0.3000 E0.0119
G1 X-0.7000 Y0.3000 E0.0119
G1 X-1.5000 Y0.0000 E0.0235
G1 X0.7000 Y0.3000 E0.0119
G1 X-0.7000 Y-0.3000 E0.0119
G1 X-1.5000 Y0.0000 E0.0235
G1 X0.7000 Y-0.3000 E0.0119
G1 X-0.7000 Y0.3000 E0.0119
G1 X-1.5000 Y0.0000 E0.0235
G1 X0.7000 Y0.3000 E0.0119
G1 X-0.7000 Y-0.3000 E0.0119
G1 X-1.5000 Y0.0000 E0.0235
G1 X0.7000 Y-0.3000 E0.0119
G1 X-0.7000 Y0.3000 E0.0119
G1 X-1.5000 Y0.0000 E0.0235
G1 X0.7000 Y0.3000 E0.0119
G1 X-0.7000 Y-0.3000 E0.0119
G1 X-1.5000 Y0.0000 E0.0235
G1 X0.7000 Y-0.3000 E0.0119
```

```
G1 X-0.7000 Y0.3000 E0.0119
G1 X-1.5000 Y0.0000 E0.0235
G1 X0.7000 Y0.3000 E0.0119
G1 X-0.7000 Y-0.3000 E0.0119
G1 X-1.5000 Y0.0000 E0.0235
G1 X0.7000 Y-0.3000 E0.0119
G1 X-0.7000 Y0.3000 E0.0119
G1 X-1.5000 Y0.0000 E0.0235
G1 X0.7000 Y0.3000 E0.0119
G1 X-0.7000 Y-0.3000 E0.0119
G1 X-1.5000 Y0.0000 E0.0235
G1 X0.7000 Y-0.3000 E0.0119
G1 X-0.7000 Y0.3000 E0.0119
G1 X-1.5000 Y0.0000 E0.0235
G1 X0.7000 Y0.3000 E0.0119
G1 X-0.7000 Y-0.3000 E0.0119
G1 X-1.5000 Y0.0000 E0.0235
G1 X0.7000 Y-0.3000 E0.0119
G1 X-0.7000 Y0.3000 E0.0119
G1 X-1.5000 Y0.0000 E0.0235
G1 X0.7000 Y0.3000 E0.0119
G1 X-0.7000 Y-0.3000 E0.0119
G1 X-1.3000 Y0.0000 E0.0235
G1 X-10.0000 Y0.0000 E0.1567
G1 F2250
G1 X120.0000 Y0.0000 E1.8808
M104 S0
```

Appendix C

G Code for third barbed suture printed

NOTE: The applied voltage was $6.25kV$.

M107
M104 S220.0000
G28
G21
G90
M83
M109 S220.0000
G1 Z0
G1 X175 Y75 F3000
G91
G1 X125 E0.4
G1 Y200 E0.8
G1 X-250 E0.8
G1 Y-200 E0.8
G1 X125 E0.4
G1 Y5
G1 X-42.0000 Y30 E2 F3000
G4 S2
G1 F2250.0000
G1 X120.0000 Y0.0000 E1.8808
G1 X-12.0000 Y0.0000 E0.1881
G1 X-1 Y-1 E0.0443
G1 X1 Y1 E0.0443
G1 X-3 Y0.0000 E0.0940
G1 X-1 Y1 E0.0443

```
G1 X1 Y-1 E0.0443
G1 X-3 Y0.0000 E0.0940
G1 X-1 Y-1 E0.0443
G1 X1 Y1 E0.0443
G1 X-3 Y0.0000 E0.0940
G1 X-1 Y1 E0.0443
G1 X1 Y-1 E0.0443
G1 X-3 Y0.0000 E0.0940
G1 X-1 Y-1 E0.0443
G1 X1 Y1 E0.0443
G1 X-3 Y0.0000 E0.0940
G1 X-1 Y1 E0.0443
G1 X1 Y-1 E0.0443
G1 X-3 Y0.0000 E0.0940
G1 X-1 Y-1 E0.0443
G1 X1 Y1 E0.0443
G1 X-3 Y0.0000 E0.0940
G1 X-1 Y1 E0.0443
G1 X1 Y-1 E0.0443
G1 X-3 Y0.0000 E0.0940
G1 X-1 Y-1 E0.0443
G1 X1 Y1 E0.0443
G1 X-3 Y0.0000 E0.0940
G1 X-1 Y1 E0.0443
G1 X1 Y-1 E0.0443
G1 X-3 Y0.0000 E0.0940
G1 X-1 Y-1 E0.0443
G1 X1 Y1 E0.0443
G1 X-3 Y0.0000 E0.0940
G1 X-1 Y1 E0.0443
G1 X1 Y-1 E0.0443
G1 X-3 Y0.0000 E0.0940
G1 X-1 Y-1 E0.0443
G1 X1 Y1 E0.0443
G1 X-3 Y0.0000 E0.0940
G1 X-1 Y1 E0.0443
G1 X1 Y-1 E0.0443
G1 X-3 Y0.0000 E0.0940
G1 X-1 Y-1 E0.0443
G1 X1 Y1 E0.0443
```

```
G1 X-3 Y0.0000 E0.0940
G1 X-1 Y1 E0.0443
G1 X1 Y-1 E0.0443
G1 X-9 Y0.0000 E0.2817
G1 X1 Y-1 E0.0443
G1 X-1 Y1 E0.0443
G1 X-3 Y0.0000 E0.0940
G1 X1 Y1 E0.0443
G1 X-1 Y-1 E0.0443
G1 X-3 Y0.0000 E0.0940
G1 X1 Y-1 E0.0443
G1 X-1 Y1 E0.0443
G1 X-3 Y0.0000 E0.0940
G1 X1 Y1 E0.0443
G1 X-1 Y-1 E0.0443
G1 X-3 Y0.0000 E0.0940
G1 X1 Y-1 E0.0443
G1 X-1 Y1 E0.0443
G1 X-3 Y0.0000 E0.0940
G1 X1 Y1 E0.0443
G1 X-1 Y-1 E0.0443
G1 X-3 Y0.0000 E0.0940
G1 X1 Y-1 E0.0443
G1 X-1 Y1 E0.0443
G1 X-3 Y0.0000 E0.0940
G1 X1 Y1 E0.0443
G1 X-1 Y-1 E0.0443
G1 X-3 Y0.0000 E0.0940
G1 X1 Y-1 E0.0443
G1 X-1 Y1 E0.0443
G1 X-3 Y0.0000 E0.0940
G1 X1 Y1 E0.0443
G1 X-1 Y-1 E0.0443
G1 X-3 Y0.0000 E0.0940
G1 X1 Y-1 E0.0443
G1 X-1 Y1 E0.0443
G1 X-3 Y0.0000 E0.0940
G1 X1 Y1 E0.0443
G1 X-1 Y-1 E0.0443
G1 X-3 Y0.0000 E0.0940
```

```
G1 X1 Y-1 E0.0443
G1 X-1 Y1 E0.0443
G1 X-3 Y0.0000 E0.0940
G1 X1 Y1 E0.0443
G1 X-1 Y-1 E0.0443
G1 X-3 Y0.0000 E0.0940
G1 X-10.0000 Y0.0000 E0.1567
G1 X120.0000 Y0.0000 E1.8808
M104 S0
```

Appendix D

G Code for fourth barbed suture printed

NOTE: The applied voltage was $6.25kV$.

M107
M104 S220.0000
G28
G21
G90
M83
M109 S220.0000
G1 Z0
G1 X175 Y75 F3000
G91
G1 X125 E0.4
G1 Y200 E0.8
G1 X-250 E0.8
G1 Y-200 E0.8
G1 X125 E0.4
G1 Y5
G1 X-42.0000 Y30 E2 F3000
G4 S2
G1 F1000.0000
G1 X120.0000 Y0.0000 E1.8808
G1 X-12.0000 Y0.0000 E0.1881
G1 X-0.7000 Y-0.3000 E0.0119
G1 X0.7000 Y0.3000 E0.0119
G1 X-1.5000 Y0.0000 E0.0235
G1 X-0.7000 Y0.3000 E0.0119

```
G1 X0.7000 Y-0.3000 E0.0119
G1 X-1.5000 Y0.0000 E0.0235
G1 X-0.7000 Y-0.3000 E0.0119
G1 X0.7000 Y0.3000 E0.0119
G1 X-1.5000 Y0.0000 E0.0235
G1 X-0.7000 Y0.3000 E0.0119
G1 X0.7000 Y-0.3000 E0.0119
G1 X-1.5000 Y0.0000 E0.0235
G1 X-0.7000 Y-0.3000 E0.0119
G1 X0.7000 Y0.3000 E0.0119
G1 X-1.5000 Y0.0000 E0.0235
G1 X-0.7000 Y0.3000 E0.0119
G1 X0.7000 Y-0.3000 E0.0119
G1 X-1.5000 Y0.0000 E0.0235
G1 X-0.7000 Y-0.3000 E0.0119
G1 X0.7000 Y0.3000 E0.0119
G1 X-1.5000 Y0.0000 E0.0235
G1 X-0.7000 Y0.3000 E0.0119
G1 X0.7000 Y-0.3000 E0.0119
G1 X-1.5000 Y0.0000 E0.0235
G1 X-0.7000 Y-0.3000 E0.0119
G1 X0.7000 Y0.3000 E0.0119
G1 X-1.5000 Y0.0000 E0.0235
G1 X-0.7000 Y0.3000 E0.0119
G1 X0.7000 Y-0.3000 E0.0119
G1 X-1.5000 Y0.0000 E0.0235
G1 X-0.7000 Y-0.3000 E0.0119
G1 X0.7000 Y0.3000 E0.0119
G1 X-1.5000 Y0.0000 E0.0235
G1 X-0.7000 Y0.3000 E0.0119
G1 X0.7000 Y-0.3000 E0.0119
G1 X-1.5000 Y0.0000 E0.0235
G1 X-0.7000 Y-0.3000 E0.0119
G1 X0.7000 Y0.3000 E0.0119
G1 X-1.5000 Y0.0000 E0.0235
G1 X-0.7000 Y0.3000 E0.0119
G1 X0.7000 Y-0.3000 E0.0119
G1 X-1.5000 Y0.0000 E0.0235
G1 X-0.7000 Y-0.3000 E0.0119
G1 X0.7000 Y0.3000 E0.0119
```

```
G1 X-1.5000 Y0.0000 E0.0235
G1 X-0.7000 Y0.3000 E0.0119
G1 X0.7000 Y-0.3000 E0.0119
G1 X-1.5000 Y0.0000 E0.0235
G1 X-0.7000 Y-0.3000 E0.0119
G1 X0.7000 Y0.3000 E0.0119
G1 X-1.5000 Y0.0000 E0.0235
G1 X-0.7000 Y0.3000 E0.0119
G1 X0.7000 Y-0.3000 E0.0119
G1 X-1.5000 Y0.0000 E0.0235
G1 X-0.7000 Y-0.3000 E0.0119
G1 X0.7000 Y0.3000 E0.0119
G1 X-1.5000 Y0.0000 E0.0235
G1 X-0.7000 Y0.3000 E0.0119
G1 X0.7000 Y-0.3000 E0.0119
G1 X-1.5000 Y0.0000 E0.0235
G1 X-0.7000 Y-0.3000 E0.0119
G1 X0.7000 Y0.3000 E0.0119
G1 X-1.5000 Y0.0000 E0.0235
G1 X-0.7000 Y0.3000 E0.0119
G1 X0.7000 Y-0.3000 E0.0119
G1 X-1.5000 Y0.0000 E0.0235
G1 X-0.7000 Y-0.3000 E0.0119
G1 X0.7000 Y0.3000 E0.0119
G1 X-1.5000 Y0.0000 E0.0235
G1 X-0.7000 Y0.3000 E0.0119
G1 X0.7000 Y-0.3000 E0.0119
G1 X-1.5000 Y0.0000 E0.0235
G1 X-0.7000 Y-0.3000 E0.0119
G1 X0.7000 Y0.3000 E0.0119
G1 X-1.5000 Y0.0000 E0.0235
G1 X-0.7000 Y0.3000 E0.0119
G1 X0.7000 Y-0.3000 E0.0119
G1 X-1.5000 Y0.0000 E0.0235
G1 X-0.7000 Y-0.3000 E0.0119
G1 X0.7000 Y0.3000 E0.0119
G1 X-1.5000 Y0.0000 E0.0235
G1 X-0.7000 Y0.3000 E0.0119
G1 X0.7000 Y-0.3000 E0.0119
G1 X-1.5000 Y0.0000 E0.0235
```

```
G1 X-0.7000 Y-0.3000 E0.0119
G1 X0.7000 Y0.3000 E0.0119
G1 X-1.5000 Y0.0000 E0.0235
G1 X-0.7000 Y0.3000 E0.0119
G1 X0.7000 Y-0.3000 E0.0119
G1 X-1.5000 Y0.0000 E0.0235
G1 X-0.7000 Y-0.3000 E0.0119
G1 X0.7000 Y0.3000 E0.00119
G1 X-1.5000 Y0.0000 E0.0235
G1 X-0.7000 Y0.3000 E0.0119
G1 X0.7000 Y-0.3000 E0.0119
G1 X-6.5000 Y0.0000 E0.1019
G1 X0.7000 Y-0.3000 E0.0119
G1 X-0.7000 Y0.3000 E0.0119
G1 X-1.5000 Y0.0000 E0.0235
G1 X0.7000 Y0.3000 E0.0119
G1 X-0.7000 Y-0.3000 E0.0119
G1 X-1.5000 Y0.0000 E0.0235
G1 X0.7000 Y-0.3000 E0.0119
G1 X-0.7000 Y0.3000 E0.0119
G1 X-1.5000 Y0.0000 E0.0235
G1 X0.7000 Y0.3000 E0.0119
G1 X-0.7000 Y-0.3000 E0.0119
G1 X-1.5000 Y0.0000 E0.0235
G1 X0.7000 Y-0.3000 E0.0119
G1 X-0.7000 Y0.3000 E0.0119
G1 X-1.5000 Y0.0000 E0.0235
G1 X0.7000 Y0.3000 E0.0119
G1 X-0.7000 Y-0.3000 E0.0119
G1 X-1.5000 Y0.0000 E0.0235
G1 X0.7000 Y-0.3000 E0.0119
G1 X-0.7000 Y0.3000 E0.0119
G1 X-1.5000 Y0.0000 E0.0235
G1 X0.7000 Y0.3000 E0.0119
G1 X-0.7000 Y-0.3000 E0.0119
G1 X-1.5000 Y0.0000 E0.0235
G1 X0.7000 Y-0.3000 E0.0119
G1 X-0.7000 Y0.3000 E0.0119
G1 X-1.5000 Y0.0000 E0.0235
G1 X0.7000 Y0.3000 E0.0119
```

```
G1 X-0.7000 Y-0.3000 E0.0119
G1 X-1.5000 Y0.0000 E0.0235
G1 X0.7000 Y-0.3000 E0.0119
G1 X-0.7000 Y0.3000 E0.0119
G1 X-1.5000 Y0.0000 E0.0235
G1 X0.7000 Y0.3000 E0.0119
G1 X-0.7000 Y-0.3000 E0.0119
G1 X-1.5000 Y0.0000 E0.0235
G1 X0.7000 Y-0.3000 E0.0119
G1 X-0.7000 Y0.3000 E0.0119
G1 X-1.5000 Y0.0000 E0.0235
G1 X0.7000 Y0.3000 E0.0119
G1 X-0.7000 Y-0.3000 E0.0119
G1 X-1.5000 Y0.0000 E0.0235
G1 X0.7000 Y-0.3000 E0.0119
G1 X-0.7000 Y0.3000 E0.0119
G1 X-1.5000 Y0.0000 E0.0235
G1 X0.7000 Y0.3000 E0.0119
G1 X-0.7000 Y-0.3000 E0.0119
G1 X-1.5000 Y0.0000 E0.0235
G1 X0.7000 Y-0.3000 E0.0119
G1 X-0.7000 Y0.3000 E0.0119
G1 X-1.5000 Y0.0000 E0.0235
G1 X0.7000 Y0.3000 E0.0119
G1 X-0.7000 Y-0.3000 E0.0119
G1 X-1.5000 Y0.0000 E0.0235
G1 X0.7000 Y-0.3000 E0.0119
G1 X-0.7000 Y0.3000 E0.0119
G1 X-1.5000 Y0.0000 E0.0235
G1 X0.7000 Y0.3000 E0.0119
G1 X-0.7000 Y-0.3000 E0.0119
G1 X-1.5000 Y0.0000 E0.0235
G1 X0.7000 Y-0.3000 E0.0119
G1 X-0.7000 Y0.3000 E0.0119
G1 X-1.5000 Y0.0000 E0.0235
G1 X0.7000 Y0.3000 E0.0119
G1 X-0.7000 Y-0.3000 E0.0119
G1 X-1.5000 Y0.0000 E0.0235
G1 X0.7000 Y-0.3000 E0.0119
G1 X-0.7000 Y0.3000 E0.0119
```

```
G1 X-1.5000 Y0.0000 E0.0235
G1 X0.7000 Y0.3000 E0.0119
G1 X-0.7000 Y-0.3000 E0.0119
G1 X-1.5000 Y0.0000 E0.0235
G1 X0.7000 Y-0.3000 E0.0119
G1 X-0.7000 Y0.3000 E0.0119
G1 X-1.5000 Y0.0000 E0.0235
G1 X0.7000 Y0.3000 E0.0119
G1 X-0.7000 Y-0.3000 E0.0119
G1 X-1.5000 Y0.0000 E0.0235
G1 X0.7000 Y-0.3000 E0.0119
G1 X-0.7000 Y0.3000 E0.0119
G1 X-1.5000 Y0.0000 E0.0235
G1 X0.7000 Y0.3000 E0.0119
G1 X-0.7000 Y-0.3000 E0.0119
G1 X-1.5000 Y0.0000 E0.0235
G1 X0.7000 Y-0.3000 E0.0119
G1 X-0.7000 Y0.3000 E0.0119
G1 X-1.5000 Y0.0000 E0.0235
G1 X0.7000 Y0.3000 E0.0119
G1 X-0.7000 Y-0.3000 E0.0119
G1 X-1.3000 Y0.0000 E0.0235
G1 X-10.0000 Y0.0000 E0.1567
G1 X120.0000 Y0.0000 E1.8808
M104 S0
```

Appendix E

G Code for fifth barbed suture printed

NOTE: The applied voltage was $6.25kV$.

M107
M104 S220.0000
G28
G21
G90
M83
M109 S220.0000
G1 Z0
G1 X175 Y75 F3000
G91
G1 X125 E0.4
G1 Y200 E0.8
G1 X-250 E0.8
G1 Y-200 E0.8
G1 X125 E0.4
G1 Y5
G1 X-42.0000 Y30 E2 F3000
G4 S2
G1 F1500.0000
G1 X120.0000 Y0.0000 E1.8808
G1 X-12.0000 Y0.0000 E0.1881
G1 X-1 Y-1 E0.0443
G1 X1 Y1 E0.0443
G1 X-3 Y0.0000 E0.0940
G1 X-1 Y1 E0.0443

```
G1 X1 Y-1 E0.0443
G1 X-3 Y0.0000 E0.0940
G1 X-1 Y-1 E0.0443
G1 X1 Y1 E0.0443
G1 X-3 Y0.0000 E0.0940
G1 X-1 Y1 E0.0443
G1 X1 Y-1 E0.0443
G1 X-3 Y0.0000 E0.0940
G1 X-1 Y-1 E0.0443
G1 X1 Y1 E0.0443
G1 X-3 Y0.0000 E0.0940
G1 X-1 Y1 E0.0443
G1 X1 Y-1 E0.0443
G1 X-3 Y0.0000 E0.0940
G1 X-1 Y-1 E0.0443
G1 X1 Y1 E0.0443
G1 X-3 Y0.0000 E0.0940
G1 X-1 Y1 E0.0443
G1 X1 Y-1 E0.0443
G1 X-3 Y0.0000 E0.0940
G1 X-1 Y-1 E0.0443
G1 X1 Y1 E0.0443
G1 X-3 Y0.0000 E0.0940
G1 X-1 Y1 E0.0443
G1 X1 Y-1 E0.0443
G1 X-3 Y0.0000 E0.0940
G1 X-1 Y-1 E0.0443
G1 X1 Y1 E0.0443
G1 X-3 Y0.0000 E0.0940
G1 X-1 Y1 E0.0443
G1 X1 Y-1 E0.0443
G1 X-3 Y0.0000 E0.0940
G1 X-1 Y-1 E0.0443
G1 X1 Y1 E0.0443
G1 X-3 Y0.0000 E0.0940
G1 X-1 Y1 E0.0443
G1 X1 Y-1 E0.0443
G1 X-3 Y0.0000 E0.0940
G1 X-1 Y-1 E0.0443
G1 X1 Y1 E0.0443
```

```
G1 X-3 Y0.0000 E0.0940
G1 X-1 Y1 E0.0443
G1 X1 Y-1 E0.0443
G1 X-9 Y0.0000 E0.2817
G1 X1 Y-1 E0.0443
G1 X-1 Y1 E0.0443
G1 X-3 Y0.0000 E0.0940
G1 X1 Y1 E0.0443
G1 X-1 Y-1 E0.0443
G1 X-3 Y0.0000 E0.0940
G1 X1 Y-1 E0.0443
G1 X-1 Y1 E0.0443
G1 X-3 Y0.0000 E0.0940
G1 X1 Y1 E0.0443
G1 X-1 Y-1 E0.0443
G1 X-3 Y0.0000 E0.0940
G1 X1 Y-1 E0.0443
G1 X-1 Y1 E0.0443
G1 X-3 Y0.0000 E0.0940
G1 X1 Y1 E0.0443
G1 X-1 Y-1 E0.0443
G1 X-3 Y0.0000 E0.0940
G1 X1 Y-1 E0.0443
G1 X-1 Y1 E0.0443
G1 X-3 Y0.0000 E0.0940
G1 X1 Y1 E0.0443
G1 X-1 Y-1 E0.0443
G1 X-3 Y0.0000 E0.0940
G1 X1 Y-1 E0.0443
G1 X-1 Y1 E0.0443
G1 X-3 Y0.0000 E0.0940
G1 X1 Y1 E0.0443
G1 X-1 Y-1 E0.0443
G1 X-3 Y0.0000 E0.0940
G1 X1 Y-1 E0.0443
G1 X-1 Y1 E0.0443
G1 X-3 Y0.0000 E0.0940
G1 X1 Y1 E0.0443
G1 X-1 Y-1 E0.0443
G1 X-3 Y0.0000 E0.0940
```

```
G1 X1 Y-1 E0.0443
G1 X-1 Y1 E0.0443
G1 X-3 Y0.0000 E0.0940
G1 X1 Y1 E0.0443
G1 X-1 Y-1 E0.0443
G1 X-3 Y0.0000 E0.0940
G1 X-10.0000 Y0.0000 E0.1567
G1 X120.0000 Y0.0000 E1.8808
M104 S0
```

Appendix F

G Code for sixth barbed suture printed

NOTE: The applied voltage was $6.45kV$.

M107
M104 S220.0000
G28
G21
G90
M83
M109 S220.0000
G1 Z0
G1 X175 Y75 F3000
G91
G1 X125 E0.4
G1 Y200 E0.8
G1 X-250 E0.8
G1 Y-200 E0.8
G1 X125 E0.4
G1 Y5
G1 X-42.0000 Y30 E2 F3000
G4 S2
G1 F2250.0000
G1 X120.0000 Y0.0000 E1.8808
G1 X-12.0000 Y0.0000 E0.1881
G1 F500
G1 X-0.7000 Y-0.3000 E0.0119
G1 X0.7000 Y0.3000 E0.0119
G1 X-3.0000 Y0.0000 E0.0470

```
G1 X-0.7000 Y0.3000 E0.0119
G1 X0.7000 Y-0.3000 E0.0119
G1 X-3.0000 Y0.0000 E0.0470
G1 X-0.7000 Y-0.3000 E0.0119
G1 X0.7000 Y0.3000 E0.0119
G1 X-3.0000 Y0.0000 E0.0470
G1 X-0.7000 Y0.3000 E0.0119
G1 X0.7000 Y-0.3000 E0.0119
G1 X-3.0000 Y0.0000 E0.0470
G1 X-0.7000 Y-0.3000 E0.0119
G1 X0.7000 Y0.3000 E0.0119
G1 X-3.0000 Y0.0000 E0.0470
G1 X-0.7000 Y0.3000 E0.0119
G1 X0.7000 Y-0.3000 E0.0119
G1 X-3.0000 Y0.0000 E0.0470
G1 X-0.7000 Y-0.3000 E0.0119
G1 X0.7000 Y0.3000 E0.0119
G1 X-3.0000 Y0.0000 E0.0470
G1 X-0.7000 Y0.3000 E0.0119
G1 X0.7000 Y-0.3000 E0.0119
G1 X-3.0000 Y0.0000 E0.0470
G1 X-0.7000 Y-0.3000 E0.0119
G1 X0.7000 Y0.3000 E0.0119
G1 X-3.0000 Y0.0000 E0.0470
G1 X-0.7000 Y0.3000 E0.0119
G1 X0.7000 Y-0.3000 E0.0119
G1 X-3.0000 Y0.0000 E0.0470
G1 X-0.7000 Y-0.3000 E0.0119
G1 X0.7000 Y0.3000 E0.0119
G1 X-3.0000 Y0.0000 E0.0470
G1 X-0.7000 Y0.3000 E0.0119
G1 X0.7000 Y-0.3000 E0.0119
G1 X-3.0000 Y0.0000 E0.0470
G1 X-0.7000 Y-0.3000 E0.0119
G1 X0.7000 Y0.3000 E0.0119
G1 X-3.0000 Y0.0000 E0.0470
G1 X-0.7000 Y0.3000 E0.0119
G1 X0.7000 Y-0.3000 E0.0119
G1 X-3.0000 Y0.0000 E0.0470
G1 X-0.7000 Y-0.3000 E0.0119
```

```
G1 X0.7000 Y0.3000 E0.0119
G1 X-3.0000 Y0.0000 E0.0470
G1 X-0.7000 Y0.3000 E0.0119
G1 X0.7000 Y-0.3000 E0.0119
G1 X-8.000 Y0.0000 E0.1359
G1 X0.7000 Y-0.3000 E0.0119
G1 X-0.7000 Y0.3000 E0.0119
G1 X-3.000 Y0.0000 E0.0470
G1 X0.7000 Y0.3000 E0.0119
G1 X-0.7000 Y-0.3000 E0.0119
G1 X-3.0000 Y0.0000 E0.0470
G1 X0.7000 Y-0.3000 E0.0119
G1 X-0.7000 Y0.3000 E0.0119
G1 X-3.000 Y0.0000 E0.0470
G1 X0.7000 Y0.3000 E0.0119
G1 X-0.7000 Y-0.3000 E0.0119
G1 X-3.0000 Y0.0000 E0.0470
G1 X0.7000 Y-0.3000 E0.0119
G1 X-0.7000 Y0.3000 E0.0119
G1 X-3.000 Y0.0000 E0.0470
G1 X0.7000 Y0.3000 E0.0119
G1 X-0.7000 Y-0.3000 E0.0119
G1 X-3.0000 Y0.0000 E0.0470
G1 X0.7000 Y-0.3000 E0.0119
G1 X-0.7000 Y0.3000 E0.0119
G1 X-3.000 Y0.0000 E0.0470
G1 X0.7000 Y0.3000 E0.0119
G1 X-0.7000 Y-0.3000 E0.0119
G1 X-3.0000 Y0.0000 E0.0470
G1 X0.7000 Y-0.3000 E0.0119
G1 X-0.7000 Y0.3000 E0.0119
G1 X-3.000 Y0.0000 E0.0470
G1 X0.7000 Y0.3000 E0.0119
G1 X-0.7000 Y-0.3000 E0.0119
G1 X-3.0000 Y0.0000 E0.0470
G1 X0.7000 Y-0.3000 E0.0119
G1 X-0.7000 Y0.3000 E0.0119
G1 X-3.000 Y0.0000 E0.0470
G1 X0.7000 Y0.3000 E0.0119
G1 X-0.7000 Y-0.3000 E0.0119
```

```
G1 X-3.0000 Y0.0000 E0.0470
G1 X0.7000 Y-0.3000 E0.0119
G1 X-0.7000 Y0.3000 E0.0119
G1 X-3.000 Y0.0000 E0.0470
G1 X0.7000 Y0.3000 E0.0119
G1 X-0.7000 Y-0.3000 E0.0119
G1 X-3.0000 Y0.0000 E0.0470
G1 X0.7000 Y-0.3000 E0.0119
G1 X-0.7000 Y0.3000 E0.0119
G1 X-3.000 Y0.0000 E0.0470
G1 X0.7000 Y0.3000 E0.0119
G1 X-0.7000 Y-0.3000 E0.0119
G1 X-3.0000 Y0.0000 E0.0470
G1 X-10.0000 Y0.0000 E0.1567
G1 F2250
G1 X120.0000 Y0.0000 E1.8808
M104 S0
```

Appendix G

G Code for seventh barbed suture printed

NOTE: The applied voltage was $6.45kV$.

M107
M104 S220.0000
G28
G21
G90
M83
M109 S220.0000
G1 Z0
G1 X175 Y75 F3000
G91
G1 X125 E0.4
G1 Y200 E0.8
G1 X-250 E0.8
G1 Y-200 E0.8
G1 X125 E0.4
G1 Y5
G1 X-42.0000 Y30 E2 F3000
G4 S2
G1 F2250.0000
G1 X120.0000 Y0.0000 E1.8808
G1 X-12.0000 Y0.0000 E0.1881
G1 F500
G1 X-0.7000 Y-0.3000 E0.0119
G1 X0.7000 Y0.3000 E0.0119
G1 X-1.5000 Y0.0000 E0.0235

```
G1 X-0.7000 Y0.3000 E0.0119
G1 X0.7000 Y-0.3000 E0.0119
G1 X-1.5000 Y0.0000 E0.0235
G1 X-0.7000 Y-0.3000 E0.0119
G1 X0.7000 Y0.3000 E0.0119
G1 X-1.5000 Y0.0000 E0.0235
G1 X-0.7000 Y0.3000 E0.0119
G1 X0.7000 Y-0.3000 E0.0119
G1 X-1.5000 Y0.0000 E0.0235
G1 X-0.7000 Y-0.3000 E0.0119
G1 X0.7000 Y0.3000 E0.0119
G1 X-1.5000 Y0.0000 E0.0235
G1 X-0.7000 Y0.3000 E0.0119
G1 X0.7000 Y-0.3000 E0.0119
G1 X-1.5000 Y0.0000 E0.0235
G1 X-0.7000 Y-0.3000 E0.0119
G1 X0.7000 Y0.3000 E0.0119
G1 X-1.5000 Y0.0000 E0.0235
G1 X-0.7000 Y0.3000 E0.0119
G1 X0.7000 Y-0.3000 E0.0119
G1 X-1.5000 Y0.0000 E0.0235
G1 X-0.7000 Y-0.3000 E0.0119
G1 X0.7000 Y0.3000 E0.0119
G1 X-1.5000 Y0.0000 E0.0235
G1 X-0.7000 Y0.3000 E0.0119
G1 X0.7000 Y-0.3000 E0.0119
G1 X-1.5000 Y0.0000 E0.0235
G1 X-0.7000 Y-0.3000 E0.0119
G1 X0.7000 Y0.3000 E0.0119
G1 X-1.5000 Y0.0000 E0.0235
G1 X-0.7000 Y0.3000 E0.0119
G1 X0.7000 Y-0.3000 E0.0119
G1 X-1.5000 Y0.0000 E0.0235
G1 X-0.7000 Y-0.3000 E0.0119
G1 X0.7000 Y0.3000 E0.0119
G1 X-1.5000 Y0.0000 E0.0235
G1 X-0.7000 Y0.3000 E0.0119
G1 X0.7000 Y-0.3000 E0.0119
G1 X-1.5000 Y0.0000 E0.0235
G1 X-0.7000 Y-0.3000 E0.0119
```

G1 X0.7000 Y0.3000 E0.0119
G1 X-1.5000 Y0.0000 E0.0235
G1 X-0.7000 Y0.3000 E0.0119
G1 X0.7000 Y-0.3000 E0.0119
G1 X-1.5000 Y0.0000 E0.0235
G1 X-0.7000 Y-0.3000 E0.0119
G1 X0.7000 Y0.3000 E0.0119
G1 X-1.5000 Y0.0000 E0.0235
G1 X-0.7000 Y0.3000 E0.0119
G1 X0.7000 Y-0.3000 E0.0119
G1 X-1.5000 Y0.0000 E0.0235
G1 X-0.7000 Y-0.3000 E0.0119
G1 X0.7000 Y0.3000 E0.0119
G1 X-1.5000 Y0.0000 E0.0235
G1 X-0.7000 Y0.3000 E0.0119
G1 X0.7000 Y-0.3000 E0.0119
G1 X-1.5000 Y0.0000 E0.0235
G1 X-0.7000 Y-0.3000 E0.0119
G1 X0.7000 Y0.3000 E0.0119
G1 X-1.5000 Y0.0000 E0.0235
G1 X-0.7000 Y0.3000 E0.0119
G1 X0.7000 Y-0.3000 E0.0119
G1 X-1.5000 Y0.0000 E0.0235
G1 X-0.7000 Y-0.3000 E0.0119
G1 X0.7000 Y0.3000 E0.0119
G1 X-1.5000 Y0.0000 E0.0235
G1 X-0.7000 Y0.3000 E0.0119
G1 X0.7000 Y-0.3000 E0.0119
G1 X-1.5000 Y0.0000 E0.0235
G1 X-0.7000 Y-0.3000 E0.0119
G1 X0.7000 Y0.3000 E0.0119
G1 X-1.5000 Y0.0000 E0.0235
G1 X-0.7000 Y0.3000 E0.0119
G1 X0.7000 Y-0.3000 E0.0119
G1 X-1.5000 Y0.0000 E0.0235
G1 X-0.7000 Y-0.3000 E0.0119
G1 X0.7000 Y0.3000 E0.0119
G1 X-1.5000 Y0.0000 E0.0235
G1 X-0.7000 Y0.3000 E0.0119
G1 X0.7000 Y-0.3000 E0.0119

```
G1 X-1.5000 Y0.0000 E0.0235
G1 X-0.7000 Y-0.3000 E0.0119
G1 X0.7000 Y0.3000 E0.0119
G1 X-1.5000 Y0.0000 E0.0235
G1 X-0.7000 Y0.3000 E0.0119
G1 X0.7000 Y-0.3000 E0.0119
G1 X-1.5000 Y0.0000 E0.0235
G1 X-0.7000 Y-0.3000 E0.0119
G1 X0.7000 Y0.3000 E0.00119
G1 X-1.5000 Y0.0000 E0.0235
G1 X-0.7000 Y0.3000 E0.0119
G1 X0.7000 Y-0.3000 E0.0119
G1 X-6.5000 Y0.0000 E0.1019
G1 X0.7000 Y-0.3000 E0.0119
G1 X-0.7000 Y0.3000 E0.0119
G1 X-1.5000 Y0.0000 E0.0235
G1 X0.7000 Y0.3000 E0.0119
G1 X-0.7000 Y-0.3000 E0.0119
G1 X-1.5000 Y0.0000 E0.0235
G1 X0.7000 Y-0.3000 E0.0119
G1 X-0.7000 Y0.3000 E0.0119
G1 X-1.5000 Y0.0000 E0.0235
G1 X0.7000 Y0.3000 E0.0119
G1 X-0.7000 Y-0.3000 E0.0119
G1 X-1.5000 Y0.0000 E0.0235
G1 X0.7000 Y-0.3000 E0.0119
G1 X-0.7000 Y0.3000 E0.0119
G1 X-1.5000 Y0.0000 E0.0235
G1 X0.7000 Y0.3000 E0.0119
G1 X-0.7000 Y-0.3000 E0.0119
G1 X-1.5000 Y0.0000 E0.0235
G1 X0.7000 Y-0.3000 E0.0119
G1 X-0.7000 Y0.3000 E0.0119
G1 X-1.5000 Y0.0000 E0.0235
G1 X0.7000 Y0.3000 E0.0119
G1 X-0.7000 Y-0.3000 E0.0119
G1 X-1.5000 Y0.0000 E0.0235
G1 X0.7000 Y-0.3000 E0.0119
G1 X-0.7000 Y0.3000 E0.0119
G1 X-1.5000 Y0.0000 E0.0235
```

G1 X0.7000 Y0.3000 E0.0119
G1 X-0.7000 Y-0.3000 E0.0119
G1 X-1.5000 Y0.0000 E0.0235
G1 X0.7000 Y-0.3000 E0.0119
G1 X-0.7000 Y0.3000 E0.0119
G1 X-1.5000 Y0.0000 E0.0235
G1 X0.7000 Y0.3000 E0.0119
G1 X-0.7000 Y-0.3000 E0.0119
G1 X-1.5000 Y0.0000 E0.0235
G1 X0.7000 Y-0.3000 E0.0119
G1 X-0.7000 Y0.3000 E0.0119
G1 X-1.5000 Y0.0000 E0.0235
G1 X0.7000 Y0.3000 E0.0119
G1 X-0.7000 Y-0.3000 E0.0119
G1 X-1.5000 Y0.0000 E0.0235
G1 X0.7000 Y-0.3000 E0.0119
G1 X-0.7000 Y0.3000 E0.0119
G1 X-1.5000 Y0.0000 E0.0235
G1 X0.7000 Y0.3000 E0.0119
G1 X-0.7000 Y-0.3000 E0.0119
G1 X-1.5000 Y0.0000 E0.0235
G1 X0.7000 Y-0.3000 E0.0119
G1 X-0.7000 Y0.3000 E0.0119
G1 X-1.5000 Y0.0000 E0.0235
G1 X0.7000 Y0.3000 E0.0119
G1 X-0.7000 Y-0.3000 E0.0119
G1 X-1.5000 Y0.0000 E0.0235
G1 X0.7000 Y-0.3000 E0.0119
G1 X-0.7000 Y0.3000 E0.0119
G1 X-1.5000 Y0.0000 E0.0235
G1 X0.7000 Y0.3000 E0.0119
G1 X-0.7000 Y-0.3000 E0.0119
G1 X-1.5000 Y0.0000 E0.0235
G1 X0.7000 Y-0.3000 E0.0119
G1 X-0.7000 Y0.3000 E0.0119
G1 X-1.5000 Y0.0000 E0.0235
G1 X0.7000 Y0.3000 E0.0119
G1 X-0.7000 Y-0.3000 E0.0119
G1 X-1.5000 Y0.0000 E0.0235
G1 X0.7000 Y-0.3000 E0.0119

```
G1 X-0.7000 Y0.3000 E0.0119
G1 X-1.5000 Y0.0000 E0.0235
G1 X0.7000 Y0.3000 E0.0119
G1 X-0.7000 Y-0.3000 E0.0119
G1 X-1.5000 Y0.0000 E0.0235
G1 X0.7000 Y-0.3000 E0.0119
G1 X-0.7000 Y0.3000 E0.0119
G1 X-1.5000 Y0.0000 E0.0235
G1 X0.7000 Y0.3000 E0.0119
G1 X-0.7000 Y-0.3000 E0.0119
G1 X-1.5000 Y0.0000 E0.0235
G1 X0.7000 Y-0.3000 E0.0119
G1 X-0.7000 Y0.3000 E0.0119
G1 X-1.5000 Y0.0000 E0.0235
G1 X0.7000 Y0.3000 E0.0119
G1 X-0.7000 Y-0.3000 E0.0119
G1 X-1.5000 Y0.0000 E0.0235
G1 X0.7000 Y-0.3000 E0.0119
G1 X-0.7000 Y0.3000 E0.0119
G1 X-1.5000 Y0.0000 E0.0235
G1 X0.7000 Y0.3000 E0.0119
G1 X-0.7000 Y-0.3000 E0.0119
G1 X-1.3000 Y0.0000 E0.0235
G1 X-10.0000 Y0.0000 E0.1567
G1 F2250
G1 X120.0000 Y0.0000 E1.8808
M104 S0
```

Appendix H

Abstract submitted in DCE 2021 Symposium on Biomedical Engineering - Poster session

Degradation and sterilization effect on polycaprolactone filament produced by melt electrospinning technology

Abstract
Electrospinning combined with 3D printing enables the use of biocompatible materials to create custom solutions with high reproducibility. This research presents preliminary results of the mechanical behaviour and degradation analysis of biodegradable polycaprolactone (PCL) filaments produced using melt electrospinning technology. No specific changes on the filament surface after sterilization and degradation were observed. The longer the degradation is, the more weight is lost. In an acidic environment, it is lost more in comparison with alkaline. Before the final product characterization, filament samples of this material should be thoroughly investigated to create mathematical models of more complex structures.

Author Keywords: Melt electrospinning, Polycaprolactone, Mechanical characterization, Degradation analysis.

1. Introduction

Pelvic organ prolapse (POP) is a condition commonly seen in older women that affects a woman's quality of life. In Portugal, from 2000 to 2012, the number of hospital admission due to POP increased by 105% and, currently, POP affects around 40% of women over 50 (Mascarenhas et al., 2015). Surgery remains the mainstay of therapy for pelvic organ prolapse (POP) (Mascarenhas et al., 2015). Meshes can be used to reinforce or substitute defective anatomical structures. However, polypropylene (PP) meshes used for pelvic organ prolapse repair might cause graft related complications (GRCs) such as infection, fistula, pain and exposure (Rynkevic et al. 2019). It is believed to be due to insufficient biocompatibility (weight, pore size, filament type, knitting pattern) and inappropriate mechanical properties of these meshes, besides patient and surgeon factors. A completely different approach may be the use of non-textile biodegradable implants made so that they mimic the biomechanical properties of the host tissue. Electrospinning, combined with 3D printing, enables using biocompatible materials with personalised dimensions, allowing for custom solutions and high reproducibility (Rynkevic et al. 2019). Before the final product characterisation, filament samples of this material should be thoroughly investigated. This research presents preliminary results of the mechanical behaviour and degradation analysis of biodegradable polycaprolactone (PCL) filaments produced using melt electrospinning technology.

2. Materials and Methods

The Polycaprolactone (PCL) (commercially available variant sold by 3D4Makers, named Facilan™ PCL 100, with density 1.1g/cm (ISO 1183), filament diameter 1.75mm, glass transition temperature -60ºC, melting point 58-60ºC, decomposition temperature 200ºC, melt flow index 11.3-5.2 g/10min) filament was used to produce the filaments.
PCL filaments were sterilised at UV irradiation for 30 min, then incubated in EtOH 70%, for 1 hour, washed with PBS 2 times during 30 min and dried within the flow chamber. Filaments were weighed before and after sterilisation.
Filament samples were placed for 60 and 180 days in pH-controlled solutions, Phosphate Buffer Saline (PBS) with pH 7.4 and Potassium Hydrogen Phthalate (KHP) with pH 4.3, to mimic a biological environment or the action of its components. Degradation analysis was conducted following the ISO 10993 standard. Each specimen's initial weight from each group (n=6), were measured before immersion mediums. After the degradation, the samples were washed in distilled water, dried at room temperature for 24 hours and weighed. The filament's

degradation and sterilisation effects were evaluated via weight loss, uniaxial testing, and Scanning electron microscope (SEM) analysis.
A total of 5 specimens were tested using an electronic testing machine, "MultiTest-dV". A preload of 0.1N was applied, and a constant elongation rate of 10mm/min was used. Outcome measurements describing the mechanical behaviour were load-elongation curves and ultimate stress-strain values.
All statistical tests were made using a statistical software package (GraphPad Prism 5, USA). Quantitative data are represented as mean ± standard error of the mean (SEM). An unpaired Student's t-test was used (two-tailed, confidence level of 95%) to determine the differences between groups. The level of significance was set to $p<0.05$.

3. Results

The SEM images of PCL electrospun filaments are displayed in Figure 1. It is possible to see some imperfections due to printing. No specific changes on the filament surface after sterilization and degradation were observed. Filaments remained uniform and solid.

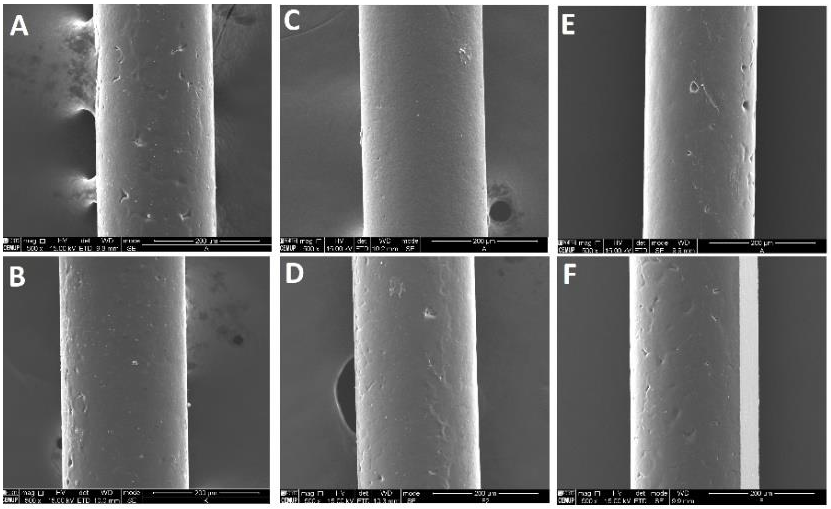

Figure 1: Scanning electron microscope (SEM) images of PCL fibers (240µm) produced by melt electrospinning (500x magnification): A-dry filament; B- sterilized filament; Filaments after degradation: C- 60d (PBS); D- 60d (KHP); E- 180d (PBS); F- 180d (KHP).

Printed filaments behaviour showed an initial elastic deformation with a small plastic deformation component (Figure 2 D). Once the elastic deformation stage is completed, the plastic deformation dominates, and a horizontal path of the graphic appears. A significant difference was observed between the filaments degraded during 180d in PBS and KHP ($p>0.05$). In acid media, filaments became fragile and were rapturing 2.5 mm elongation ($p<0.05$). A significant difference was observed between dry samples and after 60d of degradation ($p<0.05$). (Figure 2 B,C). No significant difference in filament weight loss was detect; however, a weight loss pattern due to degradation was observed (Figure 2 A). The longer the degradation is, the more weight is lost (more in an acidic environment).

4. Discussion

The most significant degradation occurred after 180 days in acid solution; however, no significant weight loss occurs after sterilization or after 60 days of degradation (period during which the implant performs tissues functions). Besides, degradation and sterilization did not cause significant surface changes on the filament.

5. Conclusions

Advantageous properties were obtained using melt electrospinning to produce PCL filaments. The study results will be used to create mathematical models, to characterize complex structures made of electrospun PCL fibres.

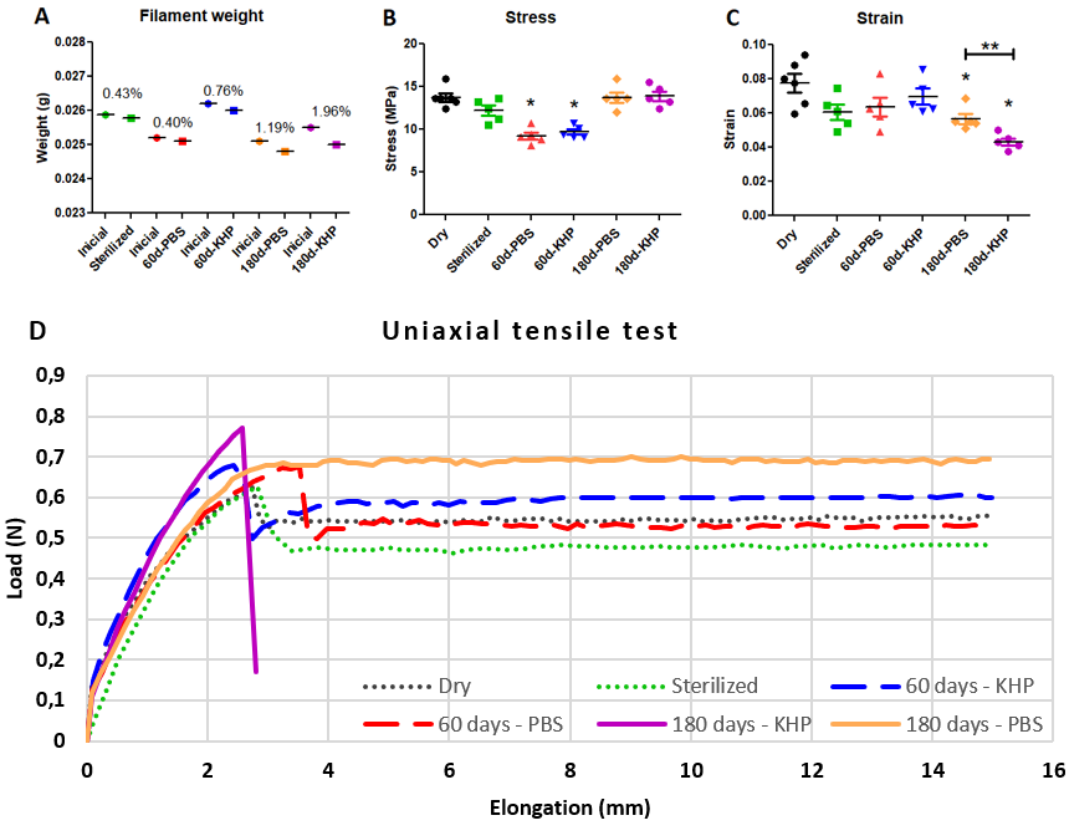

Figure 2: PCL filament sterilization and degradation analysis: A- weight loss (g); B Stress values (MPa) (mean±SEM); C- Strain (mean±SEM). Significant differences between groups are displayed above the scatter plot, when $p<0.05$ (*), within group-comparisons $p<0.05$ (**); D- uniaxial tensile tests.

References

Mascarenhas, Teresa, Miguel Mascarenhas-Saraiva, Amélia Ricon-Ferraz, Paula Nogueira, Fernando Lopes, and Alberto Freitas. 2015. "Pelvic Organ Prolapse Surgical Management in Portugal and FDA Safety Communication Have an Impact on Vaginal Mesh." *International Urogynecology Journal* 26 (1): 113–22. https://doi.org/10.1007/s00192-014-2480-0.

Rynkevic, Rita, P. Martins, Antonio Fernandes, J. Vange, Monica R. Gallego, Radoslaw A. Wach, Tristan Mes, Anton W. Bosman, and Jan Deprest. 2019. "In Vitro Simulation of in Vivo Degradation and Cyclic Loading of Novel Degradable Electrospun Meshes for Prolapse Repair." *Polymer Testing* 78 (May): 105957. https://doi.org/10.1016/j.polymertesting.2019.105957.

Acknowledgments

The authors gratefully acknowledge the funding by Ministério da Ciência Tecnologia, e Ensino Superior, FCT, Portugal and Programa Operacional Competitividade e Internacionalização - POCI the project SPINMESH - Melt eletrospining of polymeric bioabsorbable meshes for pelvic organ prolapse repair - POCI-01-0145-FEDER-029232.